12th Asian Regional Conference on SMGE, August 2003, Singapore
Keynote Lecture

Consolidation of Clay and Compaction of Sand

-An elasto-plastic description-

Akira ASAOKA
Department of Civil Engineering, Nagoya University, Furo-cho, Chikusa-ku, Nagoya, 464-8603, JAPAN
asaoka@civil.nagoya-u.ac.jp

Abstract: Naturally deposited clays/sands are mostly found in structured, and usually also in overconsolidated states. Furthermore, they exhibit what is more or less a condition of anisotropy. In order to describe the mechanical behavior of these natural soils, this study models super/subloading yield surfaces together with rotational hardening using the modified Cam-Clay model. Three evolution laws are introduced naturally into the constitutive laws of soils; the first one describes decay/collapse of soil structure, the second loss of overconsolidation, and the third evolution of anisotropy. Although all of these proceed with ongoing plastic deformation, it is newly emphasized that the decay of structure tends to promote plastic volume compression while the loss of overconsolidation leads to plastic volume expansion. Clay is clearly distinguished from sand by the difference in the rates of these evolution laws. As highly structured overconsolidated clay reverts to the normally consolidated state, it initially retains its structure. Then the clay begins to lose its structure very gradually with ongoing plastic deformation, during which process secondary consolidation and/or delayed compression is observed. In contrast, sand loses its structure very rapidly, not in the manner of a decay, but rather in a sudden collapse, while remaining in its overconsolidated state. The loss of overconsolidation for sand requires a huge amount of plastic deformation. Fundamental constitutive model responses of natural clay are illustrated through numerical simulations of secondary consolidation and/or delayed compression, during which softening is clearly observed with the occurrence of plastic volume compression. For sand, typical model responses are illustrated through numerical simulations of compaction of a loose sand deposit. Repeated application of low-level shear stress upon the loose sand leads to a huge amount of volume compression, which is due to the rapid collapse of the initial soil structure. Repetition of the loading also results in a rapid increase of the overconsolidation ratio.

1 INTRODUCTION

1.1 *Purposes of this paper*

Whether a certain soil is a sand or a clay may be easy enough to tell from such things as its color and feel, its grain size distribution and its permeability constant. Perceptual and physical properties like these can certainly tell us that what we have before us is a soil of such and such a kind rather than of some other. Yet the important problem remains that in triaxial tests in the laboratory, no matter how accurately we classify these perceptual and physical indicators, we are unable, on the basis of such variations alone, to arrive at a direct mechanical derivation of the different elasto-plastic responses of sand and clay soils with which we are so familiar. The author of this paper can remember frequently being told by his mother “Don’t play with clay, play with sand.” Even to the intuitive sense of a child, it seems, this difference between sand and clay is perfectly easy to recognize. How strange, then, that up until now there should have been virtually no clear descriptions of this difference in language appropriate to the mechanics of elasto-plasticity.

Of course, there are groups of researchers working out completely separate constitutive equations for use with sand and clay. But, given a particular soil sample, if for the initial decision of which constitutive equation to apply, these groups still go on depending on the same kind of “child’s intuition” referred to above, it can hardly be said that the two constitutive equations in question have been produced on the basis of a single consistent logic. After all, even children who have grown up healthily on clay and sand games are sometimes known to say “I don’t know if it’s sand or clay.” This is what happens to us in the case of clayey sands or sandy clays. Although the difference between sand and clay may be clear enough in principle, the fact that there is no firm borderline distinguishing between them puts us metaphorically back in the position of these children.

Even leaving aside this distinction between sand and clay, in work with sand alone there are research groups who set up separate constitutive equations and material constant parameters for “loose sand” and “dense sand,” according to density and/or void ratio. As a research attitude in soil mechanics, this is illegitimate, for the following reason. When a soil is compressed, water is drained out from the pores in it, leading to a rise in density and a lowering of the void ratio. In other words, the density and void ratio are expressions of the mechanical state of the soil material, made up as it is out of soil particles and pore water. A constitutive equation is, of its essence, a description of the changes in the mechanical state of a soil as a result of loading or unloading. Therefore, a procedure assigning different constitutive equations and material constants to the same sand depending on its density and void ratio simply does not deserve to be called research into the constitutive equations of materials. In fact, a “constitutive equation” of this kind dispenses from the start with any principled discussion of shear behavior under drained conditions, or behavior under volume compression. Such work marks a theoretical retreat even from the Cam-Clay model of 45 years ago, which set out to integrate these compression and shear behaviors.

The purposes of this paper and Invited Lecture will be:
(1) to make clear the difference between sand and clay in the language of the mechanics of elasto-plasticity,
(2) by means of a finite element method of calculation, to provide an elasto-plastic constitutive equation for sands and clays in actual engineering use,
(3) to present some examples of the calculation’s application.

The examples presented under (3) specifically include soil-water coupled computations for the compaction of loose sand and for the secondary consolidation and/or delayed compression of naturally deposited clay. The fact that these two terms "compaction" and "consolidation" have always been distinguished in classical geotechnical engineering suggests that there is a difference in the mechanisms of volume compression between sand and clay, and the inclusion in this paper of examples for both compaction and consolidation is therefore not without its good reasons.

1.2 *Content of the study*

In what will always be remembered as an outstanding achievement, the Critical State Soil Mechanics approach (e.g. Roscoe et al., 1958, 1963) established approach established some 45 years ago by the Soil Mechanics Group at the University of Cambridge was the first in the world to propose an elasto-plastic constitutive equation, the Cam-Clay model, capable of integrating both the shear and volume change behaviors of a soil. The present paper will be rearranging the essential elements of this Cam-Clay model, and arguing that a close scrutiny of the model's limits of application is an indispensable step towards an integral understanding of the relations between sand and clay.

As hardly needs mentioning, the essentials of the Cam-Clay model are that:
(1) hardening of soil accompanies plastic volume compression,
(2) softening of soil accompanies plastic volume expansion, and
(3) in the stress space, the borderline is given by the critical state line $q = \mathrm{M}p'$ (One further essential to mention, for present purposes, is that the coefficient M is constant throughout the whole process of plastic deformation). The fact that the Cam-Clay model has rarely been used for analyses of softening/expansion has to do with the limited capabilities of electronic computational technology at that time, and does not reflect any limitations in the model itself.

The limitation that does exist in the Cam-Clay model is, of course, that the only mechanical behaviors it can describe are those of fully remolded and normally consolidated soil under loading. In other words, behaviors such as
(1) hardening with plastic expansion in regions above the critical state line, such as occurs with dense sand or overconsolidated clay, or
(2) softening in regions below the critical state line, such as appears with the shearing of highly structured natural clay under undrained conditions,
cannot be represented using the Cam-Clay model. These two shortcomings can however be overcome, not by abandoning the model as such, but by supplementing it with two additional concepts, "overconsolidation" and "soil skeleton structure," from hierarchies not taken into account when the model was first put forward. These two concepts can be introduced by the definition of two new super/subloading surfaces (e.g. Hashiguchi K., 1989, Asaoka et.al., 2000a) similar in shape to the yield surface/plastic potential of the model as proposed. At the risk of repeating himself, the author again wishes to make it clear that he has no intention of renouncing the Cam-Clay model, which continues to maintain its position as the theoretical foundation of soil mechanics.

Just as was remarked above of density and void ratio, overconsolidation and soil structure are mechanical states, which will vary in the same soil depending on loading and unloading. An important consequence of introducing the super/subloading surfaces, therefore, is that it makes possible the description of two soil behaviors,
(1) loss of overconsolidation, and
(2) decay/collapse of structure in the soil skeleton,
which accompany the development of plastic deformation. As a result of these behaviors, the slope M of the critical state line can become greater or smaller depending on how plastic deformation proceeds, so that it is no longer necessarily the case that hardening always accompanies compression, and softening always expansion, as assumed in the Cam-Clay model.

Overconsolidation is explained by comparing the current loading state with the most severe loading state in the past, while the concept of structure is explained by showing how much bulk a certain soil occupies. For example, a highly structured soil is able to sustain a higher load than a less structured soil of the same void ratio, or is able to sustain the same amount of loading at a higher void ratio. For the purposes of this paper, there would be no point in pursuing more intuitive interpretations of these terms "overconsolidation" and "soil skeleton structure," by defining them physically from such visually determined characteristics as the size and configuration of soil particles. We have no need of intuitive definitions at the micro level. What is needed is a mechanical description of overconsolidation and soil structure "**at work**," or "**in action**." Nothing else matters for soil mechanics as a species of continuum mechanics. For example, we need to understand loss of overconsolidation as acting in the direction of expansion, and decay/collapse of structure as acting in the direction of compression. As the reader will appreciate, the introduction of super/subloading surfaces serves to make mechanical responses of these kinds describable.

The treatment of these matters will take us through to the end of Chapter 4. The description up to that point will make use of the terms of infinitesimal strain mechanics, and arguments concerning anisotropy will be avoided altogether. But this is only in order to simplify the formulation and — if truth be told — to make the lecture a little easier to deliver, given the author's limited command of English. No great leap of theory would be required in these first four chapters to introduce questions of anisotropy into the argument, or to reformulate the description in the terms of finite deformation theory so as to satisfy objectivity. There is no need, then, of such an undue amount of explanation. The aspects omitted here are supplied in a complete form in APPENDICES A to D (Asaoka et.al., 2002). The results presented in the concluding three chapters 5, 6 and 7 are all computed making use of this "complete model."

Chapter 5 is an account of the differences in mechanical behavior between sand and clay. In the case of sand, while any development of plastic deformation leads to a prompt collapse in the soil structure, it does not lead to any loss at all of overconsolidation. The behavior of clay is the exact opposite of this: while overconsolidated clay returns immediately to its normally consolidated state upon the development of plastic deformation, almost no collapse takes place in the structure. These behaviors are expressed by manipulating the differences in rate in the evolution laws for overconsolidation and soil structure. In this way, the use of the proposed model incorporating super/subloading surfaces is found to account consistently well for the typical mechanical responses of clay and sand, as known from laboratory experiments.

Chapter 6 offers a simulation of the compaction process in loose sand, produced through the repeated application of small-amplitude shear stresses to a quantity of loose sand in the drained condition. In this process, a considerable degree of compression occurs in the sand, accompanied by an abrupt simultaneous change to a state of overconsolidation. From this computation it is clearly seen that this degree of compression is due to the readiness

of the sand soil structure to collapse at the slightest onset of plastic deformation, while the sudden overconsolidation comes about because the loss of overconsolidation under loading is minimal. Conversely, it is also easy to see why there is hardly any compaction at all in the case of clay, which persistently resists any breakdown of soil structure while readily permitting loss of overconsolidation. The mechanical properties of sand in its various stages of compaction display considerable differences, with respect to both density and void ratio. But as this chapter makes clear, these can all be fully explained using one constitutive equation and a single set of material constants.

Chapter 7 analyzes secondary consolidation and/or delayed compression in structured clay. The causes of large-scale secondary settlement in clay naturally lie in the decay of the soil skeleton structure. As to the delay with which this happens, this is because the compression resulting from the decay of the soil structure is able to occur without any great increase in effective stress. That is to say, all that it takes for decay to proceed is that the excess pore water pressure shed from the soil pores in the course of compression should not be allowed to dissipate. In some cases compression is possible even when effective stress is decreasing. That, in fact, is what "compression accompanied by softening" refers to. When softening of this kind takes place, the excess pore pressure even increases during consolidation, due to the decrease in the effective stress level.

It may appear that compaction and secondary consolidation are quite distinct phenomena pertaining to sand and to clay, respectively. But both processes alike occur as a result of collapse or decay in the soil structure. There is therefore nothing to stop us classing them together, from a mechanical point of view, as phenomena of the same sort. One of the things that the present paper hopes to make evident is that there will be no great error in regarding compaction in sand as the equivalent of secondary consolidation in clay.

2 ESSENTIALS OF THE CAM-CLAY MODEL

For simplicity's sake, the Cam-Clay model discussed here is the original one, but exactly the same conclusions would be reached if the modified Cam-Clay model (Roscoe K.H. and Burland J. B., 1968) were considered.

2.1 *Yield function and/or plastic potential*

From isotropic consolidation tests using fully remolded clay, the following equation is obtained for the normal consolidation line.

$$1+e=\mathrm{N}-\tilde{\lambda}\ln p' \tag{2.1}$$

This is naturally for the case where stress ratio η

$$\eta=\frac{q}{p'}=0 \tag{2.2}$$

However, from a series of triaxial compression/extension tests using the same clay in undrained/drained conditions the equation obtained is

$$1+e=\Gamma-\tilde{\lambda}\ln p' \tag{2.3}$$

This, of course, is for the case where stress ratio η is in the critical state

$$\eta=\frac{q}{p'}=\mathrm{M} \tag{2.4}$$

In these equations, $\mathrm{N}, \Gamma, \tilde{\lambda}$ and M $(\mathrm{N}>\Gamma)$ are material constants of the soil, e is the void ratio, and mean effective stress p' and shear stress q are defined as:

$$p'=\frac{1}{3}\mathrm{tr}\boldsymbol{\sigma}', \quad q=\sqrt{\frac{3}{2}\boldsymbol{S}\cdot\boldsymbol{S}}, \quad \boldsymbol{S}=\boldsymbol{\sigma}'-p'\boldsymbol{I} \tag{2.5}$$

where $\boldsymbol{\sigma}'$ and $\boldsymbol{S}$ are the effective stress (compression positive) and deviatoric stress tensors, and $\boldsymbol{I}$ is the unit tensor. The curves for Equations (2.1) and (2.3) are shown in Fig. 2.1.

In the critical state expressed by Equations (2.3) and (2.4), the shear strain is indefinite even where there is no change in the effective stress, and it is well known that in these conditions, whatever variation occurs in the shear strain, there will be no corresponding change in the soil volume. The example shown in Fig. 2.2 is from a drained triaxial compression test on a fully

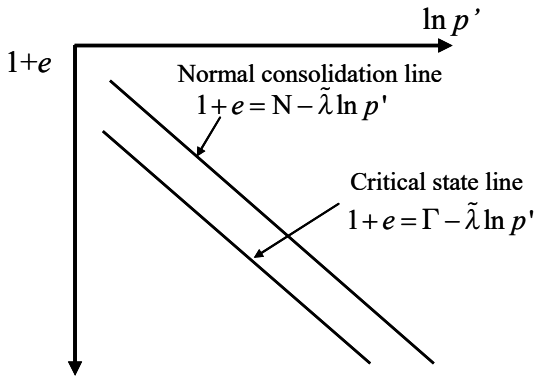

Fig. 2.1 Normal consolidation line and critical state line.

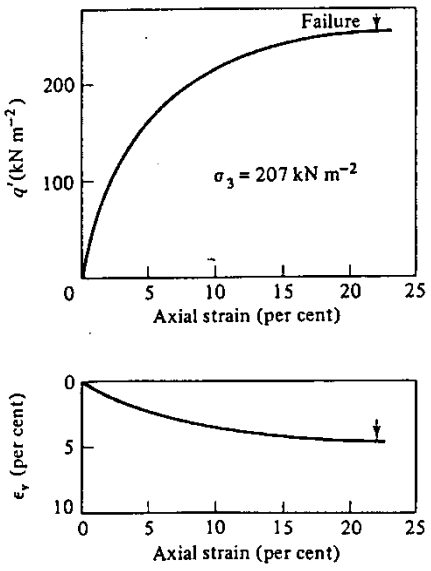

Fig. 2.2 Drained triaxial compression test of a fully remolded clay (after Bishop A.W. and Henkel D.J., 1962).

remolded clay sample. So long as the soil undergoes no change in effective stress, the change in the elastic component in the volumetric strain will naturally be 0, so that on the basis of a first-

order strain increment approximation

$$\dot{\varepsilon}_v = \dot{\varepsilon}_v^e + \dot{\varepsilon}_v^p \tag{2.6}$$

the volumetric strain at the critical state will be

$$\dot{\varepsilon}_v^p = 0 \quad \text{at} \quad q = \mathrm{M}p' \tag{2.7}$$

where ε_v stands for the volumetric strain (compression positive), the upper dot is for the material time derivative or increment, and the superscript e or p shows the elastic or plastic component.

Now, taking account of the fact that $\tilde{\lambda}$ in Equations (2.1) and (2.3) does not depend on stress ratio η, let us suppose that the relation corresponding to Equations (2.1) and (2.3) in the range $0 < \eta = q/p' < \mathrm{M}$ is of the kind

$$1 + e = x(\eta) - \tilde{\lambda} \ln p' \tag{2.8}$$

where the segment $x(\eta)$ fulfills the condition

$$x(\eta = 0) = \mathrm{N}, \quad x(\eta = \mathrm{M}) = \Gamma \tag{2.9}$$

The simplest means of fulfillment is through the linear interpolation

$$x(\eta) = \mathrm{N} + \frac{\Gamma - \mathrm{N}}{\mathrm{M}}\left(\frac{q}{p'}\right) \tag{2.10}$$

Therefore,

$$1 + e = \mathrm{N} + \frac{\Gamma - \mathrm{N}}{\mathrm{M}}\left(\frac{q}{p'}\right) - \tilde{\lambda} \ln p' \tag{2.11}$$

may most simply be assumed as the general form fitting all stress ratios obtained from Equations (2.1) and (2.3).

Let us next suppose that this clay in its normally consolidated state, without any unloading, changes from a state of $e_0, p' = p_0', q = 0$ to one of e, p', q. From Equation (2.11) in such a case, we obtain

$$1 + e_0 = \mathrm{N} - \tilde{\lambda} \ln p_0' \tag{2.12}$$

$$1 + e = \mathrm{N} + \frac{\Gamma - \mathrm{N}}{\mathrm{M}}\left(\frac{q}{p'}\right) - \tilde{\lambda} \ln p' \tag{2.13}$$

which means that the volumetric strain resulting from this change of state can be calculated as:

$$\varepsilon_v = \frac{(1+e_0)-(1+e)}{1+e_0} = \frac{1}{1+e_0}\left\{\frac{\mathrm{N}-\Gamma}{\mathrm{M}}\left(\frac{q}{p'}\right) + \tilde{\lambda} \ln \frac{p'}{p_0'}\right\} \tag{2.14}$$

Since the elastic component in this volumetric strain, calculated using elastic constant $\tilde{\kappa}$, can be given as:

$$\varepsilon_v^e = \frac{\tilde{\kappa}}{1+e_0} \ln \frac{p'}{p_0'} \tag{2.15}$$

by means of an approximation

$$\varepsilon_v = \varepsilon_v^e + \varepsilon_v^p \tag{2.16}$$

it becomes possible to express the plastic volumetric strain for this interval of change as:

$$\varepsilon_v^p = f(p', q) = \frac{1}{1+e_0}\left\{\frac{\mathrm{N}-\Gamma}{\mathrm{M}}\left(\frac{q}{p'}\right) + (\tilde{\lambda} - \tilde{\kappa}) \ln \frac{p'}{p_0'}\right\} = f_{\sigma'}(\boldsymbol{\sigma}') \tag{2.17}$$

This Equation (2.17) is well known as the yield function of the original Cam-Clay model. It is Equation (2.10) that actually gives the dilatancy component of the volume change, but since Equation (2.17) is based on the relation between the two e–$\log p'$ terms in Equation (2.1) and (2.3), the system of soil mechanics deduced from Equation (2.17) is also known as "e–$\log p'$ soil mechanics."

Equation (2.17) reveals that plastic volumetric strain does not depend on the loading path, but is determined purely in terms of the initial and final stress states. Henkel's experiment, as shown in Fig. 2.3, is famous for its demonstration of this. Invoking the mathematical 'concept of potential,' therefore, we may also think of Equation (2.17) as expressing the plastic potential surface in the original Cam-Clay model. From here a natural step leads on to the next hypothesis, the "associated plastic flow rule."

$$\dot{\boldsymbol{\varepsilon}}^p = \lambda \frac{\partial f_{\boldsymbol{\sigma}'}}{\partial \boldsymbol{\sigma}'} \tag{2.18}$$

The term $\dot{\boldsymbol{\varepsilon}}^p$ here represents the plastic strain increment tensor, while $\boldsymbol{\sigma}'$ is the effective stress tensor. Plastic multiplier $\lambda > 0$ at the time of loading. Since the term $f_{\sigma'}(\boldsymbol{\sigma}')$ in Equation (2.17) is known to be a scalar valued isotropic function, the current stress tensor and the plastic strain increment tensor are co-axial. Indeed, making use of actual results from triaxial test sets, only isotropic functions ever arise. This can only be called a stroke of genius on the part of Bishop. To express this isotropic nature of $f_{\sigma'}(\boldsymbol{\sigma}')$ in a way that is easier to understand, the following pair of related equations, having the same form as (2.18), are frequently used.

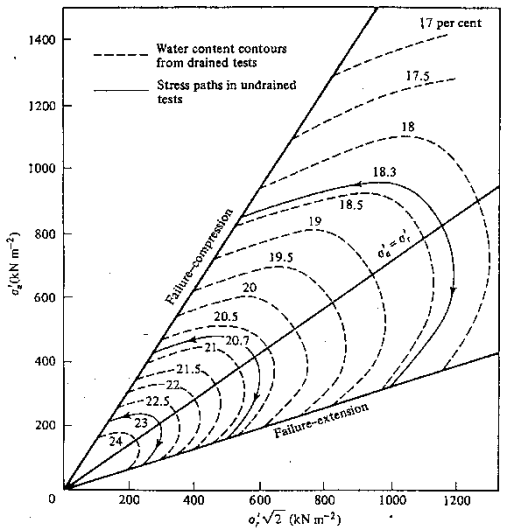

Fig. 2.3 Equi-water content contours (after Henkel D.J., 1960).

$$\begin{cases} \dot{\varepsilon}_v^p = \lambda \dfrac{\partial f}{\partial p'} \\ \dot{\varepsilon}_s^p = \lambda \dfrac{\partial f}{\partial q} \end{cases} \tag{2.19}$$

where $\dot{\varepsilon}_s^p$ and $\dot{\varepsilon}_v^p$ are the scalar valued plastic shear strain rate and the plastic volumetric strain rate, respectively, the definitions of which are as follows:

$$\begin{cases} \dot{\varepsilon}_v^p = \mathrm{tr}\dot{\boldsymbol{\varepsilon}}^p \\ \dot{\varepsilon}_s^p = \sqrt{\dfrac{2}{3}\dot{\boldsymbol{e}}^p \cdot \dot{\boldsymbol{e}}^p} \end{cases}, \quad \dot{\boldsymbol{e}}^p = \dot{\boldsymbol{\varepsilon}}^p - \frac{1}{3}(\mathrm{tr}\dot{\boldsymbol{\varepsilon}}^p)\boldsymbol{I} \tag{2.20}$$

Equation (2.19) shows the two components, compression and shear, of the plastic strain increment vector represented in a p'–q stress space (in the outward normal direction to the plastic potential surface). For this, see Fig. 2.4. The calculation in Equation (2.19) is simpler than in (2.18), making it convenient for the interpretation of triaxial test results, in which p' and q are all that occur. For example, the zero condition for the plastic volumetric strain increment in the critical state shown in Equation (2.7) can be written as:

$$\frac{\partial f}{\partial p'} = 0 \tag{2.21}$$

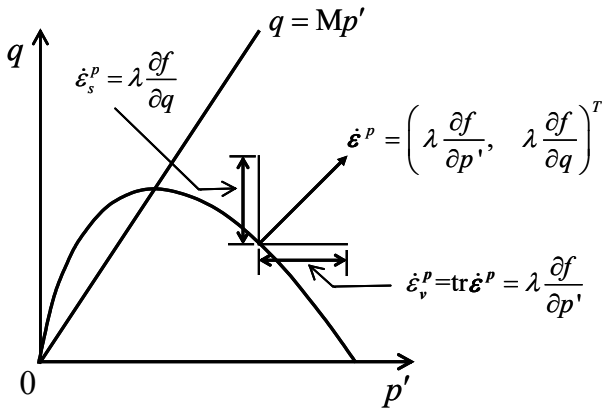

Fig. 2.4 Decomposition of plastic strain increment vector on p'–q space.

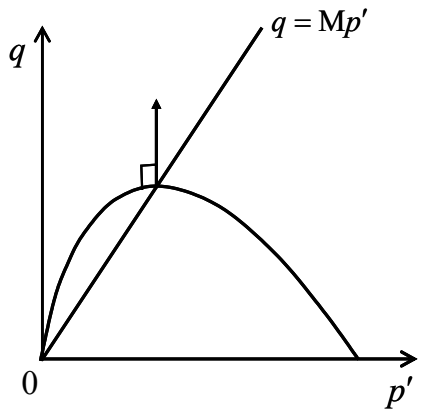

Fig. 2.5 Non plastic volume change condition at the critical state.

and if Equation (2.17) is substituted into this Equation, the following relation among the material constants is easily obtained.

$$\mathrm{N} - \Gamma = \tilde{\lambda} - \tilde{\kappa} \tag{2.22}$$

An explanation of Equation (2.21) by means of a p'–q diagram can be seen in Fig. 2.5.

The shapes of the yield function/plastic potential in Figs. 2.4 and 2.5 indicate that plastic volume expansion is occurring in the region of the stress space above the critical state line, and plastic volume compression in the region below the line. More formally,

$$\begin{cases} \dot{\varepsilon}_v^p > 0 & \text{when} \quad q < \mathrm{M}p' \\ \dot{\varepsilon}_v^p < 0 & \text{when} \quad q > \mathrm{M}p' \end{cases} \tag{2.23}$$

as summarized in Fig. 2.6.

For the yield function/plastic potential in the modified Cam-Clay model, the interpolation between Equations (2.1) and (2.3) is performed not as in Equation (2.10), but in the form

$$x(\eta) = \mathrm{N} + \frac{\Gamma - \mathrm{N}}{\ln 2} \ln \left\{ \frac{\mathrm{M}^2 + (q/p')^2}{\mathrm{M}^2} \right\} \tag{2.24}$$

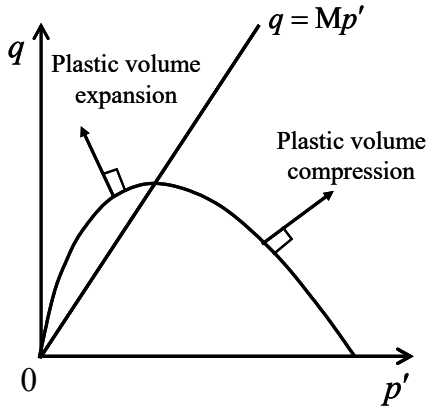

Fig. 2.6 Plastic volume compression below the critical sate line and plastic volume expansion above the critical state line in p'–q space.

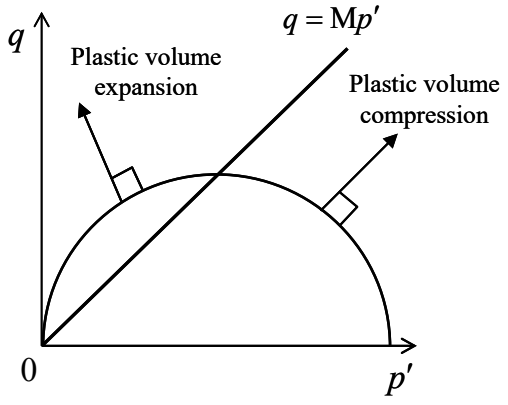

Fig. 2.7 Plastic volume compression/expansion in the modified Cam-Clay model.

However, the subsequent reasoning can be pursued in precisely the same way as above, leading also to the same outcome, with plastic expansion occurring above the critical state line, and plastic compression below it, as in Equation (2.23). This is shown in Fig. 2.7. The following two Equations may offer a little guidance:

$$\varepsilon_v^p = f(p',q) = \frac{1}{1+e_0}\left[\frac{\mathrm{N}-\Gamma}{\ln 2}\ln\left\{\frac{\mathrm{M}^2+(q/p')^2}{\mathrm{M}^2}\right\}+(\tilde{\lambda}-\tilde{\kappa})\ln\frac{p'}{p_0'}\right] = f_{\sigma'}(\boldsymbol{\sigma}') \tag{2.25}$$

$$\mathrm{N}-\Gamma = \ln 2(\tilde{\lambda}-\tilde{\kappa}) \tag{2.26}$$

2.2 *Hardening and softening*

If we take the total derivative from Equation (2.17),

$$\dot{\varepsilon}_v^p = \frac{\partial f}{\partial p'}\dot{p}' + \frac{\partial f}{\partial q}\dot{q} \tag{2.27}$$

and equate it with the first of the equations in Equation (2.19), the plastic multiplier λ is found to be

$$\lambda = \frac{\dfrac{\partial f}{\partial p'}\dot{p}' + \dfrac{\partial f}{\partial q}\dot{q}}{\dfrac{\partial f}{\partial p'}} = \frac{\dfrac{\partial f}{\partial p'}\dot{p}' + \dfrac{\partial f}{\partial q}\dot{q}}{\dfrac{\tilde{\lambda}-\tilde{\kappa}}{\mathrm{M}(1+e_0)}\dfrac{1}{p'}\left(\mathrm{M}-\dfrac{q}{p'}\right)} \tag{2.28}$$

Accordingly, for the loading condition

$$\lambda > 0 \tag{2.29}$$

we can distinguish three distinct situations, as follows:

$$\begin{cases} \dfrac{\partial f}{\partial p'}\dot{p}' + \dfrac{\partial f}{\partial q}\dot{q} > 0 & \text{when} \quad q < \mathrm{M}p' \\ \dfrac{\partial f}{\partial p'}\dot{p}' + \dfrac{\partial f}{\partial q}\dot{q} < 0 & \text{when} \quad q > \mathrm{M}p' \\ \dfrac{\partial f}{\partial p'}\dot{p}' + \dfrac{\partial f}{\partial q}\dot{q} = 0 & \text{when} \quad q = \mathrm{M}p' \end{cases} \tag{2.30}$$

Now, since $\dfrac{\partial f}{\partial p'}\dot{p}' + \dfrac{\partial f}{\partial q}\dot{q}$ represents the inner product of the outward normal vector to the plastic potential $\begin{pmatrix} \dfrac{\partial f}{\partial p'} \\ \dfrac{\partial f}{\partial q} \end{pmatrix}$ and the stress increment vector $\begin{pmatrix} \dot{p}' \\ \dot{q} \end{pmatrix}$, its positive or negative polarity will indicate whether the stress increment vector is directed out from the outer surface, or in toward the inner surface of the plastic potential. The contents of Equation (2.30) can accordingly be set out as in Fig. 2.8. Subsequent yield surfaces will either expand below the critical state (hardening) or diminish above it (softening). Thus, the critical state line $q = \mathrm{M}p'$ also marks the borderline between hardening and softening.

It is important to take Fig. 2.8 in alignment with the previous Fig. 2.6. From their combination, the following three results become evident:

① *Hardening always accompanies plastic compression, softening accompanies plastic expansion,*

② *The border between both hardening and softening, and plastic compression and plastic expansion, is represented by the critical state line* $q = \mathrm{M}p'$,

③ *The slope* M *of the critical state line is a material constant, which does not vary with changes in loading.*

These properties of the original Cam-Clay model continue to apply in exactly the same way to the modified Cam-Clay model.

2.3 *Constitutive equation and loading criterion*

If the total derivative from Equation (2.17)

$$\dot{\varepsilon}_v^p = \frac{\partial f_{\sigma'}}{\partial \boldsymbol{\sigma}'}\cdot\dot{\boldsymbol{\sigma}}' \tag{2.31}$$

is combined with the associated plastic flow rule as expressed in Equation (2.18), it can be rewritten in the form

$$\dot{\varepsilon}_v^p = \lambda \mathrm{tr}\frac{\partial f_{\sigma'}}{\partial \boldsymbol{\sigma}'} \tag{2.32}$$

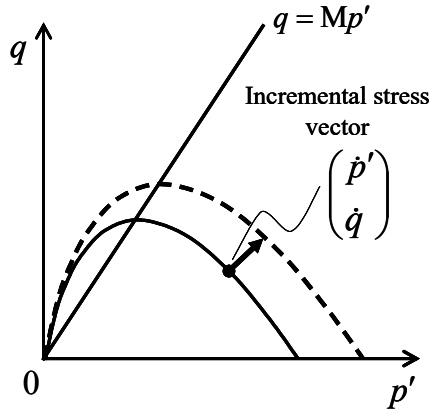

(a)

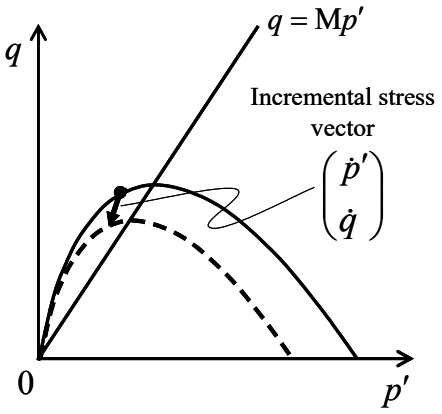

(b)

Fig. 2.8 Hardening below $q = \mathrm{M}p'$ and softening above $q = \mathrm{M}p'$.

Since (2.31) and (2.32) both express the same thing, we may equate them. Making use of the effective stress tensor $\boldsymbol{\sigma}'$, the plastic multiplier λ is then found to be

$$\lambda = \frac{\frac{\partial f_{\sigma'}}{\partial \boldsymbol{\sigma}'} \cdot \dot{\boldsymbol{\sigma}}'}{\mathrm{tr}\frac{\partial f_{\sigma'}}{\partial \boldsymbol{\sigma}'}} \tag{2.33}$$

This is known as the "plastic multiplier in terms of stress." The stress increment term in the numerator can be rewritten as:

$$\dot{\boldsymbol{\sigma}}' = \boldsymbol{E}\dot{\boldsymbol{\varepsilon}}^e \tag{2.34}$$

This is known as the "incremental elastic response," where $\boldsymbol{E}$ is a nonlinear elastic modulus tensor. It will be noticed that

$$\dot{\boldsymbol{\varepsilon}}^e = \dot{\boldsymbol{\varepsilon}} - \dot{\boldsymbol{\varepsilon}}^p = \dot{\boldsymbol{\varepsilon}} - \lambda \frac{\partial f_{\sigma'}}{\partial \boldsymbol{\sigma}'} \tag{2.35}$$

next, substituting Equation (2.34) into Equation (2.33), the plastic multiplier can be rewritten in the form

$$\lambda = \Lambda = \frac{\frac{\partial f_{\sigma'}}{\partial \boldsymbol{\sigma}'} \cdot \boldsymbol{E}\dot{\boldsymbol{\varepsilon}}}{\mathrm{tr}\frac{\partial f_{\sigma'}}{\partial \boldsymbol{\sigma}'} + \frac{\partial f_{\sigma'}}{\partial \boldsymbol{\sigma}'} \cdot \boldsymbol{E}\frac{\partial f_{\sigma'}}{\partial \boldsymbol{\sigma}'}} \tag{2.36}$$

Λ is of course the same as the λ in (2.33), but in this case is called the "plastic multiplier in terms of strain rate." Using this Λ, we can now obtain the following equation for the relation between the stress and strain increments:

$$\begin{aligned} \dot{\boldsymbol{\sigma}}' &= \boldsymbol{E}\dot{\boldsymbol{\varepsilon}}^e = \boldsymbol{E}(\dot{\boldsymbol{\varepsilon}} - \dot{\boldsymbol{\varepsilon}}^p) \\ &= \boldsymbol{E}\dot{\boldsymbol{\varepsilon}} - \Lambda \boldsymbol{E}\frac{\partial f_{\sigma'}}{\partial \boldsymbol{\sigma}'} \end{aligned} \tag{2.37}$$

Equation (2.37) is called the "incremental (linear) elasto-plastic response." Naturally, the terms on either side are in a unique inverse relation to each other, but the equation is nonetheless useful for computations of deformation using the finite element method, which takes as its starting point the weak form of the equation of equilibrium.

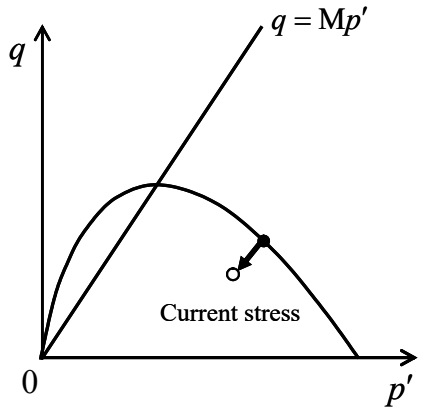

Fig. 2.9 Unloading with no movement of the yield surface.

The choice in use between elastic response Equation (2.34) and elasto-plastic response Equation (2.37) is made on the basis of the loading criterion. The second denominator term in Equation (2.36) is a positive definite quadratic form, and it tends to be the case with most soil constants that denominators come out positive, irrespective of the stress state. Generalizing from this, we may adopt the name "Cam-Clay parameters" to refer to material constants that make the denominator of Equation (2.36) positive, for any stress state. Details for this can be found in Asaoka et. al. (1994). The loading condition

$$\Lambda(=\lambda) > 0 \tag{2.38}$$

effectively guarantees that the numerator in Equation (2.36) is also positive. Thus, the loading criterion can be given as:

$$\begin{cases} \dfrac{\partial f_{\sigma'}}{\partial \boldsymbol{\sigma}'} \cdot \boldsymbol{E}\dot{\boldsymbol{\varepsilon}} > 0 & : \text{loading} \quad \text{(Equation(2.37))} \\ \dfrac{\partial f_{\sigma'}}{\partial \boldsymbol{\sigma}'} \cdot \boldsymbol{E}\dot{\boldsymbol{\varepsilon}} < 0 & : \text{unloading} \quad \text{(Equation(2.34))} \end{cases} \tag{2.39}$$

This loading criterion is indispensable for allowing us to distinguish between softening and unloading (elastic response). Softening is accompanied by a diminution of the yield surface down to the current stress state (Fig. 2.8(b)). Unloading partly resembles softening, in that the incremental stress vector is directed toward the inside of the yield surface, but in unloading the surface itself does not move but remains as it is (Fig. 2.9).

In the Cam-Clay model, once the stress has come down inside the yield surface as a result of unloading, it is assumed that an elastic response will continue, even in the event of a subsequent reloading, until such time as the current stress state reaches the previous yield surface again. It is worth noting that this is not actually stated in the loading criterion in Equation (2.39), but nonetheless this point, too, ought to be regarded as one of the essentials of the Cam-Clay model. Stated more formally:

④ *When the stress changes on the inside of the yield surface, the soil shows an elastic response (Equation (2.34)).*

In the Introduction to this paper, the author said it was not legitimate to offer separate constitutive equations for sand and clay, and to rely on childlike intuition for the choice of which equation to use. That would be the exact equivalent of presenting Equations (2.34) and (2.37), without supplementing them with loading criterion (2.39) and the above property ④.

3 LIMITATIONS OF THE CAM-CLAY MODEL

3.1 *Loss of overconsolidation*

Fig. 3.1 shows the typical experimental results obtained from a drained triaxial compression test performed on fully remolded but heavily overconsolidated clay. The effective stress path on the p'–q diagram for this test is shown in Fig. 3.2. Similar test results were reported by Bishop and Henkel, 1962, some 40 years ago. In shaded zone 1 in Fig. 3.1, the stress state is still below the critical state line, and the soil specimen is under compression. In zone 2, however, the specimen begins to display expansion as the stress state rises above the line. Expansion accompanied by softening is noticeable in zone 3. The reason we can tell that zone 3 shows softening, not unloading, is because in the case of unloading there would need to be some decrease in the axial strain.

A typical case of a phenomenon that cannot be explained using the Cam-Clay model is seen in zone 2. In the terms of the model, the stress state in this zone ought to be still on the inner side of the yield surface, where an elastic response would be expected, so that the material would have to display compression, not expansion, with the rise in p'. The expansion that actually occurs in this

zone is due to the fact that the plastic volume expansion greatly exceeds the elastic volume compression. Considering further that ① an elasto-plastic response must be occurring on the inner side of the yield surface, while ② shear stress q is also increasing, it is even possible that hardening and plastic expansion are occurring together. Phenomena ① and ② are completely inexplicable in terms of the Cam-Clay model.

In the case of a clay with an overconsolidation ratio as large as

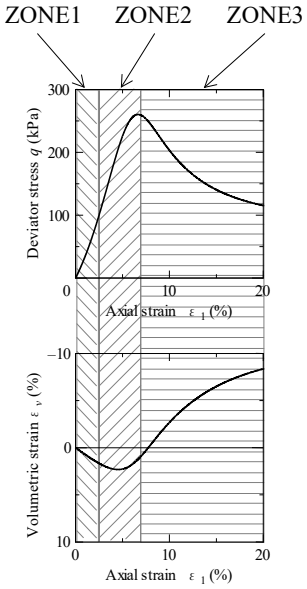

Fig. 3.1 Drained triaxial test of a fully remolded and heavily overconsolidated clay.

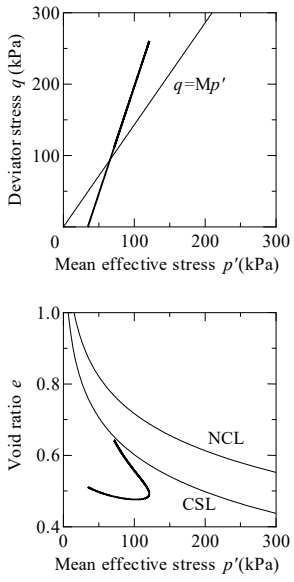

Fig.3.2 Effective stress path and volume change with p' in a draind triaxial test of remolded and overconsolidated clay.

24, the response computed by the Cam-Clay model is of the kind shown in Figs. 3.3(a) and 3.3(b), which is altogether different from what we see in Figs. 3.1 and 3.2. When the overconsolidation ratio is this high, the yield surface lies far above the current stress, and therefore in the case of reloading, assuming no movement occurs in the yield surface, the peak of the stress-strain curve will be considerably higher than in Fig. 3.1. Moreover, since the stress remains on the inside of the yield surface all the way up to the point where it reaches this peak, the material can be seen to be in elastic compression. At the peak the stress reaches the yield surface, and thereafter the material becomes normally consolidated clay. However, as the stress lies above the critical state line, the material must be subject to softening, and the peak described turns out to be correspondingly sharp and precipitous (Fig. 3.3(a)). Similarly, the stress level at this peak is also far higher than in Fig. 3.2 (Fig. 3.3(b)). It is evident from this that the Cam-Clay model is totally inadequate for expressing the shear behavior of an overconsolidated clay.

In order to model the behaviors in Figs. 3.1 and 3.2 faithfully, it is necessary

① to allow for elasto-plastic responses on the inside of the yield surface, and

② to allow for plastic expansion in accompaniment with hardening.

These problems can be completely solved by introducing the concept of a subloading surface, which was first established by Hashiguchi (Hashiguchi, 1978). It is important to emphasize here that what Hashiguchi did was not to deny the Cam-Clay model, but only to restrict its application to the loading and unloading of normally consolidated soils. Hashiguchi was the first researcher in the world to show cogently that loading leads to a progressive loss of overconsolidation, that is to say, that through the development of plastic deformation brought on by loading an overconsolidated soil returns to the normally consolidated state. Previously it had been supposed that loss of overconsolidation came about through elastic deformation, and in this sense there can be no doubt that Hashiguchi's argument, even if not a denial of the Cam-Clay model, was a considerable leap forward in theory. Typical elasto-plastic responses during reloading are shown in Figs. 3.4(a) and 3.4(b).

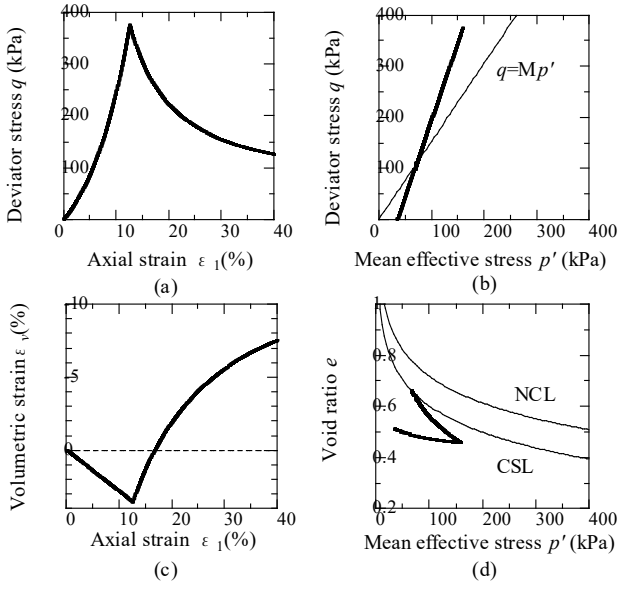

Fig. 3.3 Responses of the heavily overconsolidated Cam-Clay in a draind triaxial compression test.

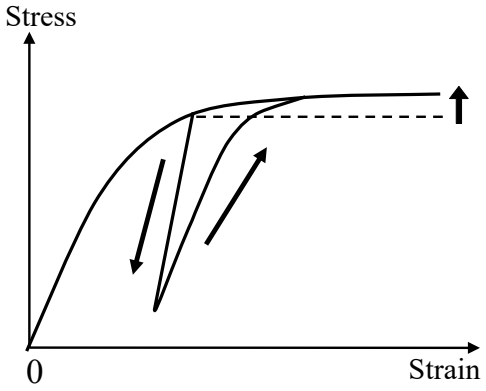

(a) Increase in "yield stress" due to hardening.

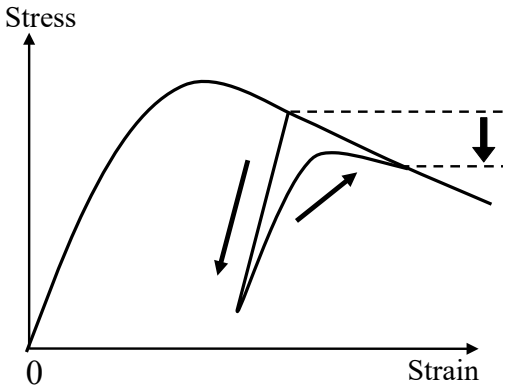

(b) Decrease in "yield stress" due to softening.

Fig. 3.4 Loss of overconsolidation due to loading.

3.2 *Decay/collapse of the soil skeleton structure*

Fig. 3.5 shows results from an oedometer test performed on highly structured natural clay material (Asaoka et. al., 2000). The straight line in the figure is the normal consolidation line for remolded clay, obtained by fully remolding the material and then running the oedometer test again. In terms of the Cam-Clay model, the area above the normal consolidation line is an impossible region, in other words, it ought to be impossible for a soil to assume this sort of state. But in fact we see that the highly structured clay can very well occur in a state of this kind that is not possible for the remolded material.

Fig. 3.5 also shows that, compared with a clay that has had its structure broken down through remolding, the highly structured clay is able to sustain greater vertical loads for the same void ratio, or to tolerate a larger void ratio while under the same load. In this paper, this is described by saying that the structured soil has a greater 'bulk.'

Fig. 3.6 presents results for comparative oedometer tests on minimally disturbed and slightly disturbed clay specimens (Leroueil S., 1996). It is evident that the minimally disturbed clay has a more developed structure, and is therefore bulkier. As for the question of *what* is slightly disturbed in the one case but not in the other, it is of course the soil skeleton structure, invisible though this may be to the naked eye.

As no normal consolidation line for fully remolded clay is indicated in Fig. 3.6, let us return again to Fig. 3.5. Here, we can see that the greater the consolidation load, and consequently the

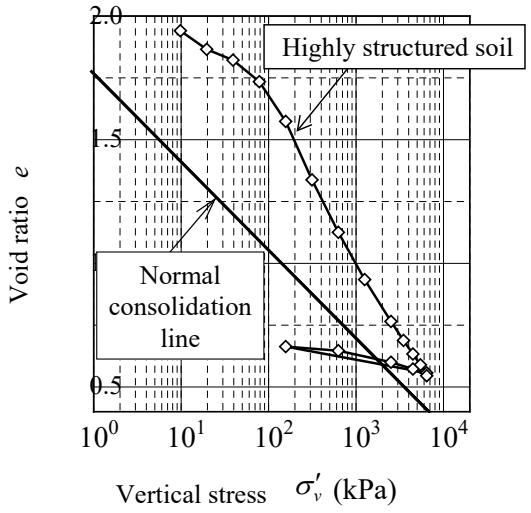

Fig. 3.5 Typical oedmeter test results on highly structured soil (after Asaoka et.al., 2000c).

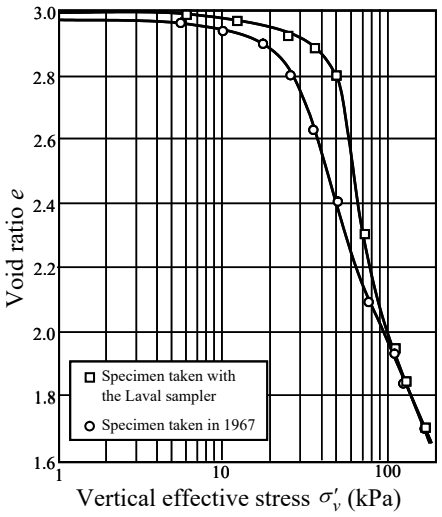

Fig. 3.6 Comparative oedometer tests on minimally disturbed and slightly disturbed clay specimens (after Leroueil S., 1996).

greater the degree of compression, the greater the tendency will be for the soil in the upper "impossible region" to revert back down toward the destructured state (that is, to approach the normal consolidation line for remolded clay). This leads us to suppose, therefore, that the collapse or progressive decay of structure is the result of the ongoing plastic deformation that occurs under loading.

From what has been said about structure in this section, and about overconsolidation in Section 3.1, it will by now be clear that the Cam-Clay model is applicable only to the loading and unloading of soils in which

① the skeleton structure has been completely destroyed through full remolding, and

② there has been a complete loss of overconsolidation, and a reversion to the normal consolidation state.

Let us from here on refer to clay of this description as "Cam-Clay."

In order to allow the Cam-Clay model to handle the mechanical states of soils in its supposedly impossible upper region, Asaoka et.al., (1998, 2000a, b) have further introduced the concept of a superloading yield surface. In conjunction with the subloading yield surface concept introduced by Hashiguchi, this has made it

possible to represent the ways in which, under ongoing loading, a progressive loss of overconsolidation and breakdown of structure leads all soils, without restriction, to approach the conditions of "Cam-Clay."

In the next chapter it will be shown how the slope M_s of the borderline between hardening and softening (from the slope formula q=Mp' of the Cam-Clay model) tends to become smaller or larger with the loss of overconsolidation, or the decay or collapse of soil structure, under loading. Soils in which these movements have come to a complete stop ("Cam-Clays") are in a

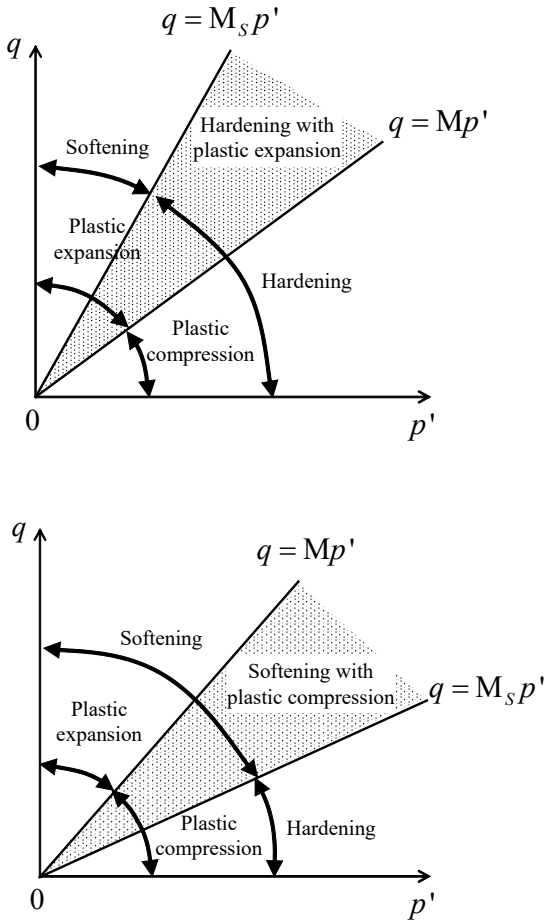

Fig. 3.7 Hardening with plastic volume expansion and softening with plastic volume compression.

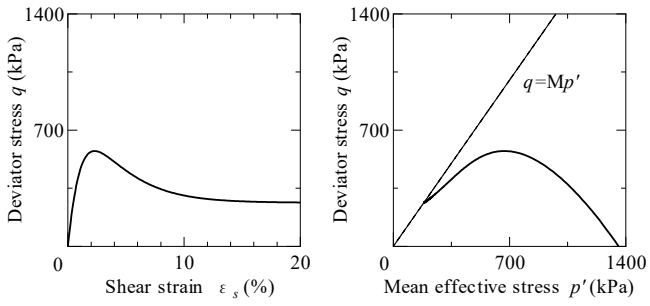

Fig. 3.8 Undrained shear behavior of a structured normally consolidated clay.

sense "dead." But in "living soils," that is, soils which retain either an overconsolidation state or a skeleton structure, or sometimes both, as M_s continues to rise or fall with the loss of overconsolidation or structure, combinations of hardening with plastic expansion, or softening with plastic compression remain a possibility, as shown in Fig. 3.7. Note that in this figure

q=Mp' : borderline between plastic compression and expansion (M constant), while

q=$M_S p'$: borderline between hardening and softening (M_s variable).

We have already seen an instance of hardening in combination with plastic expansion (Fig. 3.1, zone 2). Softening in combination with plastic compression is very commonly observed in undrained shear tests of naturally deposited clays in states close to normal consolidation. An example is shown in Fig. 3.8. A detailed explanation of this figure will be given in Chapter 4.

4 SUPER/SUBLOADING SURFACES FOR STRUCTURED AND OVERCONSOLIDATED SOILS

In this chapter we represent the elasto-plastic behaviors of structured and overconsolidated soils by introducing superloading and subloading yield surfaces into the original Cam-Clay model. The account will be in terms of an infinitesimal strain description, and there will be no discussion of anisotropy. This way of proceeding will make the explanation of new concepts relating to structure and overconsolidation much more plain and simple, and therefore facilitate understanding.

To represent anisotropy a yield surface of the form provided for in the modified Cam-Clay model is appropriate, while for a description of the kind of large deformation that leads up to the failure of soil structure a finite deformation theory is indispensable. A "complete model" satisfying these additional conditions is given in APPENDIX A. From this chapter on, all of the actual computations presented will be making use of this "complete model." But for an understanding of the accompanying explanations in each case the knowledge supplied in this chapter will be sufficient.

4.1 *Super/subloading Yield Surfaces*

Before we go on to formalize the details of the model in the next section, we need to begin here by explaining and defining some new concepts.

The Cam-Clay model

When a fully remolded and then perfectly destructured normally consolidated soil is subjected to loading, the soil is assumed to follow the elasto-plastic behavior of the Cam-Clay model.

Superloading yield surface

In a structured soil, on the outside of the yield surface as defined in the Cam-Clay model, that is to say, in the supposedly "impossible region" beyond the state boundary (or Roscoe) surface, there exists a superloading yield surface similar in form to the normal one. This is shown by the p'□ q stress space (Fig. 4.1). As can be seen in the figure, both surfaces are similar in relation to the point of origin. Since the current stress $\bar{p}'$, $\bar{q}$ shown on the superloading yield surface in the figure corresponds to the stress $\tilde{p}'$, $\tilde{q}$ on the yield surface in the Cam-Clay model, the similarity ratio between the two can be expressed as R^*, as in Fig. 4.1, and will lie between 0 and 1.

Normally consolidated state

When a current stress state is situated on the superloading yield

surface, the soil is said to be in a normally consolidated state. When a soil in this state undergoes loading, its elasto-plastic response can be described by applying the associated flow rule on the superloading yield surface.

Evolution law for R^*

Let the degree of the structural be denoted by R^*. A complete decay of structure would then correspond to $R^*=1$, and an infinitely developed state of structure to $R^*=0$. Since decay of structure is a consequence of plastic deformation, R^* will increase with the development of plastic deformation and eventually attain the value of 1. In other words, the material time derivative of R^*, $\dot{R}^*$, is a function of the plastic strain rate, and will always be positive (evolution law for R^*). Only in the state $R^*=1$, representing a complete decay of structure, will the superloading yield surface completely come to overlie the Cam-Clay yield surface beneath it.

Overconsolidated state

When a soil in a normally consolidated state undergoes unloading, the soil is said to be in an overconsolidated state.

Subloading yield surface

When a soil in an overconsolidated state is subjected to reloading, an elasto-plastic response occurs. This response can be described by applying the associated flow rule on the subloading yield surface. That is to say, in an overconsolidated soil the current stress will invariably be on the subloading yield surface, as shown in Fig. 4.2. Again, as shown in the figure, this subloading surface is taken to be similar in form to the Cam-Clay yield surface in relation to the point of origin.

In Fig. 4.2, as seen from the fact that p', q give the current stresses and $\bar{p}'$, $\bar{q}$ the size of the superloading yield surface under unloading, the similarity ratio R between the subloading and superloading yield surfaces will represent the state of overconsolidation ($0<R\le 1$). In fact, the reciprocal of R, $1/R$, is equivalent to the overconsolidation ratio as defined in classical soil mechanics. That is, $R=1$ represents the normal consolidation state, and in this state, only, the subloading and superloading yield surfaces will coincide. In general, however, the subloading surface lies on the inside of the superloading one, where $R<1$.

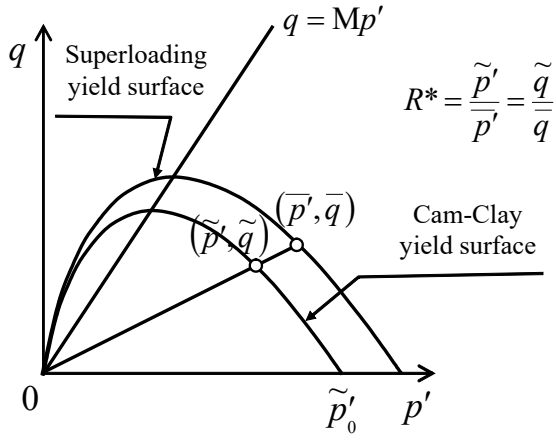

Fig. 4.1 Superloading yield surface.

Evolution law for R

As an overconsolidated soil undergoes progressive plastic deformation under loading, its overconsolidated state will come to approach a normally consolidated state. In other words, if an overconsolidated soil is allowed to evolve in its loaded state, the value of R will steadily increase and eventually reach 1 (normal consolidation). In such cases the plastic strain rate function $\dot{R}$, the material time derivative of R, will always be positive (evolution law for R).

A crucial point to notice is that during plastic deformation not only R, but also R^* increases. That is, when soil in an overconsolidated state reverts back toward the normally consolidated state, the superloading yield surface also changes from its initial unloading position, either increasing or decreasing. This means that the change in the overconsolidation ratio results not only from the change in current stress, but also from this movement of the superloading yield surface. This can also be appreciated from the previous Figs. 3.4(a) and (b) in Chapter 3. Naturally, when this plastic deformation leads to a change in the plastic volumetric strain, this will also result in a change of position for the Cam-Clay yield surface, which will either increase or decrease in size.

Four possible states for soils

From the preceding explanations, it is evident that soils can exist in the following four states:

① overconsolidated structured state ($0<R<1$, $0<R^*<1$)
② normally consolidated structured state ($R=1$, $0<R^*<1$)
③ overconsolidated non-structured state ($0<R<1$, $R^*=1$)
④ normally consolidated non-structured state ($R=1$, $R^*=1$)

Soils in states ①, ② and ③ pass through a process of plastic deformation before finally arriving at state ④. This process will be the central concern of Chapter 5.

4.2 *Model formulation*

Three yield surfaces

It is assumed here that for a structured soil in an overconsolidated state after unloading, the current stresses p', q are situated on the subloading yield surface. Noting that the center of similarity is at the point of origin, we next denote the corresponding stresses on the superloading and Cam-Clay yield surfaces as $\bar{p}'$, $\bar{q}$ and $\tilde{p}'$, $\tilde{q}$ respectively. Thus R^* and R can be given as:

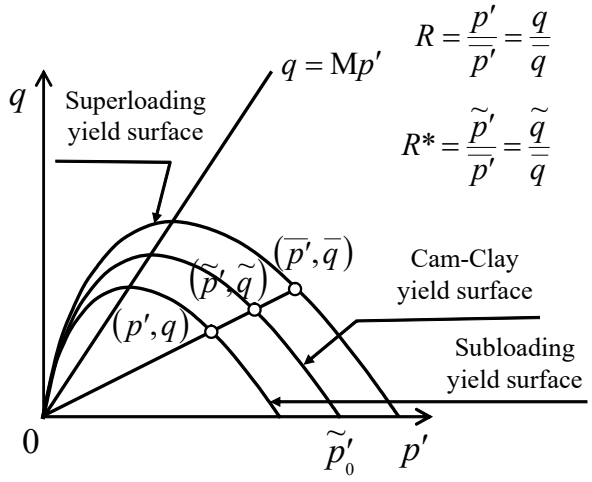

Fig. 4.2 Three yield surfaces.

$$R^*=\frac{\tilde{q}}{\bar{q}}=\frac{\tilde{p}'}{\bar{p}'} \tag{4.1}$$

$$R = \frac{q}{\bar{q}} = \frac{p'}{\bar{p}'} \tag{4.2}$$

This has already been shown in Fig. 4.2.

The Cam-Clay yield surface can be expressed in the form

$$\varepsilon_v^p = f(\tilde{p}', \bar{q}) = \frac{\tilde{\lambda} - \tilde{\kappa}}{1 + e_0} \ln \frac{\tilde{p}'}{\tilde{p}'_0} + \frac{\tilde{\lambda} - \tilde{\kappa}}{\mathrm{M}(1 + e_0)} \frac{\bar{q}}{\tilde{p}'} \tag{4.3}$$

$\tilde{p}'_0$ has already been shown in Figs. 4.1 and 4.2. Substituting Equation (4.1) in Equation (4.3), the superloading yield surface can be expressed as:

$$\begin{aligned} \varepsilon_v^p &= f(\bar{p}', \bar{q}) + \frac{\tilde{\lambda} - \tilde{\kappa}}{1 + e_0} \ln R^* \\ &= \frac{\tilde{\lambda} - \tilde{\kappa}}{1 + e_0} \ln \frac{\bar{p}'}{\tilde{p}'_0} + \frac{\tilde{\lambda} - \tilde{\kappa}}{\mathrm{M}(1 + e_0)} \frac{\bar{q}}{\bar{p}'} + \frac{\tilde{\lambda} - \tilde{\kappa}}{1 + e_0} \ln R^* \end{aligned} \tag{4.4}$$

By the same procedure, substituting Equation (4.2) in Equation (4.4) allows the subloading yield surface to be written as:

$$\begin{aligned} \varepsilon_v^p &= f(p', q) + \frac{\tilde{\lambda} - \tilde{\kappa}}{1 + e_0} \left(\ln R^* - \ln R \right) \\ &= \frac{\tilde{\lambda} - \tilde{\kappa}}{1 + e_0} \ln \frac{p'}{\tilde{p}'_0} + \frac{\tilde{\lambda} - \tilde{\kappa}}{\mathrm{M}(1 + e_0)} \frac{q}{p'} + \frac{\tilde{\lambda} - \tilde{\kappa}}{1 + e_0} \left(\ln R^* - \ln R \right) \\ &= f_{\boldsymbol{\sigma}'}(\boldsymbol{\sigma}') + \frac{\tilde{\lambda} - \tilde{\kappa}}{1 + e_0} \left(\ln R^* - \ln R \right) \end{aligned} \tag{4.5}$$

Normality rule and consistency condition

In the present research, as in the Cam-Clay model, the plastic response of the soil is assumed to follow the associated flow rule:

$$\dot{\varepsilon}_v^p = \lambda \frac{\partial f}{\partial p'} \tag{4.6}$$

$$\dot{\varepsilon}_s^p = \lambda \frac{\partial f}{\partial q} \tag{4.7}$$

where λ is the plastic multiplier. The size of the subsequent loading surface following the hardening or softening of the soil is calculated from the material time derivatives, or increment forms,

$$\dot{\varepsilon}_v^p = \dot{f} + \frac{\tilde{\lambda} - \tilde{\kappa}}{1 + e_0} \left(\frac{\dot{R}^*}{R^*} - \frac{\dot{R}}{R} \right) \tag{4.8}$$

from Equation (4.5) (Prager's consistency condition). This equation shows the necessity of evolution laws that give the material time derivatives $\dot{R}^*$ and $\dot{R}$ of R^* and R.

Equation (4.8) further expresses the two facts that

① the loss of overconsolidation ($\dot{R} > 0$, $R \to 1$) acts in the direction of the soil's plastic volume expansion;

② the decay or collapse of structure ($\dot{R}^* > 0$, $R^* \to 1$) acts in the direction of the soil's plastic volume compression.

Both of these two occurrences have hitherto been understood intuitively, ① from the breakdown of the interlocking bonds between soil particles, and ② from the card house-like collapse of overall structure.

*Evolution laws for R and R**

The evolution laws for R and R^* express the fact that as plastic deformation proceeds both R and R^* increase and approach a value of 1. Here, this is written as

$$\dot{R} = U \dot{\varepsilon}_s^p \tag{4.9}$$

$$\dot{R}^* = U^* \dot{\varepsilon}_s^p \tag{4.10}$$

where U and U^* are the positive definite scalar functions of R and R^* respectively. It is to be noted in Equations (4.9) and (4.10) that the evolution in the plastic deformation is represented by the plastic shear strain rate $\dot{\varepsilon}_s^p$, and that under conditions of loading this $\dot{\varepsilon}_s^p$ is invariably positive. In place of plastic shear strain rate $\dot{\varepsilon}_s^p$, it might also be possible to take the norm of the plastic strain rate tensor $\dot{\boldsymbol{\varepsilon}}^p$ (see APPENDIX A). The only reason for using the plastic shear strain rate in this chapter is in order to keep the subsequent computations as simple as possible.

The following restrictions apply to U, the positive definite scalar function of R:

$$U(R = 1) = 0 \tag{4.11}$$

$$U(R = 0) = \infty \tag{4.12}$$

Equation (4.11) expresses the fact that loss of overconsolidation ends once the soil reaches the normally consolidated state. Equation (4.12) signifies that as the overconsolidation ratio becomes infinitely large the elasto-plastic response of the soil approaches closer to a pure elastic response. The reason for this is because

$$U = \frac{\dot{R}}{\dot{\varepsilon}_s^p} = \infty \tag{4.13}$$

which entails that $\dot{\varepsilon}_s^p \to 0$. The simplest function U satisfying the two restrictions (4.11) and (4.12) is of the form

$$U = -\frac{\mathrm{M}(1 + e_0)}{\tilde{\lambda} - \tilde{\kappa}} m \ln R \tag{4.14}$$

The larger the value of material constant m, the faster will be the rate of overconsolidation loss. For this reason, m is called the degradation parameter of the overconsolidated state. The first researchers to present this line of argument from Equations (4.11) to (4.14) were Hashiguchi et al. (1989).

Next, the following restrictions can similarly be presented for U^*, the postive scalar function of R^*:

$$U^*(R^* = 1) = 0 \tag{4.15}$$

$$U^*(R^* = 0) = 0 \tag{4.16}$$

Equation (4.15) expresses the condition where the decay or collapse of structure is about to cease, and Equation (4.16) the point at which a saturated soil, maximally advanced in both its structural development and its void ratio, is said to "liquefy," making an elasto-plastic response altogether unthinkable. The simplest function U^* satisfying the restrictions (4.15) and (4.16) is given by the beta function

$$U^* = \frac{\mathrm{M}(1 + e_0)}{\tilde{\lambda} - \tilde{\kappa}} a R^{*b} (1 - R^*)^c \tag{4.17}$$

Three parameters are used in this, but generally it is taken that

$b=1$, $c=1$. These are called the degradation parameters of structure. The argument from (4.15) to (4.17) was first presented by Asaoka et. al. (1988, 2000a, 2002).

The curves for the functions U in Equation (4.14) and U^* in Equation (4.17) are shown in Fig. 4.3.

Plastic multiplier λ in terms of stresses

Recalling the rates of plastic volumetric strain and plastic shear strain shown in Equations (4.6) and (4.7), and substituting the two evolution laws, Equations (4.9) and (4.10), into the consistency condition given by Equation (4.8), we obtain

$$\dot{\varepsilon}_v^p = \lambda\frac{\partial f}{\partial p'} = \frac{\partial f}{\partial p'}\dot{p}' + \frac{\partial f}{\partial q}\dot{q} + \lambda\frac{\tilde{\lambda}-\tilde{\kappa}}{1+e_0}\left(\frac{U^*}{R^*}\frac{\partial f}{\partial q} - \frac{U}{R}\frac{\partial f}{\partial q}\right) \tag{4.18}$$

Given the fact that

$$\frac{\partial f}{\partial q} = \frac{\tilde{\lambda}-\tilde{\kappa}}{\mathrm{M}(1+e_0)}\frac{1}{p'} \tag{4.19}$$

the plastic multiplier λ in Equation (4.18) can be calculated from the second and third parts of the equation as

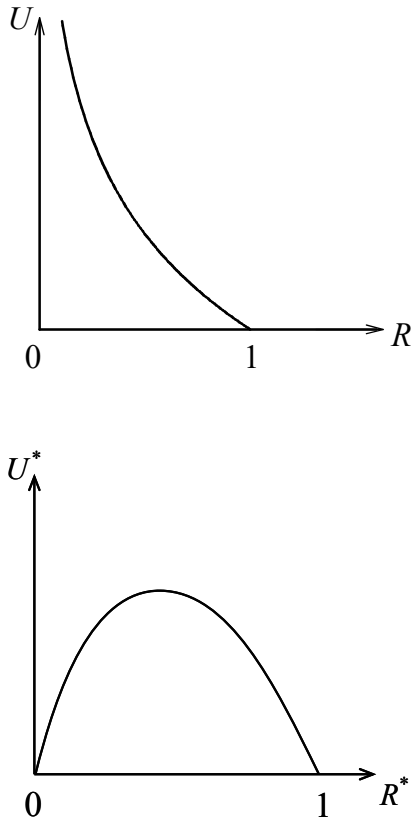

Fig. 4.3 U and U^* functions.

$$\lambda = \frac{\dfrac{\partial f}{\partial p'}\dot{p}' + \dfrac{\partial f}{\partial q}\dot{q}}{\dfrac{\tilde{\lambda}-\tilde{\kappa}}{\mathrm{M}(1+e_0)}\dfrac{1}{p'}\left(\mathrm{M}_s - \dfrac{q}{p'}\right)} \tag{4.20}$$

Here,

$$\mathrm{M}_s = \mathrm{M}\left\{1 - \frac{\tilde{\lambda}-\tilde{\kappa}}{\mathrm{M}(1+e_0)}\frac{U^*}{R^*} + \frac{\tilde{\lambda}-\tilde{\kappa}}{\mathrm{M}(1+e_0)}\frac{U}{R}\right\} \tag{4.21}$$

Comparing the plastic multiplier λ in Equation (4.20) with the λ in the Cam-Clay model (Equation (2.28) in Chapter 2), it can be seen that constant M stands in place of variable M_s.
From the loading condition,

$$\lambda > 0 \tag{4.22}$$

we see that the loading state can be divided into the three following phases, exactly as was the case with the Cam-Clay model in Chapter 4:

$$\begin{cases} \dfrac{\partial f}{\partial p'}\dot{p}' + \dfrac{\partial f}{\partial q}\dot{q} > 0 & \text{when} \quad q < \mathrm{M}_s p' \quad : \text{hardening} \\ \dfrac{\partial f}{\partial p'}\dot{p}' + \dfrac{\partial f}{\partial q}\dot{q} < 0 & \text{when} \quad q > \mathrm{M}_s p' \quad : \text{softening} \\ \dfrac{\partial f}{\partial p'}\dot{p}' + \dfrac{\partial f}{\partial q}\dot{q} = 0 & \text{when} \quad q = \mathrm{M}_s p' \quad : \text{perfectly plastic} \end{cases} \tag{4.23}$$

However, unlike the case of the Cam-Clay model, the slope M_s of the borderline

$$q = \mathrm{M}_s p' \tag{4.24}$$

between hardening and softening will increase and decrease considerably depending on the development of plastic deformation. This matter will be discussed in the next section.

Constitutive equation and loading criterion

The plastic multiplier λ can be generally written in the form

$$\lambda = \frac{\dfrac{\partial f_{\boldsymbol{\sigma}'}}{\partial \boldsymbol{\sigma}'}\cdot\dot{\boldsymbol{\sigma}}'}{\dfrac{\tilde{\lambda}-\tilde{\kappa}}{\mathrm{M}(1+e_0)}\dfrac{1}{p'}\left(\mathrm{M}_s - \dfrac{q}{p'}\right)} \tag{4.25}$$

using the effective stress tensor and function $f_{\boldsymbol{\sigma}'}$ from Equation (4.5). Substituting the elastic response of the soil

$$\dot{\boldsymbol{\sigma}}' = \boldsymbol{E}\,\dot{\boldsymbol{\varepsilon}}^e \tag{4.26}$$

in this equation gives

$$\Lambda = \lambda = \frac{\dfrac{\partial f_{\boldsymbol{\sigma}'}}{\partial \boldsymbol{\sigma}'}\cdot\boldsymbol{E}\,\dot{\boldsymbol{\varepsilon}}}{\dfrac{\partial f}{\partial \boldsymbol{\sigma}'}\cdot\boldsymbol{E}\dfrac{\partial f}{\partial \boldsymbol{\sigma}'} + \dfrac{\tilde{\lambda}-\tilde{\kappa}}{\mathrm{M}(1+e_0)}\dfrac{1}{p'}\left(\mathrm{M}_s - \dfrac{q}{p'}\right)} \tag{4.27}$$

just as in Chapter 2. Accordingly, this means that the elasto-plastic response

$$\begin{aligned} \dot{\boldsymbol{\sigma}}' &= \boldsymbol{E}\dot{\boldsymbol{\varepsilon}}^e = \boldsymbol{E}(\dot{\boldsymbol{\varepsilon}} - \dot{\boldsymbol{\varepsilon}}^p) \\ &= \boldsymbol{E}\dot{\boldsymbol{\varepsilon}} - \Lambda\boldsymbol{E}\frac{\partial f_{\sigma'}}{\partial \boldsymbol{\sigma}'} \end{aligned} \tag{4.28}$$

can also be written the same way as in the Cam-Clay model. Also,

the question of whether the soil shows an elastic or an elasto-plastic response to the change in stress — in other words, the use of the relation

$$\frac{\partial f_{\sigma'}}{\partial \boldsymbol{\sigma}'} \cdot \boldsymbol{E}\dot{\boldsymbol{\varepsilon}} = 0 \qquad (4.29)$$

in selecting between the uses of Equations (4.26) and (4.28) — is again precisely the same as for the Cam-Clay model.

4.3 *Model characteristics*

If Equations (4.14) and (4.17), for U and U^* respectively, are substituted for M_s in Equation (4.21) in conditions where $b=1$, $c=1$, we obtain

$$\mathrm{M}_s = \mathrm{M}\left\{1-\frac{m}{R}\ln R - a\left(1-R^*\right)\right\} \qquad (4.30)$$

This equation shows, more distinctly than Equation (4.21), that
① the loss of overconsolidation ($R \to 1$) leads to a decrease in M_s ;
② the decay or collapse of structure ($R^* \to 1$) leads to an increase in M_s .

This is also shown in Figs. 4.4(a) and 4.4(b). The straight line $q = \mathrm{M}p'$ in these figures naturally marks the border between plastic compression and plastic expansion. This being so, Fig. 4.4(a) indicates that the region in which hardening can occur together with plastic expansion will decrease and eventually disappear with a decrease in M_s , while Fig. 4.4(b) similarly indicates that the region in which softening can occur together with plastic compression will decrease and eventually disappear with an increase in M_s .

Let us now present two extreme examples that clearly illustrate these behaviors. These two examples have already been shown in Fig. 3.1 and Fig. 3.8 in Chapter 3, which showed the limitations of the Cam-Clay model.

Fully remolded, but overconsolidated clay
The elasto-plastic and evolution parameters of this clay material are as given below.

Table 4.1 Material constants.

Elasto-plastic parameters	
Compression index $\tilde{\lambda}$	0.15
Swelling index $\tilde{\kappa}$	0.035
Critical state constant M	1.43
Void ratio at $p'=98.1$kPa on NCL N	1.72
Poisson's ratio ν	0.15
Evolution parameters	
Degradation parameter of overconsolidation state m	2.0
Degradation parameter of structure a ($b=c=1.0$)	1.5

The initial conditions of the material (subscript 0 indicates initial values) are:

Table 4.2 Initial conditions.

Initial conditions	
Initial void ratio e_0	0.51
Initial mean effective stress p_0' (kPa)	34.5
Initial value of R^* (R^*_0)	1.00
Initial overconsolidation ratio $1/R_0$	24.0

As $R^*_0 = 1$, we may say that the clay has been completely remolded to leave no structure. Therefore the superloading yield surface already falls together with the Cam-Clay yield surface. However, since the current stress is situated on the subloading yield surface (overconsolidation ratio 24), the material's elasto-plastic response to reloading is also dominantly determined on this subloading surface.

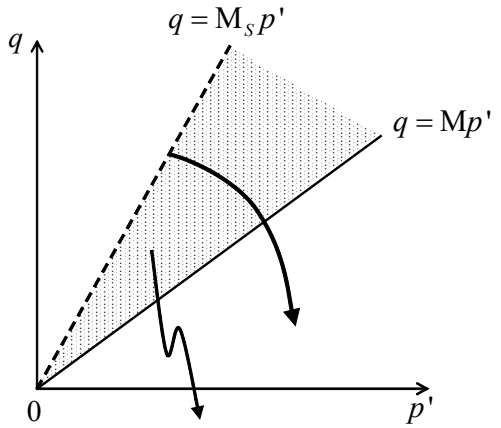

Hardening with plastic volume expansion

(a)

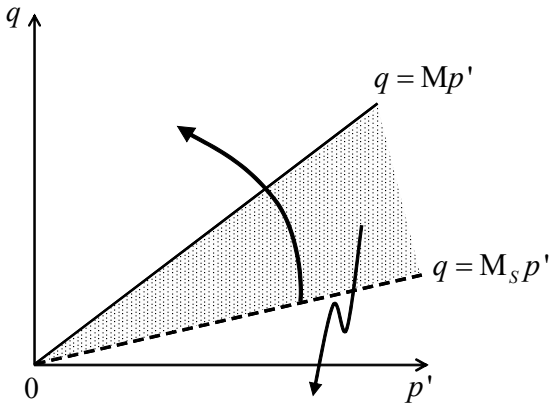

Softening with plastic volume compression

(b)

Fig. 4.4 Movement of M_s .

Using the model presented in this chapter, let us now try to compute the mechanical behavior exhibited by this material in a drained triaxial compression test. The calculated results are shown in Figs. 4.5(a) and 4.5(b). The figures show that this soil material initially displays hardening together with elastic compression, but

that once the stress state crosses the line $q = \mathrm{M}p'$, beyond which

$$\mathrm{M}p' < q < \mathrm{M}_s p' \tag{4.31}$$

there is a resulting switch in behavior to hardening together with plastic expansion. However, as plastic deformation proceeds further, there is a progressive loss in overconsolidation ($R \to 1$) and a consequent decrease in M_s (Fig. 4.4(a)), until eventually

$$\mathrm{M}_s p' < q \tag{4.32}$$

at which stage the clay undergoes another reversal in behavior, to softening together with plastic expansion. Finally, the material then reaches the state of normally consolidated clay,

$$\mathrm{M}_s = \mathrm{M} \tag{4.33}$$

Here, the stress state also comes down from its previous higher position to overlie line $q = \mathrm{M}p'$, where it settles into a so-called residual state, with no volumetric change and an indefinite shear strain. Fig 4.5(a) also includes an indication of the variation in value of $1/R$ (overconsolidation ratio) in relation to shear strain deformation. In this way, it has now become possible to understand the mechanical behavior of an overconsolidated clay soil in all of its aspects.

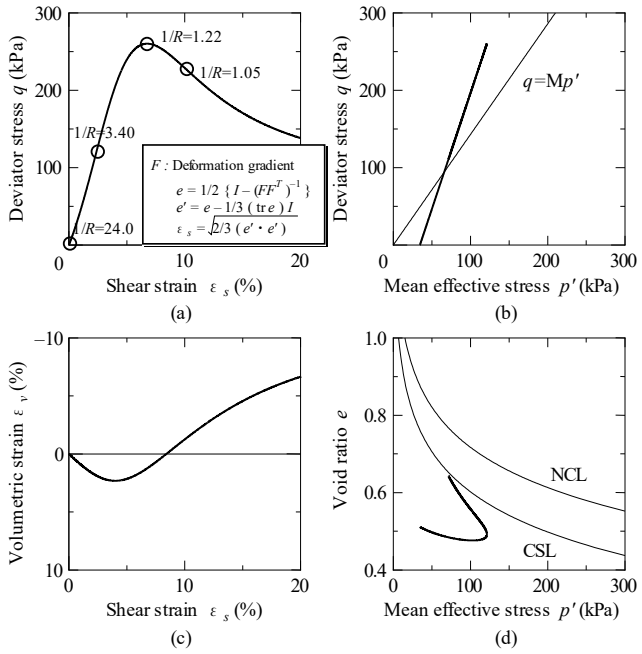

Fig. 4.5 Model responses of a drained triaxial compression test on a fully remolded but heavily overconsolidated clay (initial OCR=24).

Normally consolidated, but highly structured clay

Next let us consider the case of a normally consolidated but highly structured clay, which is of interest for its so-called "sensitivity ratio." Let us assume that the elasto-plastic and evolution parameters for this material are exactly the same as for the overconsolidated clay just discussed. Furthermore, the initial void ratio is also the same. However, the other initial conditions for the material will be different. For the purposes of this example, we may give them as:

Table 4.3 Initial conditions.

Initial conditions	
Initial void ratio e_0	0.51
Initial mean effective stress p_0' (kPa)	1357
Initial value of R^* (R^*_0)	0.2
Initial overconsolidation ratio $1/R_0$	1.0

As $R_0 = 1$ (normally consolidated state), the subloading and superloading yield surfaces can already be taken as falling together, but the Cam-Clay yield surface, for which $R^*_0 = 0.2$, will be situated inside the superloading yield surface, with a similarity ratio of 5. The current stress is, of course, on the superloading surface.

Let us use the model presented in this chapter to compute the mechanical behavior exhibited by this material, this time in an undrained triaxial compression test. The results can be seen in Figs. 4.6(a) and 4.6(b). In Fig. 4.6(b), the R^* values show the state of structural decay in relation to the evolution of plastic deformation. At the initial stage of shear deformation, the material shows plastic compression accompanied by hardening.

This is because the initial stress state is of the kind

$$q < \mathrm{M}_s p' < \mathrm{M}p'. \tag{4.34}$$

However, the stress state later changes to

$$\mathrm{M}_s p' < q < \mathrm{M}p' \tag{4.35}$$

and the material accordingly displays a behavior of plastic compression accompanied by softening. But as the plastic deformation evolves still further, bringing further decay in the soil structure ($R^* \to 1$), M_s steadily increases (Fig. 4.4(b)) until eventually

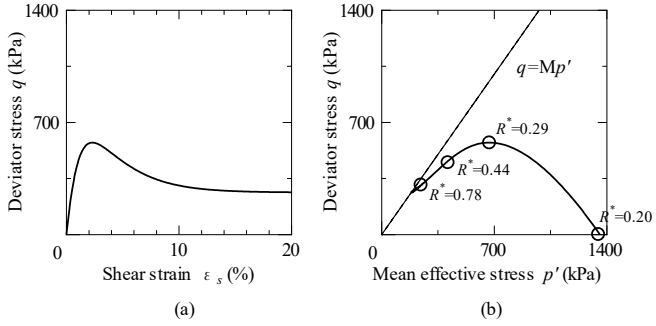

Fig. 4.6 Model responses of an undrained triaxial compression test on a highly structured normally consolidated clay (e_0 =0.51).

$$\mathrm{M}_s = \mathrm{M} \tag{4.36}$$

at which point the stress also comes to settle into a steady state on line $q = \mathrm{M}p'$, showing no more change in the excess pore water pressure and an indefinite shear strain.

Let us now consider the case of an undrained triaxial

compression test on a normally consolidated soil, obtained by thoroughly remolding the same clay material so as to return it to the same void ratio as in the above example. Since we are dealing with the same clay, the elasto-plastic parameter will be the same as before. (The evolution parameter is no longer needed.) However, the initial conditions of the material are different. They can be given as:

Table 4.4 Initial conditions.

Initial conditions	
Initial void ratio e_0	0.51
Initial mean effective stress p_0' (kPa)	395.2
Initial value of R^* (R^*_0)	1.0
Initial overconsolidation ratio $1/R_0$	1.0

The results of an undrained triaxial compression test performed on this clay material are computed in Figs. 4.7(a) and 4.7(b). Of course, these Fig. 4.7 responses are precisely the ones indicated by the Cam-Clay model. The result of superimposing Fig. 4.7 on Fig. 4.6 is shown in Fig. 4.8. Taking the sensitivity ratio as the ratio between the peak strength and the strength of the remolded clay, it can further be seen that this clay had a sensitivity ratio of about 2. In ways like this, it can be appreciated that the meaning

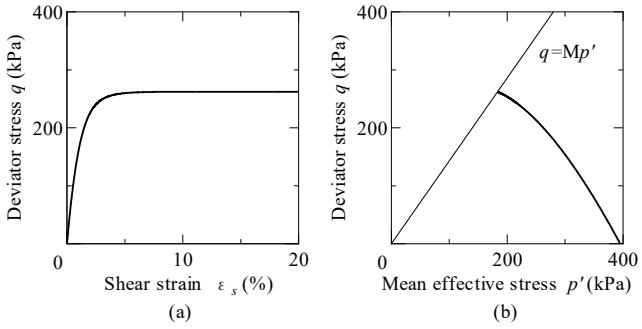

Fig. 4.7 Model responses of an undrained triaxial compression test on a fully remolded normally consolidated clay with e_0 =0.51.

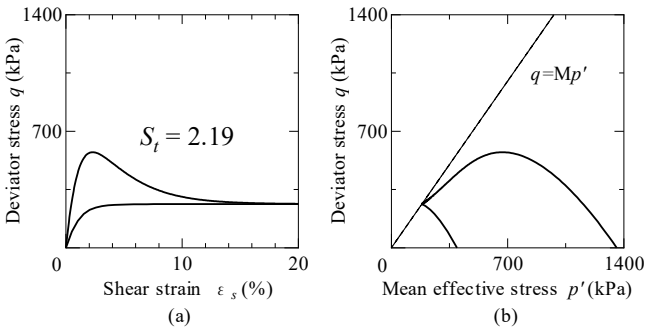

Fig. 4.8 Sensitivity ratio.

of classical soil mechanics concepts such as “soil disturbance” and “sensitivity ratio” in terms of actual elasto-plastic mechanics is steadily becoming clearer.

5 THE DIFFERENCE BETWEEN CLAY AND SAND

5.1 *Changes of overconsolidation and structure state*

In Chapter 4 it was mentioned that a soil always exists in one of the following four states:

① overconsolidated structured state $(0<R<1,\ 0<R^*<1)$
② normally consolidated structured state $(R=1,\ 0<R^*<1)$
③ overconsolidated non-structured state $(0<R<1,\ R^*=1)$
④ normally consolidated non-structured state $(R=1,\ R^*=1)$

Soils in states ①, ② and ③ pass through a process of plastic deformation before ultimately arriving at state ④.

Naturally sedimented soils, whether clays or sands, can generally be considered as occurring in state ①, that is to say, they have well developed structures and, while there may be differences of degree, basically exist in an overconsolidated state. In the process of plastic deformation by which soils of this kind evolve toward state ④, the two following routes may roughly be distinguished:

Route C: ① overconsolidated + structured → ② normally consolidated + structured → ④ normally consolidated + non-structured

Route S: ① overconsolidated + structured → ③ overconsolidated + non-structured → ④ normally consolidated + non-structured

In soils that move along route C, plastic deformation evolves in such a way that there is a more rapid progress in the loss of overconsolidation than in the decay of soil structure. Also, for the breakdown of structure, a greater plastic deformation is required. Conversely, in soils that move along route S, the soil structure collapses as soon as plastic deformation begins to develop, while the loss of overconsolidation makes no progress at all.

Anticipating the conclusion of an argument to come, when a soil undergoes loading, a typical clay soil will follow route C, whereas a typical sand soil will follow route S. For this, see Fig. 5.1.

The reasoning from which this Fig. 5.1 conclusion is drawn will be made clear in the latter half of this chapter and in Chapters 6 and 7 to follow, but first let us explain the details of the conclusion itself, in five principal points.

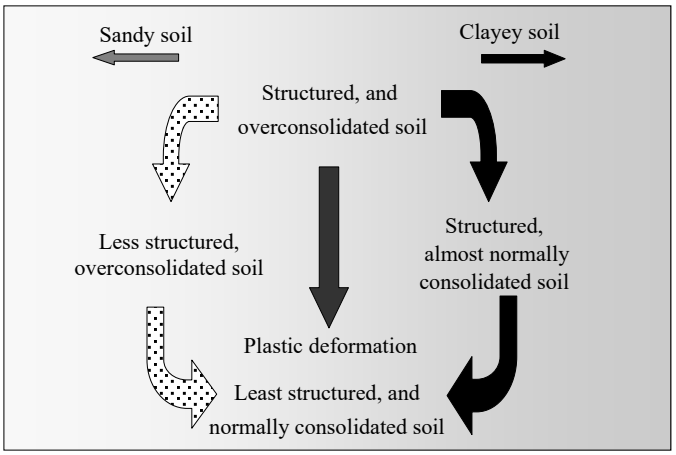

Fig. 5.1 Route S and route C (after Asaoka et. al., 2002).

(1) A major claim made in this paper is that the ways a soil has of changing its state with regard to overconsolidation and soil structure, and more particularly the different ways different soils proceed with their changes of state, provide us with a means for distinguishing between sand and clay. Suppose we are given a

sample of soil, and also told that it is currently in state ①. Since that information alone is not enough to tell us how its state will change under loading, we are not yet in a position to tell whether the soil is a sand or a clay. A similar point can be made regarding a soil in state ④. Once we have been told that its present state is ④, there is no further need to draw the distinction between sand and clay, because, either way, no amount of additional loading will bring about any further change of state. Be it sand or clay, when a soil has reached state ④ its elasto-plastic response can be described in terms of the Cam-Clay model, so that there is no difference as far as that is concerned. However, there *are* differences regarding the elasto-plastic parameter values. For example, clay is soft and sand is hard. Differences of that sort still remain.

(2) In the model presented above, involving the introduction of super/subloading yield surfaces, the degradation rate of overconsolidation is dominated by a parameter m in the evolution law for R, while the structure decay (or collapse) rate is dominated by the parameters a, b and c (of which b and c generally have a value 1) in the evolution law for R^*. Depending on the value differences on these parameters, the model is therefore capable of describing a development either on route C or on route S. In other words, there is no need to provide separate models for clay and for sand. In fact:

(3) It is not impossible to conceive of a soil in which loss of overconsolidation and decay of structure might proceed together at the same rate, with the result that the state of the soil would change directly from ① to ④, without passing through either state ② or state ③. A clayey sand or a sandy clay might perhaps fit this description. That is why the adjective 'typical' was attached to "clay" and "sand" in the above conclusion statement. It is both difficult and unnecessary to draw an absolutely precise dividing line between clay and sand.

(4) Let us next think back to the two examples calculated in Chapter 4. The first calculation was for a remolded, but overconsolidated clay. The soil material was obtained by unloading a soil in state ④ so as to return it to state ③. (It should be noted with regard to route C above that no claim was made that a clay soil can never exist in state ③. One reason for adding the restriction "when a soil undergoes loading" to the conclusion statement was to allow for such special cases.) Now as this material was converted from state ③ to state ④ in the course of the drained shear test, it might seem possible, in terms of the routes as summarized above, to identify it as a sand. But as the rate of structure decay or collapse was not measured in the test, that is to say, no observation was made of the route of change from state ①, we cannot judge on the basis of this test alone whether the soil in question was a sand or a clay. The same point can be made about the second calculation, concerning the results of an undrained shear test for a normally consolidated but highly structured clay. In this case, too, there was no observation of the route of change from state ①, and therefore there can be no way of judging from the test alone whether the material was a sand or a clay.

(5) Since any soil in state ④ will shift into state ③ under unloading, an occurrence in state ③ is clearly conceivable for both sands and clays. The problem here is rather state ②. Structure cannot be recovered (revived) by unloading. Hypothesizing from the above conclusion only, therefore, it might seem impossible for a typical sand to occur in state ②. But that would be a false conclusion. If a loose sand is formed by a "water sedimentation method" in a cylinder, it will be at a consolidation level very close to normal, and also possess a high degree of structure. If this sand then shears repeatedly at a very low stress level, it will immediately enter into state ①. In other words, this sand has been in state ② prior to arriving in state ①. The repeated shearing is equivalent to a repeated succession of loadings and unloadings, but since there is no chance in the loading phases for any loss of overconsolidation to get underway, the increases in overconsolidation that occur in the unloading phases can go on accumulating with each repetition cycle. Meanwhile, as the shearing takes place at such a low stress level, the structure remains intact. In this way, state ① conditions are generated in this sand, which was originally in state ②. If the same material is then subjected to loading only (without any unloading), it follows a route of ① → ③ → ④. More explanations will be needed concerning this particular topic, to which we shall be returning in Chapter 6.

5.2 *Medium dense sand and structured overconsolidated clay*

In this section we consider the undrained shear behavior of two soils, one of them a sand and the other one a clay.

Undrained shear behavior of medium dense sand

The elasto-plastic and evolution parameters for the medium dense sand on which the following calculation is based are set out in Table 5.1. Using these evolution law parameters, it can be seen that while a rapid collapse in structure occurs per unit plastic deformation, there is next to no loss in overconsolidation. This will also be evident from the calculation. The parameters in Table 5.1 are thus indicative of a typical sand.

The initial conditions of this sand, prior to its investigation in an undrained triaxial compression test, are shown in Table 5.2. The overconsolidation ratio, $1/R_0$, is 3.5, the state of the structure $R_0^* = 0.26$.

Table 5.1 Material constants.

Elasto-plastic parameters	
Compression index $\tilde{\lambda}$	0.05
Swelling index $\tilde{\kappa}$	0.012
Critical state constant M	1.00
Void ratio at $p' = 98.1$kPa on NCL N	0.97
Poisson's ratio ν	0.3
Evolution parameters	
Degradation parameter of overconsolidation state m	0.08
Degradation parameter of structure a ($b = c = 1.0$)	2.3

Table 5.2 Initial conditions.

Initial conditions	
Initial void ratio e_0	0.92
Initial mean effective stress p_0' (kPa)	294.3
Initial value of R^* (R^*_0)	0.26
Initial overconsolidation ratio $1/R_0$	3.5

The grounds for calling this material "a medium dense sand" will be explained presently, in Chapter 6.

Figs. 5.2(a), 5.2(b), 5.2(c) and 5.2(d) show calculated results obtained from the Super/subloading Yield Surface model, for the response behaviors of the material during the test. From Figs. 5.2(c) and 5.2(d), showing the changes in R and R^*, it is clear

that this is a typical sand.

The change in M_s in the course of the test is shown in Fig. 5.3. Given that initially $M_s < M$, at a point where the stress state reaches

$$M_s p' < q < Mp', \tag{5.1}$$

the sand exhibits a softening behavior, together with plastic compression. However, the breakdown of the soil structure is then rapid, and as M_s very quickly increases straight up to $M_s > M$, the stress reaches a state

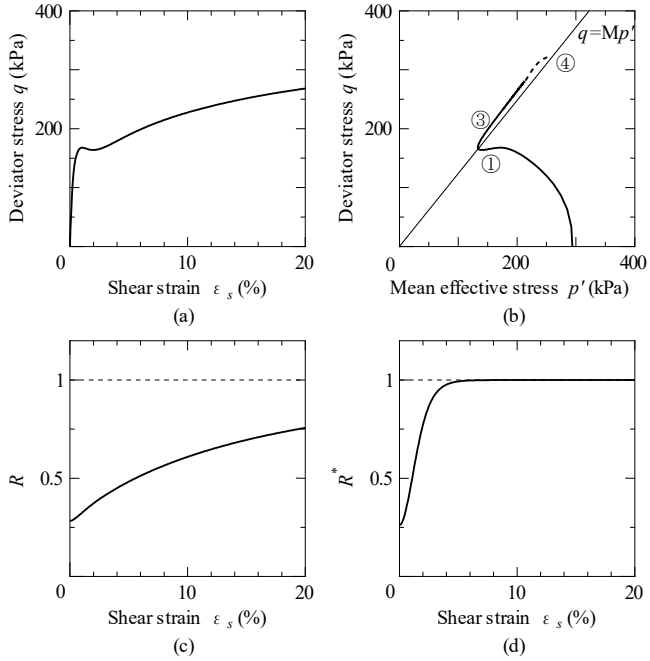

Fig. 5.2 Model responses of the undrained triaxial compression test on a medium dense sand.

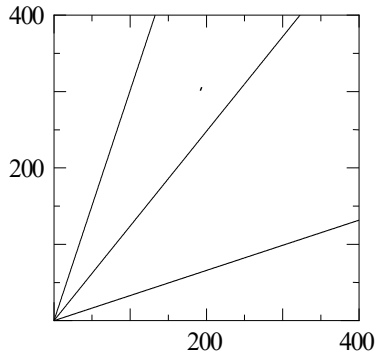

Fig. 5.3 Movement of M_s.

$$Mp' < q < M_s p', \tag{5.2}$$

where the behavior switches to hardening, together with plastic expansion. If the plastic deformation is allowed to proceed further, M_s will of course settle at $M_s = M$, and the material will ultimately attain a steady state on $q = Mp'$. In other words, stress, volume and excess pore water pressure will all cease to vary in response to the ongoing development of shear strain on $q = Mp'$.

Undrained shear behavior of structured overconsolidated clay

The elasto-plastic and evolution parameters for the clay on which the calculation is performed are given in Table 5.3. Using these evolution parameters, while a rapid loss in overconsolidation per unit plastic deformation can be seen, there is virtually no decay in soil structure. The same is also evident from the calculation. Thus, the parameters in Table 5.3 are indicative of a typical clay.

The initial conditions of this clay material, prior to subjecting it to an undrained triaxial compression test, are as shown in Table 5.4. The overconsolidation ratio, $1/R_0$, is 4.5, and the state of the structure is $R_0^* = 0.46$.

Figs. 5.4(a), 5.4(b), 5.4(c) and 5.4(d) show calculated results, obtained using the Super/subloading Yield Surface model, for the response behaviors of the material during the compression test. From Figs. 5.4(c) and 5.4(d), which show the changes in R and R^*, it is clear that this is a typical clay.

The changes in M_s during the test are shown in Fig. 5.5. Given that initially $M_s > M$, even at a point where

$$Mp' < q < M_s p' \tag{5.3}$$

the clay will still go on exhibiting hardening, in spite of the plastic expansion that accompanies this. However, the loss of overconsolidation in the clay then proceeds rapidly, and as M_s steeply decreases to a level where $M > M_s$, the stress eventually comes to a state

Table 5.3 Material constants.

Elasto-plastic parameters	
Compression index $\tilde{\lambda}$	0.25
Swelling index $\tilde{\kappa}$	0.045
Critical state constant M	1.25
Void ratio at $p' = 98.1$kPa on NCL N	1.73
Poisson's ratio ν	0.3
Evolution parameters	
Degradation parameter of overconsolidation state m	10.0
Degradation parameter of structure a ($b = c = 1.0$)	0.5

Table 5.4 Initial conditions.

Initial conditions	
Initial void ratio e_0	1.58
Initial mean effective stress p_0' (kPa)	98.1
Initial value of R^* (R^*_0)	0.46
Initial overconsolidation ratio $1/R_0$	4.5

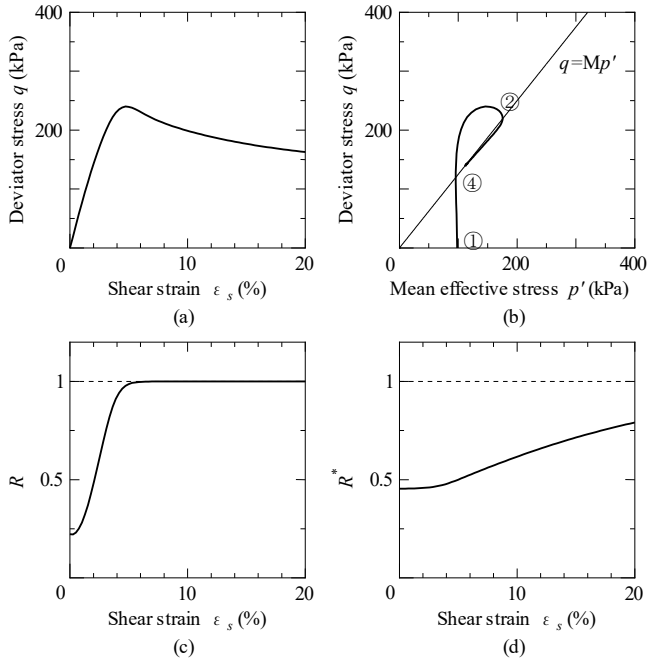

Fig. 5.4 Model responses of the undrained triaxial compression test on a structured heavily overconsolidated clay.

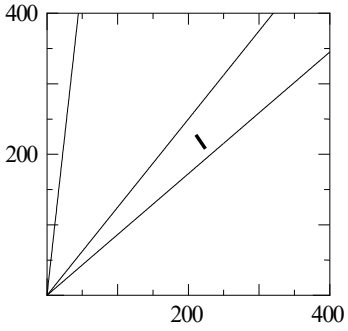

Fig. 5.5 Movement of M_s .

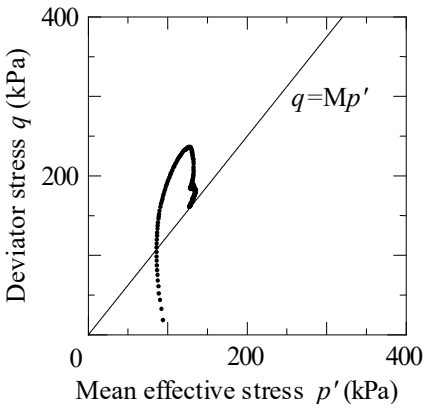

Fig. 5.6 "Rewinding" observed in laboratory (after Asaoka A., 2000).

$$M_s p' < q < M p' \qquad (5.4)$$

where the behavior switches to softening, together with plastic compression. If the plastic deformation is allowed to proceed further, M_s will of course settle at $M_s = M$, and the material will attain a steady state of $q = Mp'$. In other words, stress, volume and excess pore pressure will all cease to vary in response to the ongoing development of shear strain at $q = Mp'$.

Another important point is that because of the residual structure that remains even after the loss of overconsolidation, the clay material in the latter half of the test displays a softening behavior, together with plastic compression. This is called "rewinding" (Tatsuoka F. and Kohata Y., 1995). An example of an experiment in which rewinding is observed is given in Fig. 5.6.

6. COMPACTION/DENSIFICATION OF SAND

As clearly represented in Equation (4.8) in Chapter 4

$$\dot{\varepsilon}_v^p = \dot{f} + \frac{\tilde{\lambda} - \tilde{\kappa}}{1 + e_0}\left(\frac{\dot{R}^*}{R^*} - \frac{\dot{R}}{R}\right) \qquad (6.1)\ (\text{bis } (4.8))$$

a decay or collapse of the soil structure ($\dot{R}^* > 0$), whether in clay or in sand, is conducive to plastic volume compression. However, in the case of sand, while the structure is quick to collapse, loss of overconsolidation hardly makes any progress at all. What results from the combination of these two causes is the classical sand phenomenon of large volume compression under repeated loading, or in other words, the "compaction" of sand.

6.1 *Densification of loose sand under repeated drained shear stress application*

As the phenomenon of the densification of drained loose sand under repeated shear stress is a complicated thing to grasp, let us explain it here with the aid of numerically computed examples obtained from the Super/subloading Yield Surface model.

The sand used is the same as in Table 5.1 in Chapter 5. But since we are now taking account of the evolution law for anisotropy, it is necessary to present the elasto-plastic and evolution parameters again, in a new Table 6.1. The details concerning anisotropy are given in APPENDIX A, but for the understanding of the present chapter they are not of great importance. It will be recalled that the sand in Chapter 5 was initially in a medium dense state (①), and that the investigation concerned the undrained application of shear stress. The sand under consideration here is the same as in Chapter 5, but its initial state is different, in that before undergoing repeated shear stress under drained conditions it is as indicated in Table 6.2. The significance of this is that, in the terms of Chapter 5, the sand in the present test begins in the "normally consolidated structured state" ②. It will be easy to see that the values in Table 6.2 correspond to the classic initial conditions for loose sand.

A triaxial repeated compression/extension test was performed on this material, under drained conditions, at a constant lateral pressure $\sigma_2 = \sigma_3$ and a relatively low shear stress amplitude q. The deviator stress amplitude was 60kPa. The elasto-plastic response to this, according to the Super/subloading Yield Surface model, can be seen in Figs. 6.1(a) to 6.1(d). Fig. 6.1(a) shows the effective stress path for the test, Fig. 6.1(c) the nature of the volume compression undergone by the sand specimen under the repeated shear stress, and Figs. 6.1(b) and 6.1(d) the variations of R and R^* under the same repeated shear stress, taking shear

strain ε_s, as the horizontal axis scale.

Table 6.1 Material constants.

Elasto-plastic parameters	
Compression index $\tilde{\lambda}$	0.05
Swelling index $\tilde{\kappa}$	0.012
Critical state constant M	1.00
Void ratio at $p' = 98.1$kPa on NCL N	0.97
Poisson's ratio ν	0.3
Evolution parameters	
Degradation parameter of overconsolidation state m	0.08
Degradation parameter of structure a ($b = c = 1.0$)	2.3
Evolution parameter of $\boldsymbol{\beta}$ b_r (see APPENDIX A)	200.0
Limit of rotation m_b (see APPENDIX A)	0.7

Table 6.2 Initial conditions.

Initial conditions	
Initial void ratio e_0	1.09
Initial mean effective stress p_0' (kPa)	294.3
Initial value of R^* (R^*_0)	0.01
Initial overconsolidation ratio $1/R_0$	1.00
Initial anisotropy $\zeta_0 = \sqrt{3/2\boldsymbol{\beta}_0 \cdot \boldsymbol{\beta}_0}$ (see APPENDIX A)	0.00

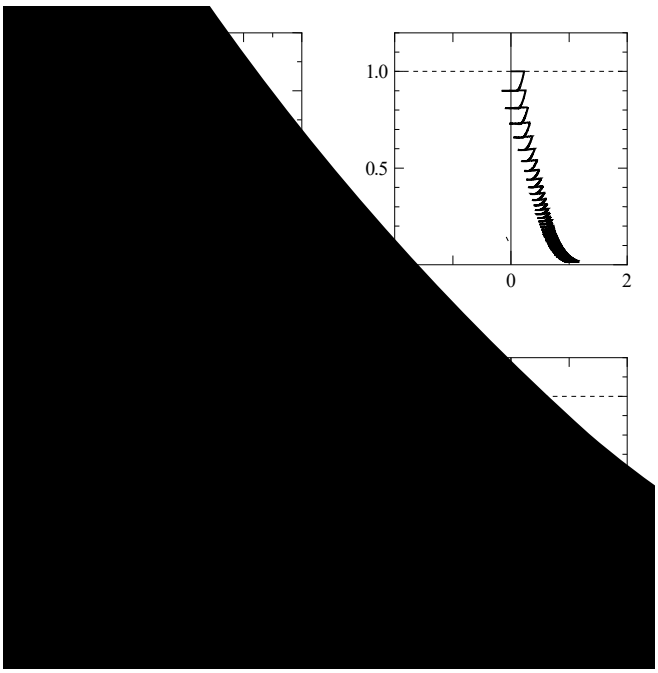

Fig. 6.1 Overall behavior of "compaction" of a loose sand under repeated shear stress application.

Fig. 6.1(c) shows the extreme degree of volume compression undergone by this sand. The two lines drawn in the figure represent the normal consolidation and critical state lines from the modified Cam-Clay model, using the elasto-plastic parameters for this sand: $\tilde{\lambda}$, $\tilde{\kappa}$, N, Γ $(= \mathrm{N} - (\tilde{\lambda} - \tilde{\kappa})\ln 2)$. Looking at these results, it can be seen that the soil compression theory of classical soil mechanics, based on the e – $\log p'$ relation and dilatancy $\mathrm{N} - \Gamma \propto \tilde{\lambda} - \tilde{\kappa}$, is powerless to deal with the compaction/densification of sand.

Fig. 6.2 is an enlargement of Fig. 6.1(c). This illustrates vividly the impossibility of trying to compact loose sand under monotonic loading. At a pressure above 2000kPa, the sand particles are finally crushed to destruction.

Fig. 6.2 is also important for showing that no concept of "maximal past loading" is needed for a definition of the overconsolidation ratio. Let us next look more closely at that aspect.

The changes in the void ratio and in R and R^* are shown enlarged in Figs. 6.3(a) to 6.3(d), for the third cycle of the repeated shear stress. Although these figures are simply a blowing up of Figs. 6.1(a) to 6.1(d), the larger scale does aid comprehension. How large a compression occurs in the loading stages (a)–(b) and (c)–(d) can be appreciated from Equation (6.1) as well as from the increase of R^* in Fig. 6.3(d). However, the loss of overconsolidation accompanying the loading process is extremely small (Fig. 6.3(c)). By contrast, the increase in overconsolidation that occurs in the unloading stages (b)–(c) and (d)–(e) of the repeated loading is highly conspicuous. In this way, while the structure is destroyed early on by the repeated loading, overconsolidation goes on accumulating, leading to a diminution in R. The same story can be gleaned from Figs. 6.1(b) and 6.1(d).

The fact that there is so little loss of overconsolidation in the loading stage implies that the increases in size of the subloading and superloading yield surfaces under loading must be comparable, so that there is almost no change in the ratio between them. However, whereas the superloading surface, after increasing in size under loading, hardly alters its position in response to the subsequent unloading, the subloading surface follows the response of diminution in the current stress and reduces its shape in turn. Since the overconsolidation ratio is determined as the size ratio between the superloading and subloading yield surfaces, and since every repeated cycle of loading means that the superloading surface will increase in size while the size of the subloading surface will remain tied to the position of current stress, the overconsolidation ratio, in a case of

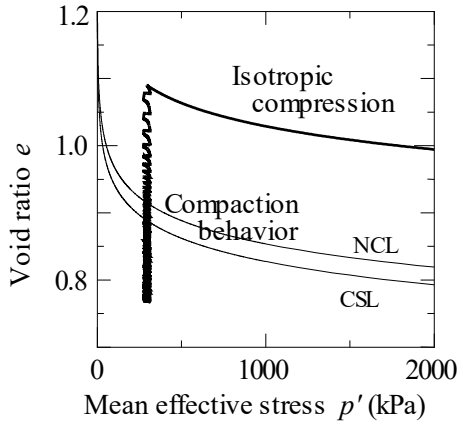

Fig 6.2 "Compaction" and isotropic compression of a loose sand.

sand like this, will go on and on rising.

In the contrary case of clay, it is the loss of overconsolidation under loading that is conspicuous, so that the superloading and subloading yield surfaces very soon come to fall together. For this reason, there is no rapid accumulation of overconsolidation for clay under repeated loading, as there is for sand.

6.2 *Variation in shear behavior of sand with decrease in void ratio and increase in overconsolidation*

Let us now return to Fig. 6.1(b), relabeled here as Fig. 6.4. Fig. 6.4 shows five states of the sand, [1]-[5], as indicated by void ratio e, R and R^*, obtained in the course of compaction at five stages of repeated loading, beginning at initial state [1]. (n indicates the number of each shear cycle.) Looking at the five states, we recognize them as:

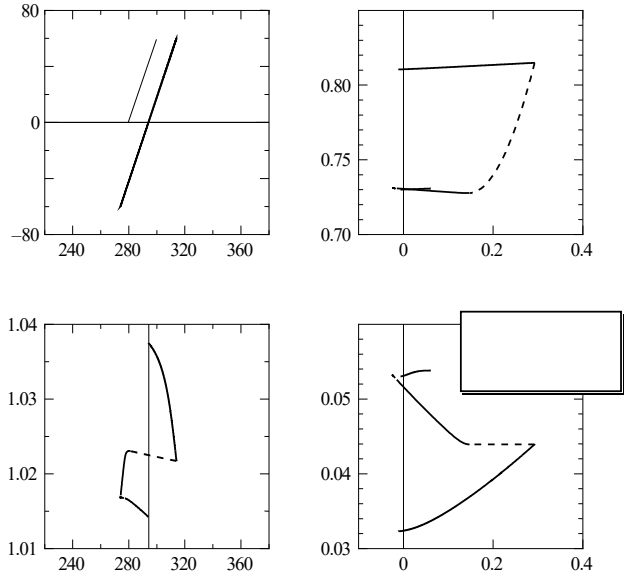

Fig. 6.3 Detailed behavior during “compaction” procedure.

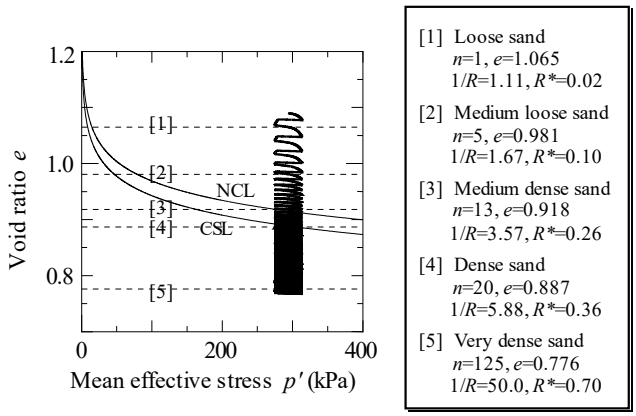

Fig. 6.4 Five different sand specimens as distinguished by “compaction” procedure.
[1] : loose sand
[2] : medium loose sand
[3] : medium dense sand
[4] : dense sand
[5] : very dense sand

These five states of sand are all occur in the same sand material. That is to say, the five states [1]-[5]of this sand have all been generated spontaneously by assigning the elasto-plastic and evolution parameters of Table 6.1 to the Super/subloading Yield Surface model and then computing the responses to repeated shear stresses on the basis of the initial conditions shown in Table 6.2. It is to be stressed that they are not simply five states that the author invented arbitrarily and assigned to suit his own needs.

Let us next use the model to compute how these five different kinds of sand will respond to undrained and drained triaxial tests. Figs. 6.5(a) to 6.5(e) show the elasto-plastic responses obtained from the Super/subloading Yield Surface model for an undrained triaxial compression test with constant lateral cell pressure. All of these sand responses are derived from the same elasto-plastic and evolution parameters (Table 6.1). Moreover, as was stressed above, the initial conditions of the specimen in each of the five cases were obtained by successive calculations from the original loose state of the same sand. It will therefore be evident that the undrained shear responses in Fig. 6.5 are all the results of a variation of void ratio, overconsolidation ratio and degree of structure in the same sand specimen.

What happens when the test is actually performed in a laboratory is shown in Figs. 6.6(a) to 6.6(c). These test results come from work by Nakano and Nakai (2003a). The physical specifications of the sand used are given in Table 6.3, and the grain size distribution in Fig. 6.7. It is important to notice the good qualitative and quantitative match between Figs. 6.5 and 6.6. The qualitative tendencies of the test findings in Fig. 6.6 have long been familiar in experimental soil mechanics. Experiments by Castro (1969) are referred to in the REFERENCES at the end.

As was mentioned in the INTRODUCTION to this paper, there have been attempts by some researchers and research groups to explain the experimental findings of Fig. 6.6 by setting up separate models, or separate elasto-plastic parameters. It was also remarked that such approaches are hard to accept as constitutive formula research. This is because of the shared shortcoming found in them all, of offering no concepts for “structure” or a “superloading yield surface.”

Another common shortcoming of all these researchers and groups who construct separate models or parameters is that they have virtually nothing to say on the subject of the drained shearing of sand. This is because, in drained conditions, both loose and dense sand undergo very noticeable changes in sedimentation through shearing.

The responses calculated in accordance with the Super/subloading Yield Surface model for the five kinds of sand in triaxial drained compression tests under constant cell pressure (results as in Fig. 6.4) are set out in Fig. 6.8. The qualitative tendencies appearing in this figure are already well-known in experimental soil mechanics.

Figs. 6.5(c) and 6.5(e), and Figs. 6.8(c) and 6.8(f), show the variations in R and R^* in relation to the development of axial strain. We can confirm, yet again, that the decay of structure is rapid in sand, while the loss of overconsolidation is very slow.

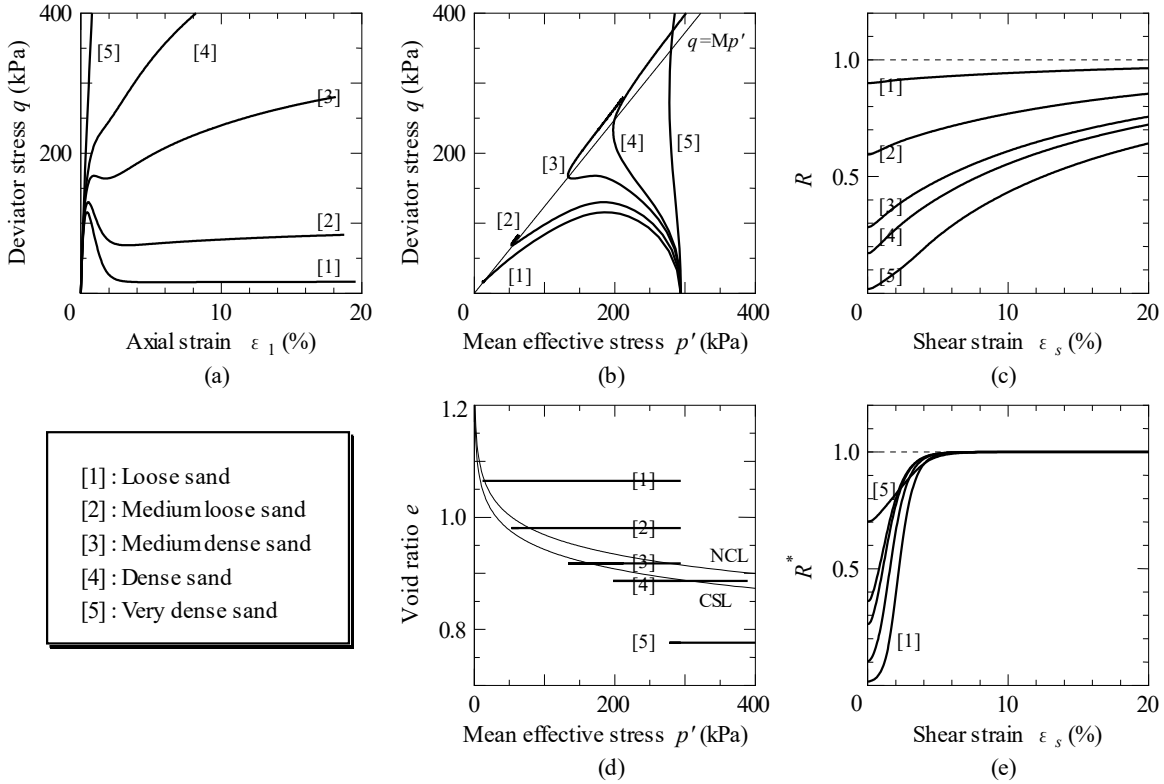

Fig. 6.5 Undrained triaxial compression behaviors of the five sand specimens of different densities.

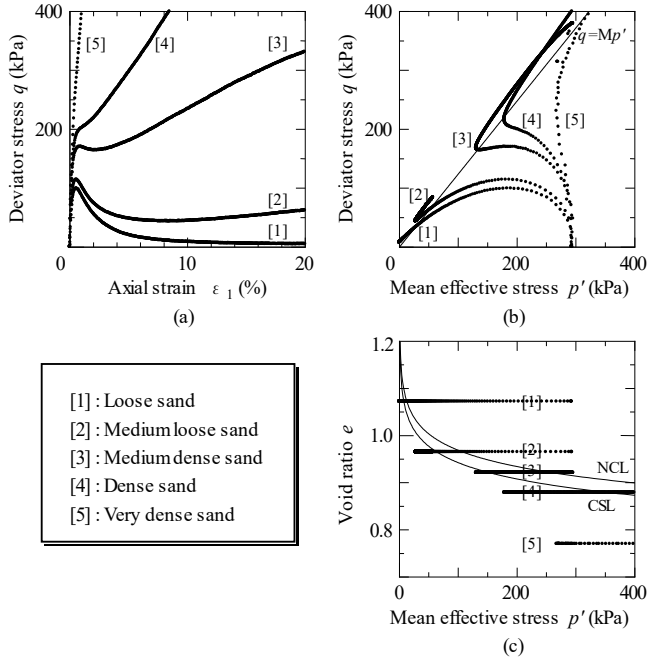

Fig. 6.6 Experimental results corresponding to Fig. 6.5 (after Nakano and Nakai, 2003a).

Table 6.3 Physical properties of the sand tested in laboratory.

Specific gravity of grains G_s	2.65
Maximum void ratio e_{max}	1.06
Minimum void ratio e_{min}	0.64

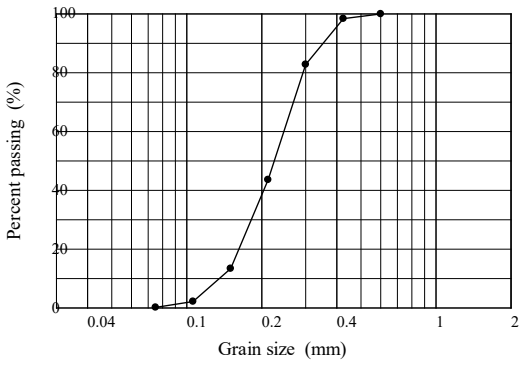

Fig. 6.7 Grain size distribution.

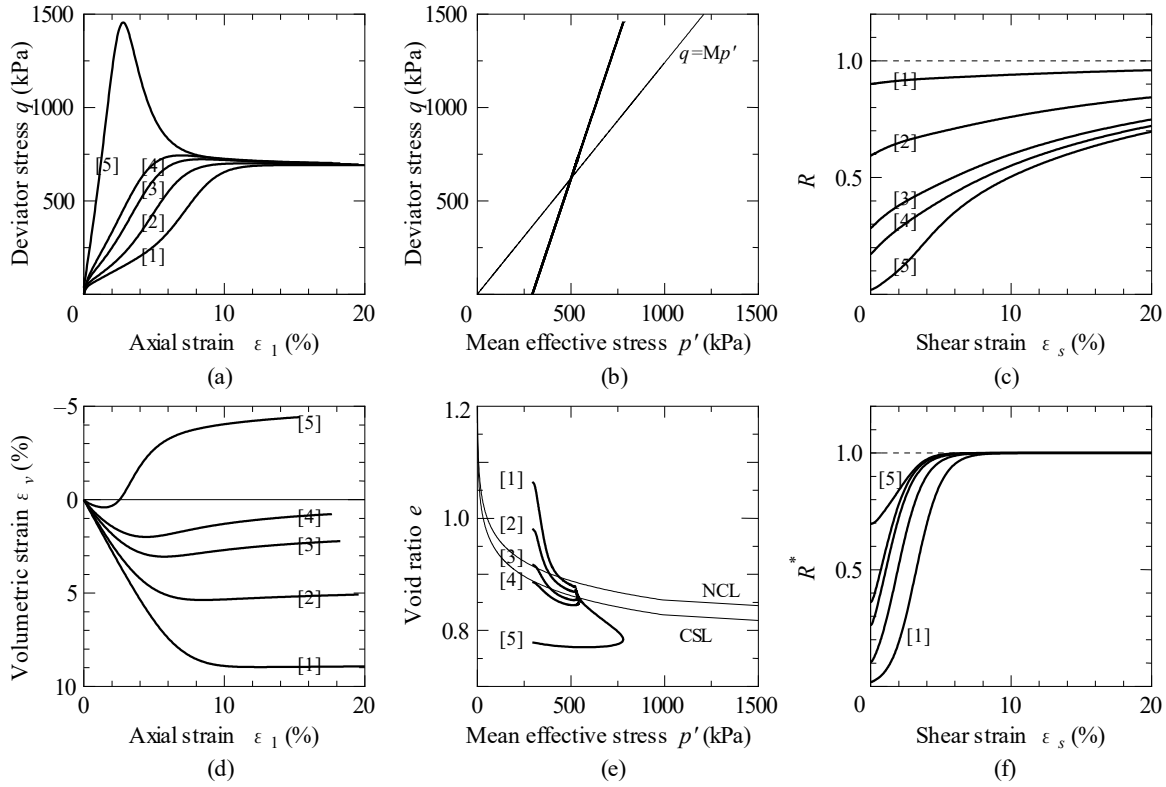

Fig. 6.8 Drained triaxial compression behaviors of the five sand specimens of different densities.

Concerning the characteristics of shear behavior in sand, it is difficult to comment in any greater detail without bringing in some discussion of

① grain size distribution, and

② anisotropy.

In the case of ①, if the grain size distribution is not gently graded but abrupt in contour, it will be difficult for the sand to exhibit a medium loose or medium dense state, for the grain size distribution is closely related to the evolution parameters for the structure and overconsolidation. As for ②, sand is very conspicuous for induced anisotropy, i.e. changes in anisotropy co-occurring with changes in current stress states. This induced anisotropy has a considerable effect on shear behavior characteristics, especially for a sand existing in a loose condition.

There are various further things we might say about these topics ① and ②. But as they lie too far out outside the main scope of our paper, they are best omitted.

7. "SECONDARY CONSOLIDATION" OF STRUCTURED CLAY

As a phenomenon, the secondary consolidation of clay was long regarded as being due to the intrinsic viscosity characteristic of the clay soil skeleton itself, and from Suklje to the present day, visco-plasticity theory has been taken as the theoretical statement of this outlook. The main steps of this theory, if we sum them up, are that, first, "clay skeleton elements are intrinsic to a visco-plastic material," and second, "if the question of the clay mass is accordingly approached as a boundary value problem, the creep - i.e. secondary consolidation/delayed compression - can be "calculated." However, seeing that the "viscosity" of the soil skeleton elements and the "creep" of the clay mass are originally two synonyms for the same concept, the fact that one can be "calculated" from the other is trivial. For all the theory says is that creep (secondary consolidation) occurs in a clay ground as a result of creep (secondary consolidation) occurring in the clay of which that ground is composed." What is not explained by this kind of theorizing is the reason why secondary consolidation should occur in the first place.

Let us think back to the investigative attitudes with which our predecessors in soil mechanics approached their research. They were well aware that the visco-elasticity theory could deliver the same solutions as Terzaghi's one-dimensional consolidation settlement, but nonetheless continued to take Terzaghi's consolidation theory, grounded in the concept of "effective stress," as their theoretical basis in soil mechanics. This was because Terzaghi's account, with its layered structural presentation of concept and theory, was able to offer explanations for why consolidation settlement occurred.

What is needed in soil mechanics is a theory that can answer questions of the sort: "What mechanisms are secondary consolidation, or delayed compression, caused by?", "What are the conditions in which they do not occur?", and "Why does secondary consolidation occur in clay, but not in sand?" If it is granted that the present paper has given "a successful description of the difference between sand and clay," then the Super/subloading Yield Surface model, by means of which this has been achieved, must also be the source from which this theory can best be deduced (Asaoka et al., 2000b).

7.1 *Terminology*

In this chapter we shall be investigating the progressive consolidation phenomenon that appears in a structured clay as its structure decays. No term yet exists in soil mechanics to express this "progressive consolidation with decay of structure." Terms existing hitherto, such as "secondary consolidation" and "delayed compression," are the names given to particular phenomena displayed in extreme cases of "progressive consolidation with decay of structure." Certainly, in extreme cases it may take an inordinate length of time for progressive consolidation of this kind to arrive at its end stage, and large-scale occurrences of delayed compression are always possible. But it is not the case that all instances of "progressive consolidation with decay of structure" require this inordinate length of time, or result in delayed compression on a large scale. Therefore it is not appropriate to assign automatic equivalence labels like "secondary consolidation" etc. to this term.

It is difficult to give strict mechanical definitions for terms like "secondary consolidation" and "delayed compression," the uses of which have been based on experience. Nor, mechanically speaking, is there any need to. It will be sufficient if we are able to analyze and investigate "progressive consolidation with decay of structure" as a phenomenon. For reasons of this kind, when we have occasion to use these terms "secondary consolidation" and "delayed compression" in what follows, we shall always put them in quotation marks.

7.2 *A possible mechanism of "secondary consolidation" and/or "delayed compression"*

This section opens with an explanation of how, in a highly structured clay, a progressive consolidation with decay of structure may lead to plastic compression accompanied by softening, which then considerably delays consolidation/ compression. The co-occurrence of softening with compression may be an "extreme case" among the mechanical behaviors of clay, but sometimes the consideration of "extreme cases" proves helpful for the thorough understanding of a mechanism.

The argument in both this section and the one that follows will confine itself to conditions of one-dimensional consolidation. Also, in order to keep things easily understandable, the explanation will at times make use of one-dimensional mechanics (Figs. 7.2 and 7.3). It may be that these expedients lead to further "extreme cases," for in real problems of engineering conditions of one-dimensional consolidation deformation are very rare and one-dimensional mechanics, as an apparatus, represents an extreme simplification. But, as said above, the consideration of simple, stark cases can sometimes prove helpful for the understanding. Problems of multidimensional consolidation will be dealt with in Section 7.4.

We look first at the example of a clay which is already in a heavily overconsolidated state initially. Therefore, even assuming a starting state in which $M_s > M$, considering that the loss of overconsolidation in clay generally proceeds faster than the degradation of structure, M_s will decrease as a result of the plastic deformation process accompanying the loading until it eventually becomes smaller than M, arriving at the kind of stress state shown in Fig. 7.1, where

$$M_s p' < q < M p' . \qquad (7.1)$$

In this state, as already explained in Chapters 4 and 5, there will be an occurrence of softening together with plastic compression. If this phenomenon continues in the same clay, delayed consolidation settlement is bound to result. Let us first explain why.

Even if compression goes on, the continuing softening will eventually bring down effective stress, leading to a new rise in pore water pressure in the clay, assuming that the applied load remains constant. This is shown in Fig. 7.2, in terms of one-dimensional mechanics. Assuming the pore pressure is not dissipated, this is what causes the delayed consolidation. Naturally, if the loading continues, the further evolution of the plastic deformation will sooner or later lead to the development of decay in the structure, causing M_s to increase and approach closer to M, which means that the state of $M_s p' < q < M p'$ in Equation (7.1) will not last indefinitely, but eventually give way to the relation

$$q < M_s p' < M p' , \qquad (7.2)$$

whereupon the soil will revert to hardening. Once this state in Equation (7.2) is reached, the clay returns to the usual kind of consolidation state for clay, familiar from textbooks, in which "stiffness/Young's modulus are positive." Therefore if we do

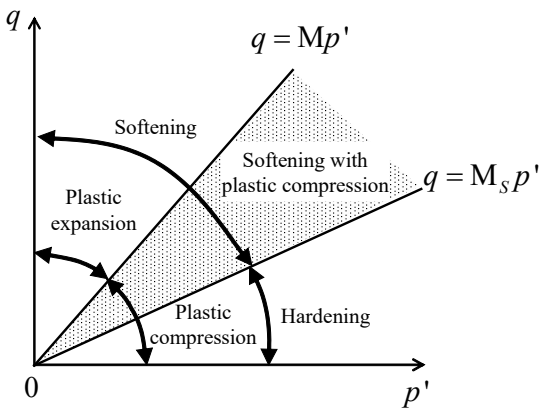

Fig. 7.1 Softening with plastic compression.

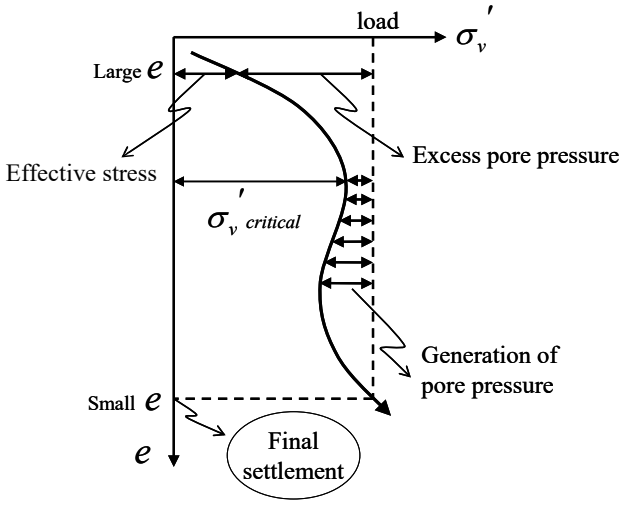

Fig.7.2 $\sigma_v' \sim e$ relation with $\sigma_{v\,critical}'$ in "one-dimensional mechanics."

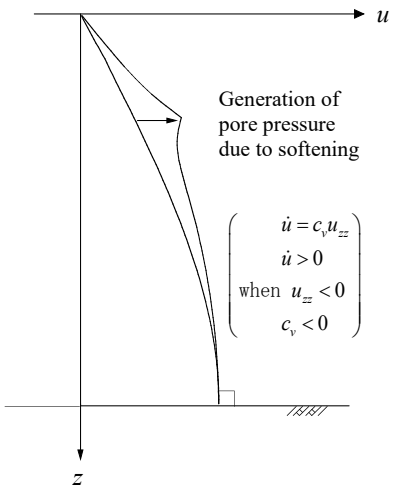

Fig.7.3 Generation of pore pressure due to softening during one-dimensional consolidation.

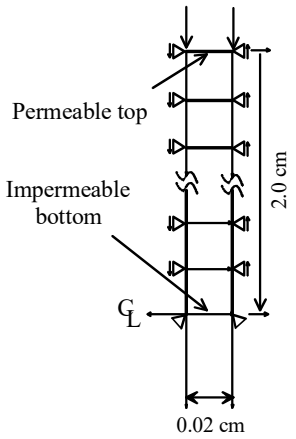

Fig. 7.4 Finite element array for one dimensional consolidation/compression.

Table 7.1 Material constants, initial conditions and permeability constant.

Elasto-plastic parameters	
Compression index $\tilde{\lambda}$	0.13
Swelling index $\tilde{\kappa}$	0.075
Critical state constant M	1.53
Void ratio at $p' = 98.1$kPa on NCL N	1.97
Poisson's ratio ν	0.3
Evolution parameters	
Degradation parameter of overconsolidation state m	10.0
Degradation parameter of structure a (b=c=1.0)	0.59
Initial conditions	
Initial void ratio e_0	1.19
Initial mean effective stress p_0' (kPa)	9.8
Initial value of R^* (R^*_0)	0.05
Initial overconsolidation ratio $1/R_0$	100.0
Permeability k (cm/sec)	7.8×10^{-9}

decide to apply the name of "secondary consolidation" to the state represented in Equation (7.1), we can say that secondary consolidation leads up to a primary consolidation state to follow.

As the time variation in the pore pressure at some material point in a clay deposit will depend on the gradient of the excess water pressure field at that point, consolidation is a concept that essentially has to be treated as a boundary value problem. Thus, even in a problem of one-dimensional mechanics, the representation of the material point's behavior in Fig. 7.2 is, if taken alone, insufficient for explaining aspects such as the regeneration and dissipation of pore pressure. For this reason, Fig. 7.3, using Terzaghi's one-dimensional consolidation equation (here again, in terms of one-dimensional mechanics), serves to explain the effect of softening on consolidation. As seen in the figure, a negative value of the coefficient of consolidation c_v corresponds, in one-dimensional mechanics, to softening. If softening were to go on exclusively, localization of the sort shown in Fig. 7.3 would run on too far, and the calculation would explode exponentially. But fortunately, as Equation (7.2) and Fig. 7.2 indicate, there is no real fear of that happening, since at some point the clay's behavior is bound to revert to hardening.

Let us say a little more about this need to treat consolidation as a boundary value problem.

Once softening has set in at a certain depth in the clay deposit so that the pore water pressure there begins to increase, since the pressure in the clay is continuously distributed there will be a corresponding increase in the soil elements on all adjoining sides, as well as above and below, leading to unloading in those elements. In this kind of way, even if deformation occurs in a one-dimensional state, the clay in the ground undergoing the consolidation pressure will be subject, as Fig. 7.2 shows, not just to hardening, softening and re-hardening, but also to incidental unloading along the way. The resulting stress state will be three-dimensionally highly complex, and the loading history and effective stress paths will be of extreme complexity, too. Furthermore, since these effective stress paths will all differ from the top of the clay to the bottom, the elasto-plastic mass of the whole, once consolidation is complete, will become quite heterogeneous in the depth direction, reflecting the differences in loading history. The variable void ratios and other heterogeneities that our researchers regularly find in naturally deposited clay strata do in fact show, according to the ways described above, whether or not a given clay deposit has undergone co-occurrences of compression and softening in the course of its deposition process. There is no hiding these geological footprints.

We now confirm the above account by means of a numerically computed example of one-dimensional consolidation. The computation itself, of course, makes use of three-dimensional componential rules to calculate the one-dimensional deformation according to a multidimensional consolidation theory. It simulates an oedometer test on a clay specimen of thickness 2cm. Fig. 7.4 shows the various conditions assumed for the finite element calculation, and Table 7.1 the parameter and other initial values used. The specimen was a structured clay, but the initial overconsolidation ratio of 100 is intended to simulate its state when brought into the laboratory after being sampled. Fig. 7.5 shows the relation between the void ratio and load, for the specimen as a whole, when consolidated under gradual loading at a constant incremental rate. "Void ratio," here, means the average of the void ratio values occurring from top to bottom in the specimen. In other words, in a case where compression is advanced at the drained end, but not so advanced at the undrained end of the sample, it is the average value that is taken.

In Fig. 7.5, the compression curves extend further to the right

for the faster rates of loading. When the loading rate is rapid the draining is unable to keep pace, and this causes a rise in pore water pressure. Or conversely, for the same void ratio the clay specimen is able to withstand higher loads if these are applied at a slower rate. On first sight, the figure appears to show a difference in loading rate leading to a different shape in the compression curve for the same soil. However, this can be recognized as only apparent when we take into account the increase in pore drainage resistance, that is to say, the rise in the pressure on the pore water. By working out the coupled soil-water relation in which the rate of volume change in the soil skeleton is governed by Darcy's law, the problem of calculating this behavior takes care of itself. It should be noted that it has nothing to do with, and does not depend upon, Suklje's "isotache hypothesis" (Suklje L., 1957) concerning the small element of the soil skeleton.

As seen in Fig. 7.5, loading is first applied at a rapid rate at one of three levels, A (392kPa), B (833kPa) or C (1179kPa). The load is then kept constant, and the procedure changes to that of a usual consolidation test. The settlement observed at the top end of the specimen after the change to constant loading is shown

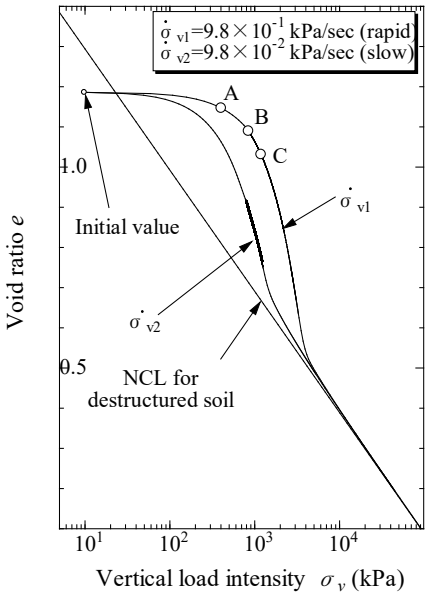

Fig. 7.5 Apparent σ_v – e curves with different loading rates.

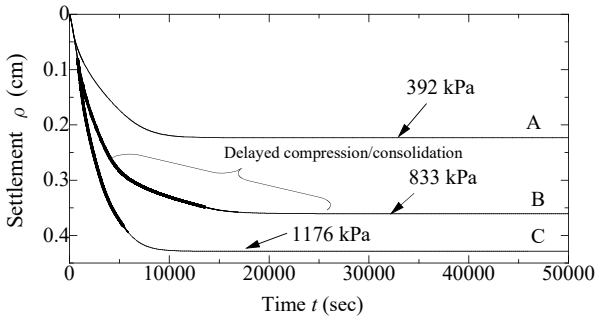

Fig. 7.6 Delayed compression/consolidation due to softening with volume compression (bold lines indicate the occurrence of softening).

plotted against time in Fig. 7.6. In this example, a remarkable delay in consolidation settlement is observed at loading level B. Fig. 7.7 shows the isochrones for the excess pore pressure at this level, from top to bottom inside the specimen. From this we can make out a gradual shift with time in the portion exhibiting a rise in pore pressure due to softening, from the top end (drained) to the bottom (undrained). The delay in the dissipation of excess pore pressure is also evident. Fig. 7.8 shows the heterogeneous condition of the clay specimen after consolidation is complete, by depth, in comparison with the reference configuration observed prior to the test.

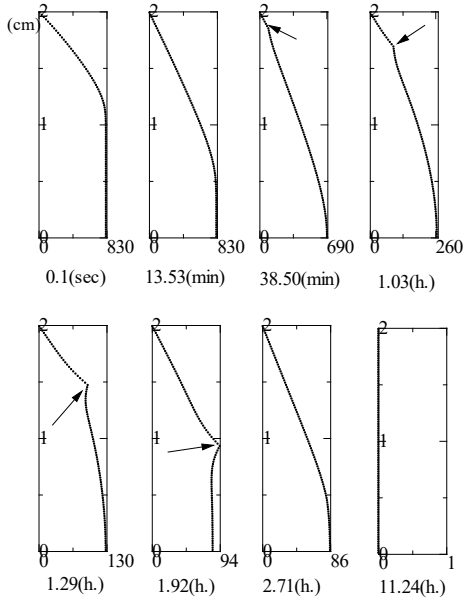

Fig. 7.7 Isochrones (kPa) (arrows indicate the generation of pore pressure).

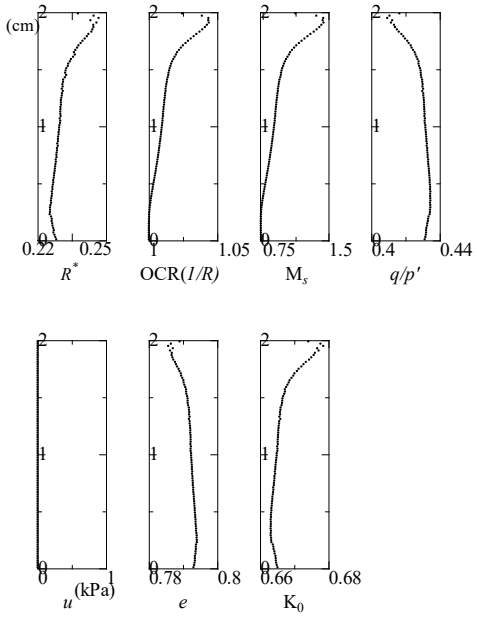

Fig. 7.8 Heterogeneity of the clay specimen with depth after completion of consolidation.

For the clay in Figs. 7.5 to 7.8, there is a certain load level between loading levels A (392kPa) and B (833kPa) at which softening begins to occur ($\sigma_v{}'_{critical}$ in Fig. 7.2; around 700kPa in

the present calculation). The nearer loading level B approaches to this $\sigma_v{}'_{critical}$, the greater the consolidation delay becomes. This can be seen from Fig. 7.9, where loading level B is at 785kPa. For the isochrones, see Fig. 7.10. For a loading level as high as C, softening begins at the very onset of compression, as shown in Fig. 7.6. A large compression due to the decay or collapse of the soil structure is inevitable, but the consolidation delay is small.

In Fig. 7.5, loading levels A and B both appear to be close to the "consolidation yield stress." It has long been said that consolidation pressures in the area straddling this consolidation yield stress lead to "secondary consolidation" and/or "delayed compression." This can be regarded as a rule of experience, based on the fact that the kind of loading level that destroys the soil skeleton and leads to the softening phenomenon lies close to the consolidation yield stress observed in consolidation tests for structured overconsolidated clays. Since the soil is in fact always yielding (the current stress is always on the subloading yield surface), this name "consolidation yield stress" refers only to an apparent yield stress, and is not a strictly defined mechanical term. Further details in this connection are given for Figs. 7.16 and 7.17 below.

The phenomenon evident from Fig. 7.9, that consolidation settlement can accelerate while underway, and the fact that a vertical consolidation pressure occurs in the vicinity of the "consolidation yield stress," have both been reported previously. Observations by the Laval University Geotechnical Group (Leroueil et al., 1985), are presented in Fig. 7.11. These indicate that a sudden rise in the settlement rate occurs around a certain particular loading level. Similar observations have been reported from alluvial clay deposits in land reclamation sites in Japan.

It was said above that Fig. 7.5 "shows the relation between the void ratio and load for the specimen as a whole when consolidated under gradual loading at a constant rate." In such a case, what kind of compression curve will result from taking this 2cm thick specimen as a single soil element, compressing the clay soil at an infinitely slow rate while no load is supported from the pore water? This is the situation shown in Fig. 7.12, overlaid on Fig. 7.5. As can be seen from this figure, a $\sigma_v{}'_{critical}$ level occurs between loading levels A (392kPa) and B (833kPa), leading to softening within the specimen.

Let us note that the softening that occurs with compression in the stress state of Equation (7.1) (Fig. 7.2) is a special phenomenon, appearing in the most extreme cases of delayed consolidation/compression. So far we have explained the time-lag effect exerted on consolidation by "softening with plastic compression." But it needs to be pointed out that this kind of softening is not necessarily a precondition for delayed consolidation. Even in a highly structured clay soil, there is no automatic guarantee that softening and a $\sigma_v{}'_{critical}$ phenomenon of the type seen in Fig. 7.2 will be observable in a one-dimensional compression process. This is shown clearly in Fig. 7.13. Nevertheless, even in a case like this it remains true that where the clay in the deposit finds itself on the loading path X → Y there will be a delay in consolidation and a considerable degree of compression as a result of the coefficient of consolidation c_v approaching close to zero. The "consolidation yield stress" is also situated very close to this X → Y load level, which explains, again, why it has long been said that "secondary consolidation" and/or "delayed compression" occurs at loads straddling the "consolidation yield stress." This is evident both from Fig. 7.13 and from Fig. 7.2, and further remarks regarding the same point will made in connection with Figs. 7.16 and 7.17 in the next section.

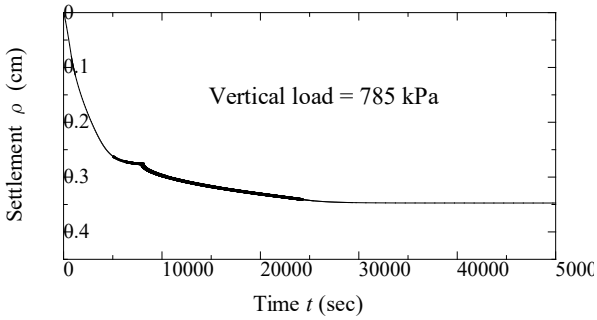

Fig.7.9 Suddenly accelerated consolidation settlement.

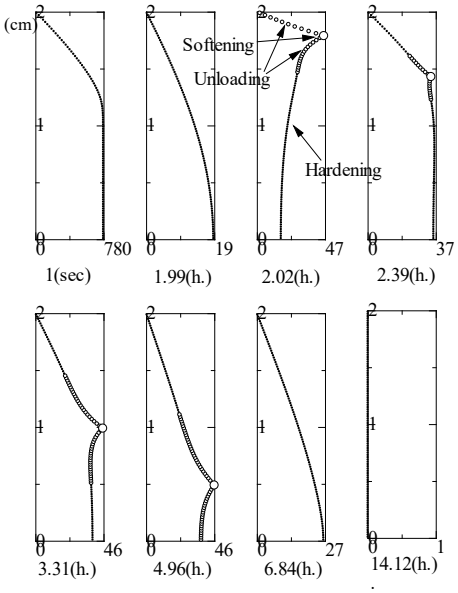

Fig. 7.10 Isochrones of excess pore pressure (kPa).

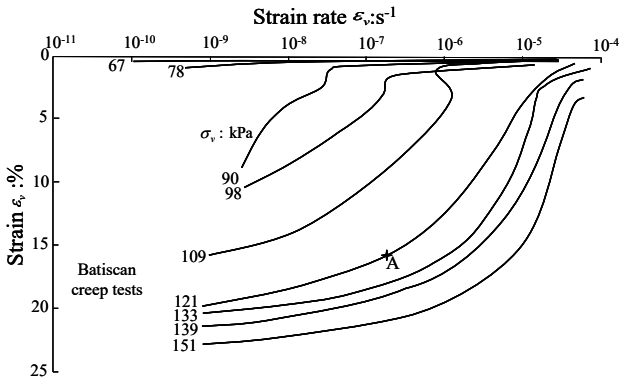

Fig. 7.11 Field observation of the rate of consolidation settlement (after Leroueil et al., 1985).

7.3 *Limitations of the laboratory oedometer test*

Taking a sample of a highly structured naturally deposited clay without disturbing its structure is far from easy. Its transfer from its initial location in the clay deposit to the laboratory involves

inevitable unloading, so that the specimen ends up in a heavily overconsolidated condition. In consequence, the effective stress path during the laboratory reloading turns out quite differently from the effective stress path of its original loading *in situ*. For all these reasons, it is exceedingly difficult in the laboratory environment to recreate the loading process at the natural deposition site. All of these problems have always been well known, but nowadays it is possible to factor most of them into the computation in detail, including the problem of the "disturbance of the soil specimen." In this section, using

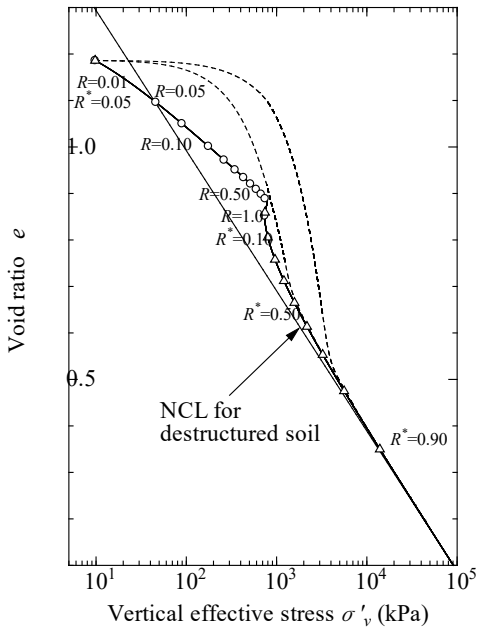

Fig. 7.12 Compression behavior of the clay material, by elements.

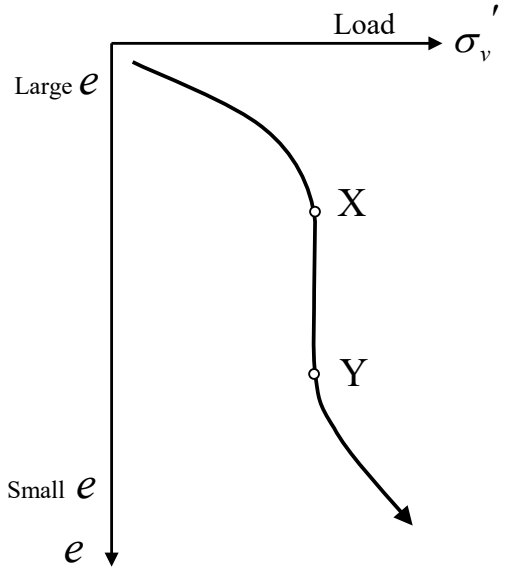

Fig. 7.13 σ_v' □ e relation without peak.

computed results from a numerical experiment, we shall be looking at the limitations of laboratory consolidation tests, taking the main problem points in order.

Overconsolidated state of laboratory clay specimen

We shall here be considering briefly a numerical simulation of *in-situ* soil sampling, the mounting of the clay material on the test apparatus, and the subsequent one-dimensional consolidation test. For the details, see Noda et al., 2003a and Nakano et al.,2003b.

The initial conditions at the *in-situ* sampling location of Fig. 7.14 (depth 20m) are set out in Table 7.2. The assumed material is a structured clay with an overconsolidation ratio of 2.5. The elasto-plastic and evolution parameters of this clay are given in Table 7.3. They are typical clay parameters, in that the loss of overconsolidation proceeds more rapidly than the decay of the soil structure. This set of conditions is the general departure point for the numerical simulation.

The sample, still in a strictly maintained undrained condition, is next brought into an isotropic stress state. The effective stress path for this process is marked $A \rightarrow A'$ in Fig. 7.15. The subloading yield surface shown in the figure for the *in-situ* sampling position follows the form of the yield function in the modified Cam-Clay model, for which anisotropy is taken into account. The details of this are as explained in APPENDIX A. Effective stress path $A \rightarrow A'$ (undrained path) leads outside of this subloading yield surface, and is thus a loading, not an unloading path. This means that plastic deformation has been occurring along this path $A \rightarrow A'$, causing a slight but real change in both the structural state and the overconsolidation ratio of the clay, as compared with the original *in-situ* state. The state of the clay at point A' is calculated to be as in Table 7.4. Comparing this with Table 7.2, it is evident that a small amount of disturbance has crept in during the process of sampling.

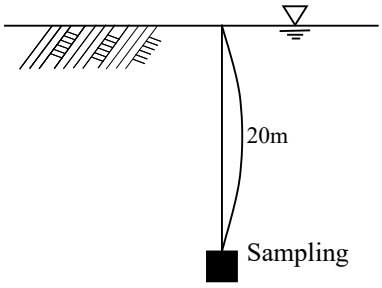

Fig. 7.14 Soil sampling.

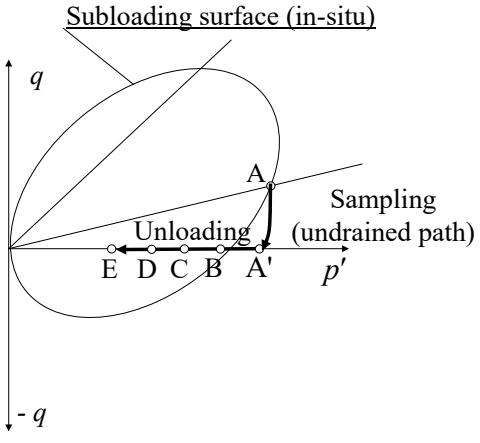

Fig. 7.15 Sampling and isotropic unloading.

Table 7.2 Initial soil sates *in-situ*, lightly overconsolidated clay.

Vertical effective stress σ'_v (kPa)	153.7
Coefficient of lateral pressure σ'_h/σ'_v	0.7
Overconsolidation ratio $1/R_0$	2.5

Value of R^*_0	0.1
Anisotropy $\zeta_0 = \sqrt{3/2\boldsymbol{\beta}_0 \cdot \boldsymbol{\beta}_0}$ (see APPENDIX A)	0.7

Table 7.3 Material constants and permeability constant.

Elasto-plastic parameters	
Compression index $\tilde{\lambda}$	0.131
Swelling index $\tilde{\kappa}$	0.06
Critical state constant M	1.2
Void ratio at $p' = 98.1$kPa on NCL N	1.97
Poisson's ratio ν	0.1
Evolution parameters	
Degradation parameter of overconsolidation state m	5.0
Degradation parameter of structure a ($b = c = 1.0$)	1.73
Evolution parameter of $\boldsymbol{\beta}$ b_r (see APPENDIX A)	0.0001
Limit of rotation m_b (see APPENDIX A)	1.0
Permeability k (cm/sec)	7.8×10^{-9}

Table 7.4 State of a lightly overconsolidated clay specimen of point A' in Fig. 7.15 after sampling.

Vertical effective stress σ'_v (kPa)	121.4
Coefficient of lateral pressure σ'_h / σ'_v	1.07
Overconsolidation ratio $1/R$	2.3
Value of R^*	0.1
Anisotropy $\zeta = \sqrt{3/2\boldsymbol{\beta} \cdot \boldsymbol{\beta}}$ (see APPENDIX A)	0.7

Table 7.5 Initial conditions for laboratory oedometer test.

Four different unloading stages	B	C	D	E
Initial vertical load (kPa)	78.5	39.2	19.6	9.8
Vertical effective stress σ'_v (kPa)	78.5	39.2	19.6	9.8
Coefficient of lateral pressure σ'_h / σ'_v	1.0	1.0	1.0	1.0
Overconsolidation ratio $1/R$	3.58	7.16	14.3	28.6
Value of R^*	0.10	0.10	0.10	0.10
Anisotropy $\zeta = \sqrt{2/3\boldsymbol{\beta} \cdot \boldsymbol{\beta}}$ (see APPENDIX A)	0.7	0.7	0.7	0.7

The sample is next mounted on the one-dimensional consolidation test apparatus, and subjected to unloading with swelling down to the first stage vertical loading level. The process varies depending on the magnitude of the first stage loading, as shown in Table 7.5.

Taking the conditions in Table 7.5 as initial values, the soil element response to the one-dimensional compression can be calculated right away from the constitutive equation of the Super/subloading Yield Surface model. The result is seen in Fig. 7.16. Examining this in alignment with the earlier Figs. 7.2 and 7.13, the following three points emerge.

① None of the four clay specimens represented in Table 7.5 displays a one-dimensional compression response at the point of *in-situ* sampling (A in Fig.7.16).

② Even supposing the clay specimens were exposed to one-dimensional compression from the *in-situ* sampling state on, the shapes in Fig. 7.13 indicate that there was no co-occurrence of softening and compression.

③ But in the laboratory one-dimensional consolidation test, a clay specimen unloaded with swelling down to 9.81kPa does invariably display this behavior of softening with compression. Looking at the enlargement in Fig. 7.16, the material unloaded with swelling shows plain evidence of softening in the vicinity of $\sigma_v{}'_{critical} = 230$kPa . The same phenomenon is seen with the specimen unloaded down to 19.62kPa, again with swelling. In both cases, the shapes displayed are the same as in Fig. 7.2.

It can be seen from this that a clay specimen overconsolidated through the sampling process, as well as through unloading and swelling, displays "secondary consolidation" and/or "delayed compression" phenomena in this laboratory test at a lower consolidation load than would be the case with clay left *in situ*. Whatever the precise details, it is important to be aware that a laboratory one-dimensional consolidation test does not provide assured information about the one-dimensional compression response of clay in its natural deposition environment.

Fig. 7.16, as we said, is calculated from the constitutive equation, but let us now examine how reliably results like these can be observed in laboratory consolidation tests using staged loading of the conventional kind. Fig. 7.17 shows the results of a standard consolidation test for a specimen (of a typical kind for this sort of test) unloaded with swelling down to 9.81kPa. The line of black points in the figure shows the results obtained by maintaining the specimen under a staged load for 24 hours. (Of course, these are numerically simulated results, not real test values; the assumptions for the staged loading simulation were loading for one second, followed by 24 hours under constant load.) The "consolidation yield load" for Fig. 7.17 was sought by means of the Casagrande method, giving a result of 230kPa, a value extremely close to $\sigma_v{}'_{critical}$. A comparison of this standard consolidation test result with the stress response behavior in Fig.

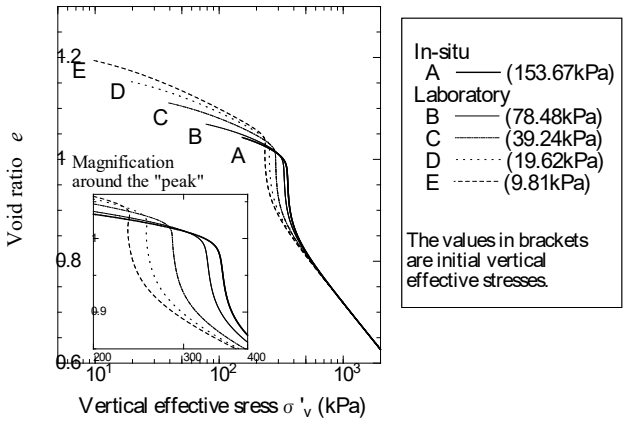

Fig. 7.16 One-dimensional compression behaviors of the five clay elements, A to E, in Fig. 7.15.

7.16, above, is presented in Fig. 7.18. With the exception of the portion just before and after the "consolidation yield load," the accuracy of the oedometer test is very good. But the most important thing to remark is that Figs. 7.17 and 7.18, with the laboratory test findings, fail to supply any information at all about the soil response at the original sampling site (the heavy black line A in Fig. 7.16). Of this, we have already said something above.

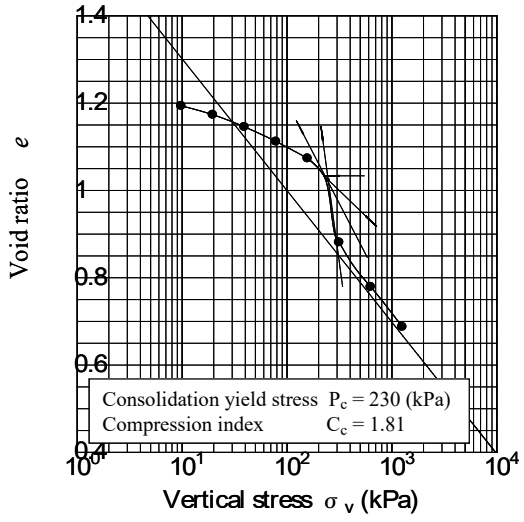

Fig. 7.17 Oedometer test results obtained from the clay specimen E in Fig. 7.15.

7.15). This procedure is summarized in Fig. 7.19. Table 7.6 presents the computed states of the material after disturbance in this manner. Three degrees of disturbance were simulated, by varying the number of undrained shear load cycles. Results of unconfined compression tests for four such materials before and after disturbance are shown in Fig. 7.20. It will be seen that the observations center on the clay with a sensitivity ratio of around 2.5.

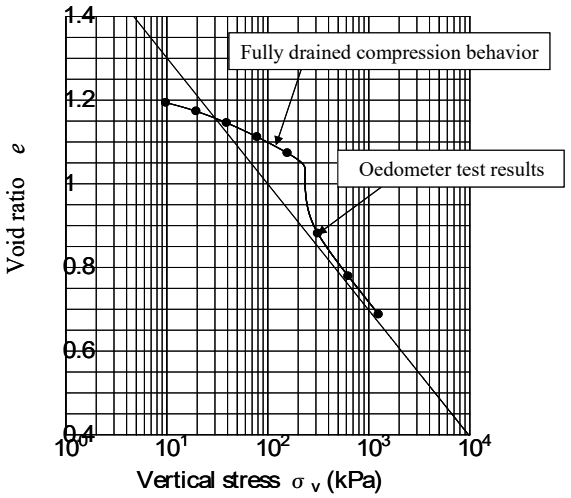

Fig. 7.18 Comparison between fully drained compression behavior and oedometer test results.

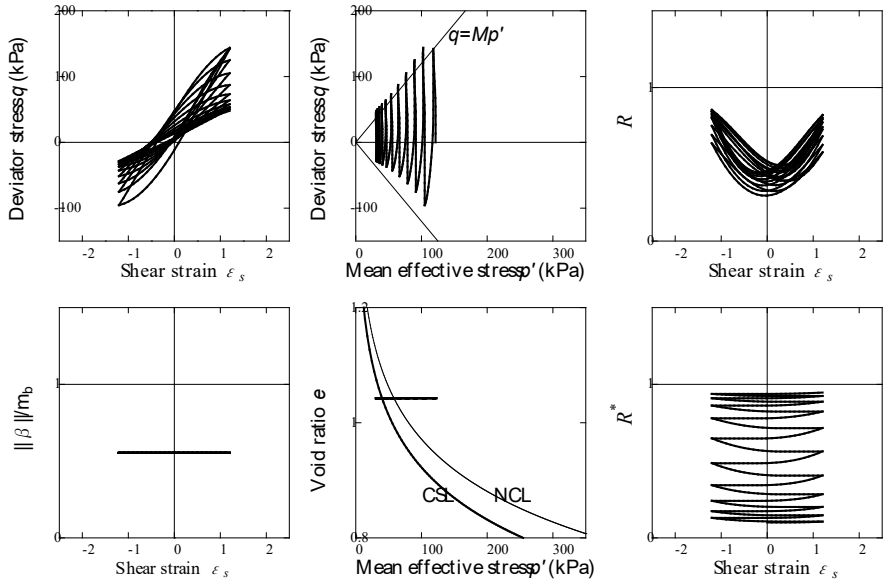

Fig. 7.19 Artificial soil disturbance by repeated undrained shear stress application.

Effect of soil disturbance during sampling and testing

Just what the effects are of conducting a laboratory test on disturbed soil materials was next investigated using numerical simulations. The disturbance in the soil was simulated by bringing materials into an undrained isotropic stress state, and then subjecting them to repeated undrained shearing before any unloading and swelling took place (material at point A' in Fig.

Table 7.6 State of clay specimens after repeated undrained shear stress application.

Number of cycles	0	5	10	15
Vertical effective stress σ'_v (kPa)	121	91.5	69.7	51.7

Coefficient of lateral pressure σ'_h/σ'_v	1.0	1.0	1.0	1.0
Overconsolidation ratio $1/R$	2.32	2.96	3.48	3.36
Value of R^*	0.10	0.14	0.19	0.34
Anisotropy $\zeta = \sqrt{3/2\boldsymbol{\beta}\cdot\boldsymbol{\beta}}$ (see APPENDIX A)	0.7	0.7	0.7	0.7

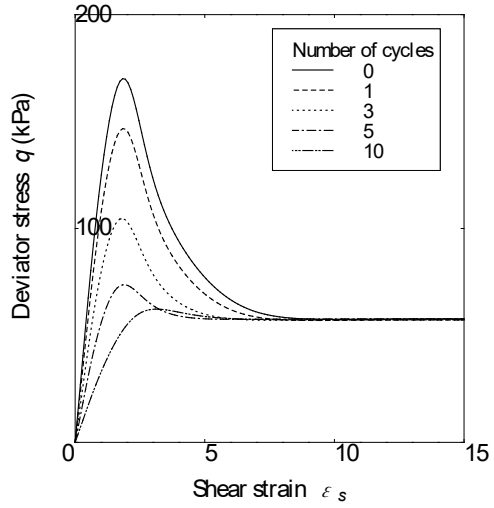

Fig. 7.20 Sensitivity ratio.

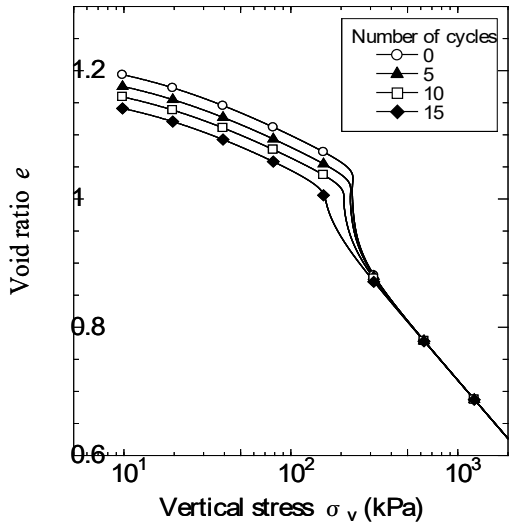

Fig. 7.21 Change of compression behavior due to different degrees of soil disturbance.

Performing oedometer tests on the above four clay materials for unloading with swelling down to 9.81kPa gives the kind of results presented in Fig. 7.21. These show a close resemblance to the imaginary curves formerly drawn by Schmertmann, J. H. (1953) (Fig. 7.22). The disturbance leads to a diminution in the "consolidation yield stress," reflected in the reduced slope of the e – $\log\sigma_v'$ compression curve. Recalling the earlier explanations for Figs. 7.2 and 7.13, it will be apparent here that Fig. 7.21 shows that:

① so long as the material is subjected to a small amount of disturbance only, there is a drop in the load level at which "secondary consolidation"/"delayed compression" occurs, but

② if the applied disturbance is sufficient, and the material remolded, the occurrence of "secondary consolidation" and "delayed compression" is thereby impeded.

7.4 *Long-term settlement of a multi-layered system under embankment loading*

Fig. 7.23 shows an example of long-term settlement due to embankment loading on an alluvial clay foundation at the Kanda site on the Joban Expressway. The soil profile in the lower part

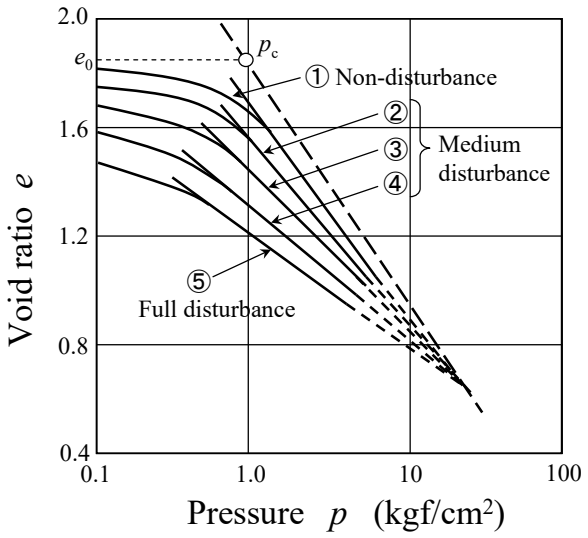

Fig. 7.22 Imaginary curves drawn by Schmertmann (after Schmertmann, J. H., 1953).

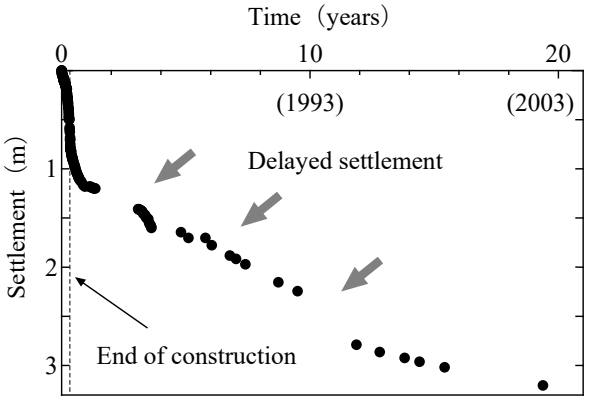

Fig. 7.23 Long-time settlement at the Kanda site on the Joban Expressway.

of the embankment foundation can be seen in Fig. 7.24. An 8m thick layer of sand rests on top of a 15m thick base of alluvial soft clay. Consolidation settlement has been occurring continuously over the 20 years since the embankment's completion, and has not yet come to a stop.

In fact, the settlement problem at this site has been so serious as

to require repeated overlays of asphalt since completion, as a result of which the load on the embankment is now some 20% larger than at the time of its construction.

The time-settlement curve is not smooth, but, as indicated by the arrows in Fig. 7.23, shows repeated bouts of accelerated settlement, followed by intervals of slower change. However, the intervals are steadily increasing in time length. Fig. 7.24 shows an example of rising pore pressure observed when one of the bouts of consolidation settlement was in progress. The cause lies in the softening that co-occurs with the plastic compression of the soil skeleton. In other words, we can consider the consolidation settlement in Fig. 7.23 as an example of "progressive consolidation with decay of structure."

In this section we compute the "progressive two-dimensional plane strain consolidation with decay of structure" at this site, and examine the typical characteristics of "secondary consolidation" and/or "delayed compression" that are observed along with it.

Fig. 7.25 shows the finite element array of the foundations, and the shape of the embankment load. Fig. 7.26 shows the time-load relations used in the computation. The 10m high embankment was built over a 120-day period, and the load on it has since been kept constant. The unit weight of the embankment materials is taken as 17kN/m^3. These figures both match with the embankment and the foundations as shown in Fig. 7.23. Additional load increments due to repeated overlays of asphalt are not taken into account in the computation.

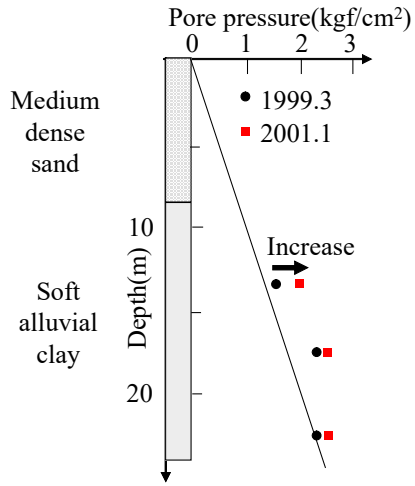

Fig. 7.24 Field observation of the increase in pore pressure.

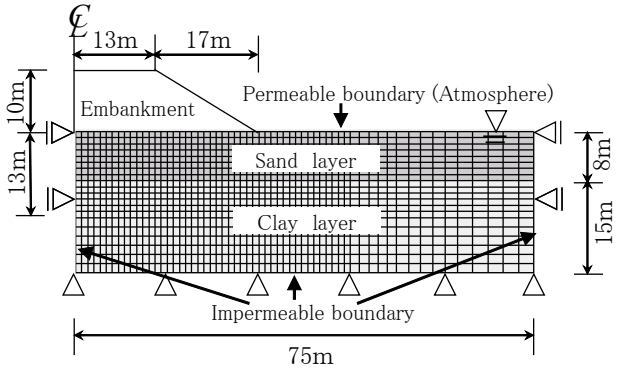

Fig. 7.25 Boundary conditions, loading conditions and finite element array used in the numerical analysis.

Table 7.7 displays the material constants used in the computation. Fig. 7.27 shows the initial conditions in the foundation. The sand is taken to be of the typical medium dense type with an initial overconsolidation ratio of 5, and the clay of a highly structured natural alluvial type, with an initial overconsolidation ratio of 3. The values in Table 7.7 and Fig. 7.27 are imaginary ones assigned by the author, however, and do not necessarily match the actual state of the foundation or the initial conditions in Fig. 7.23, as might be obtained from strict survey measurements.

Results of the two-dimensional plane strain consolidation computation can be seen in Figs. 7.28 and 7.29. Consolidation settlement is computed 100 years into the future. Fig. 7.29 shows the same contents as Fig. 7.28, but with time represented on a log scale. The pattern of sudden change in the rate of settlement whenever a bout of settlement is in progress shows an extremely close match to the observed changes in Fig. 7.23. Rises in pore pressure, apparent at times when consolidation settlement is in progress, are indicated by the arrows in Figs. 7.28 and 7.29.

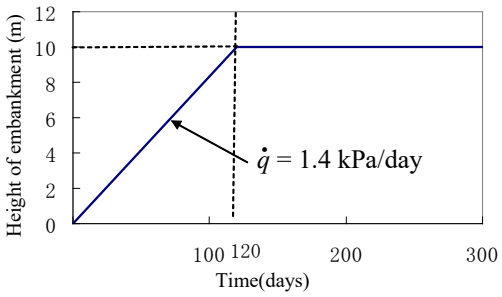

Fig. 7.26 Loading history.

Table 7.7 Material constants and permeability constants.

Elasto-plastic parameters	Clay	Sand
Compression index $\tilde{\lambda}$	0.25	0.042
Swelling index $\tilde{\kappa}$	0.13	0.012
Critical state constant M	1.20	1.08
Void ratio at $p'=98.1$kPa on NCL N	1.97	1.99
Poisson's ratio ν	0.2	0.3
Evolution parameters		
Degradation parameter of overconsolidation state m	7.0	0.04
Degradation parameter of structure a ($b=c=1.0$)	1.25	1.5
Evolution parameter of $\boldsymbol{\beta}$ b_r (see APPENDIX A)	10^{-3}	0.51
Limit of rotation m_b (see APPENDIX A)	1.0	0.5
Permeability k (cm/sec)	7.4×10^{-8}	4.1×10^{-2}
Density of soils ρ_s (t/m^3)	2.60	2.65

The consolidation settlement of highly structured natural alluvial clay does not proceed with anything like the smoothness of an exponential curve. Structural decay spreads through the clay foundation in the manner of a progressive failure, as seen in Fig. 7.30. That is what makes the settlement curve so jerky.

In Figs. 7.28 and 7.29, complete consolidation settlement takes upward of 100 years. From the results for the actual clay

foundation in Fig. 7.23, too, settlement would seem to have a long way still to run.

Even from the remarks made about one-dimensional consolidation up to Section 7.3, it is easy to imagine that "secondary consolidation" and/or "delayed compression" are outcomes that occur when the size of the load on an embankment exceeds a certain threshold value. The broken lines in Figs. 7.28 and 7.29 show patterns for consolidation settlement in an embankment of height 6m. The "secondary consolidation" and/or "delayed compression" is not observed when the lightweight embankment load is applied. It is clear that a lightweight embankment material such as EPS (polystyrene foam) would be highly effective as a precaution against "secondary consolidation" and/or "delayed compression."

Another cause of the thoroughly bad settlement behavior in Fig. 7.23 is the thick layer of sand laid on top of the clay layer, as shown in Fig. 7.24. This sand layer acts as a counterweight, keeping the soft clay from slipping away in spite of the enormous load of the 10m embankment. If the sand layer had been thinner, allowing destructive slippages to occur, another mode of engineering might well have been adopted, and the kind of settlement seen in Fig. 7.23 might never have happened. All of the above points were verified through the numerical computation, but for reasons of space the details are omitted here (for these, see Noda et al., 2003b).

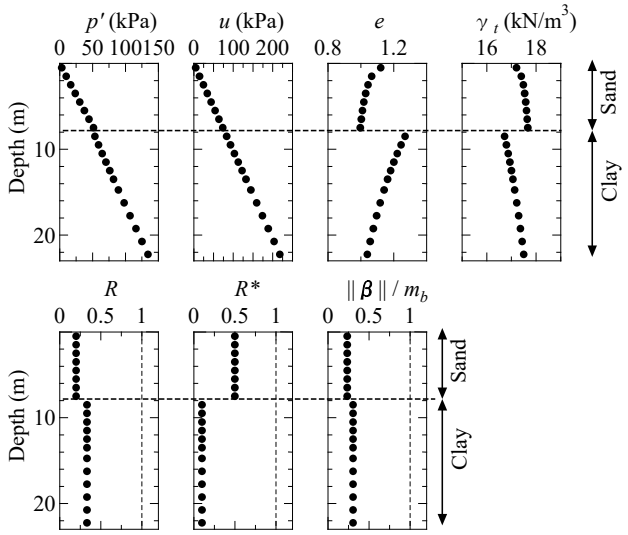

Fig. 7.27 Initial conditions for computation.

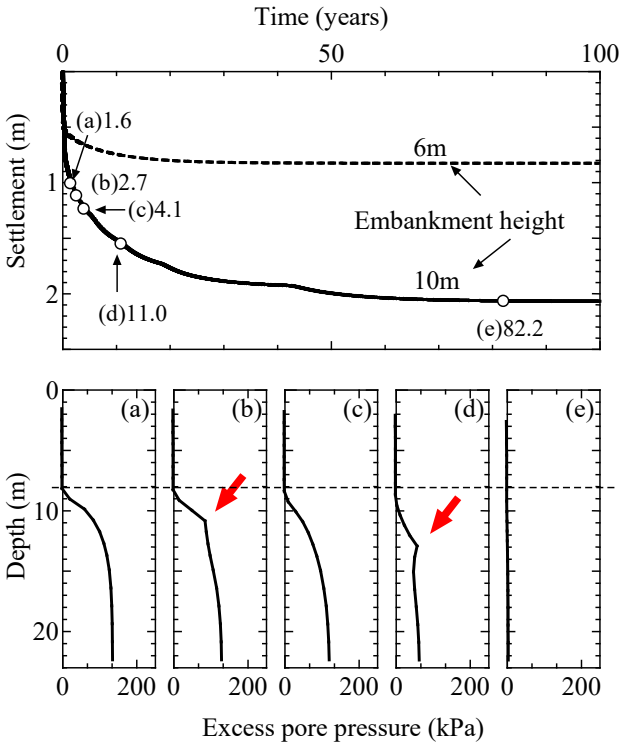

Fig. 7.28 Settlement - time curve and isochrones of the center of foundation.

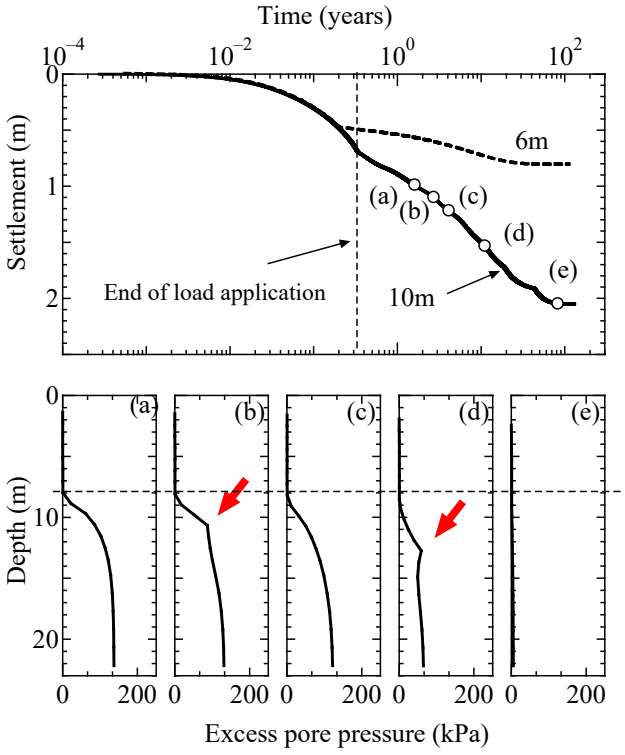

Fig. 7.29 Settlement - time curve on log scale.

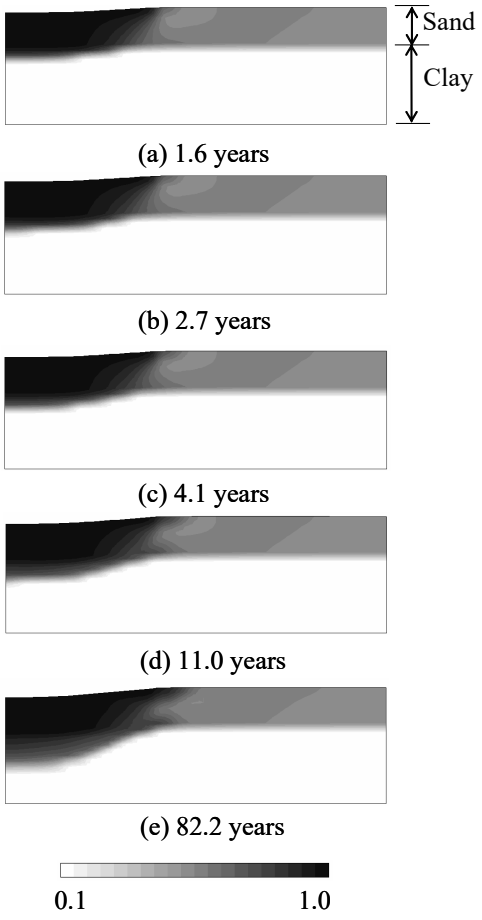

Fig. 7.30 Progressive failure of soil skeleton structure.

8. CONCLUSIONS

(1) In order to give an elasto-plastic theoretical account of actions or processes behind the "structure" and "overconsolidation" of naturally deposited clay and of sand, a *superloading yield surface* and (Hashiguchi's) *subloading yield surface* were introduced as additions to the *Cam-Clay model*. In the new model thus constituted, these two yield surfaces are taken as similar in shape to the yield surface of the Cam-Clay model, as viewed in relation to the origin point of the stress space. In terms of this Super/subloading Yield Surface model, the state of the soil structure is expressed through the degree of similarity between the superloading and the Cam-Clay yield surfaces, while the state of overconsolidation ("overconsolidation ratio", OCR) is expressed through the degree of similarity between the superloading and subloading yield surfaces.

Structure and overconsolidation are both 'mechanical states' of soils, and changes of state may occur from one to the other in the same soil depending on conditions of loading and unloading.

This new model is capable, first, of describing the following two kinds of mechanical behavior. ① In any kind of soil, with the development of plastic deformation, there is a collapse or progressive decay of structure until finally the soil reaches a state of complete disturbance. ② In any kind of soil, with the development of plastic deformation, there is also a progressive loss of overconsolidation until finally the soil reaches a state of normal consolidation. Further, the model also accounts for the facts that ③ collapse or decay of structure acts in the direction of an increase in plastic volume compression, while ④ loss of consolidation acts in the direction of an increase in plastic volume expansion.

Additionally, in the new model, the coefficient M_s of the threshold line $q=M_s p'$ which divides the p'–q stress space into regions of hardening and softening is a variable which changes with plastic deformation, showing that it is possible for a soil to soften and be compressed, or harden and expand, at the same time.

By using these features of the new model it becomes possible to describe almost all of the mechanical properties of clay and sand known hitherto from compression and shear tests.

(2) For the same amount of plastic deformation, the loss of overconsolidation outruns the decay in structure in clay, whereas in sand the opposite is true: the decay or collapse of structure proceeds faster than the loss of overconsolidation. By manipulating the parameters for the rates of evolution of these two states of structure and overconsolidation, it becomes possible to control both processes. Distinguishing between sand and clay in this way also makes it possible to account almost perfectly for virtually all the known differences in mechanical response between the two materials.

(3) The abrupt compression and densification that occurs in loose sand upon the repeated application of a shear load can be explained as a result of the rapid collapse in structure that proceeds from even a minimal amount of plastic deformation. The accumulation of overconsolidation in loose sand repeatedly subjected to the same kind of shear load is explained by the fact that small amounts of plastic deformation lead to almost no loss of overconsolidation.

(4) The "secondary consolidation" and/or "delayed compression" of structured clay is explained by the decay that goes on occurring in the remaining soil structure after the near-total loss of the overconsolidation state. Because the loss of overconsolidation is so nearly complete, the high degree of remaining structure causes M_s to become very small, which means that even at the low stress ratios found in states of one-dimensional compression, plastic compression accompanied by softening becomes a possibility. As a result, there is also a notable delay in the dissipation of pore water pressure, which causes consolidation settlement to persist for a great length of time.

Further details of the new model, making it possible to take account of the evolution of induced anisotropy and thus deal with finite deformations in ways that satisfy objectivity, are given in APPENDICES A－D.

ACKNOWLEDGEMENT

Consolidation of Clay and Compaction of Sand-An elasto-plastic description-, Akira ASAOKA, Copyright @ 2004 with permission from World Scientific Publishing Co. Pte. Ltd.

References

1) Asaoka, A., Nakano, M and Noda, T. (1994): Soil-water coupled behavior of saturated clay near/at critical state, *Soils and Foundations*, Vol.34, No.1, pp.91-106.
2) Asaoka, A., Nakano, M. and Noda, T. (1998): Super loading yield surface concept for the saturated structured soils, *Proc. of the fourth European conference on numerical methods in geotechinical engineering-NUMGE98*, pp.232-242.
3) Asaoka, A. (2000): Recent topics in soil-water coupled

problems, *J. of the Japan Society of Civil Engineers*, Vol.85, pp.46-49.
4) Asaoka, A., Nakano, M. and Noda, T. (2000a): Superloading yield surface concept for highly structured soil behavior, *Soils and Foundations*, No.40, Vol.2, pp.99-110.
5) Asaoka, A., Nakano, M., Noda, T. and Kaneda, K. (2000b): Delayed compression/consolidation of naturally clay due to degradation of soil structure, *Soils and Foundations*, No.40, Vol.3, pp. 75-85.
6) Asaoka, A., Nakano, M and Noda, T. (2000c): Elasto-plastic behavior of structured overconsolidated soils, *J. Appl. Mech. JSCE*, Vol.3, pp.335-342.
7) Asaoka, A., Noda, T., Yamada, E., Kaneda, K. and Nakano, M. (2002): An elasto-plastic description of two distinct volume change mechanisms of soils, *Soils and Foundations*, Vol.42, No.5, pp.47-57.
8) Bishop, A. W. and Henkel, D. J. (1962): The Measurement of Soil Properties in the Triaxial Test, *Edward Arnold,* London.
9) Castro, G. (1969): Liquefaction of sands, *ph.D. Thesis, Harvard Soil Mech. Series*, No.81.
10) Green, A. E. and Naghdi, P. M. (1965): A general theory of an elastic-plastic continuum, *Archive for Rational Mechanics and Analysis*, Vol.18, pp.251-281.
11) Hashiguchi, K. (1978): Plastic constitutive equations of granular materials, *Proc. of US-Japan Seminar on Continuum Mechanics and Statistical Approaches in the Mechanics of Granular Materials* (*Cowin, S.C. and Satake, M. eds.*), Sendai, JSSMFE, pp.321-329.
12) Hashiguchi, K. (1989): Subloading surface model in unconventional plasticity, *Int. J. of Solids and Structures*, Vol.25, pp.917-945.
13) Hashiguchi, K. and Chen, Z. -P. (1998): Elastoplastic constitutive equations of soils with the subloading surface and the rotational hardening, *Int. J. Numer. Anal. Meth. Geomech.*, Vol.22, pp.197-227.
14) Henkel, D. J. (1960): The shear strength of saturated remolded clay, *Proc. of Research Conf. on Shear Strength of Cohesive Soils at Boulder*, Colorado, pp.533-540.
15) Leroueil, S., Kabbaj, M., Tavenas, F. (1985): Stress-strain-strain rate relation for the compressibility of sensitive natural clays, *Geotechnique*, Vol.35, No.2, pp.159-180.
16) Leroueil, S. (1996): Compressibility of clays; fundamental and practical aspects, *J. of Geotech. Engrg.*, ASCE, Vol.122, No.7, pp.534-543.
17) Muir Wood, D. (1995): Soil behavior and critical state soil mechanics, Cambridge.
18) Nakano, M. and Nakai, K. (2003a): Description of undrained behaviors of sands with some kinds of grain size distributions based on soil skeleton structure at work, *Soils and Foundations*, under contribution.
19) Nakano, M., Nakai, K., Noda, T. and Asaoka, A. (2003b): Simulation of shear and one-dimensional compression behaviors of natural deposited clays by Super/subloading yield surface model, *Soils and Foundations*, under contribution.
20) Noda, T., Yamada, S. and Asaoka, A. (2003a): Effects of destructuration and overconsolidation during sampling of clay on the subsequent mechanical behavior, *Soils and Foundations*, under contribution.
21) Noda, T., Yamada, E., Nakano, M., Tashiro, M. and Asaoka, A. (2003b): Delayed consolidation behavior of naturally deposited clayey soil under embankment loading, *Soils and Foundations*, under contribution.
22) Roscoe, K. H., Schofield, A. N. and Wroth, C. P. (1958): On the yielding of soils, *Geotechnique*, Vol.8, pp.22-53.
23) Roscoe, K. H., Schofield, A. N. and Thurairajah, A. (1963): Yielding of clays in state wetter than critical, *Geotechnique*, Vol.13, pp.211-240.
24) Roscoe, K. H., and Burland, J. B. (1968): On the generalized stress-strain behavior of 'wet' clay, in J. Heyman and F. A. Leckie (eds.), *Engineering plasticity* (Cambridge: Cambridge University Press), pp.535-609.
25) Schmertmann, J. H. (1953): Estimating the True Consolidated Behavior of Clay from Laboratory Test Results, *Proc. Am. Soc. Civ. Engrs.*, pp.79-311.
26) Sekiguchi, H. and Ohta, H. (1977): Induced anisotropy and time dependency in clays, *Constitutive Equations of Soils* (*Proc, 9th Int. Conf. Soil Mech. Found. Eng., Spec. Session9*), Tokyo, pp.229-238.
27) Suklje, L. (1957): The analysis of the consolidation process by the isotaches method, *Proc of the IV-th I. C. S. M. F. E.*, Vol.1, pp.200-206.
28) Tatsuoka, F. and Kohata, Y.(1995): Stiffness of hard soils and soft rocks in engineering applications, *Proc. of 1st int. conf. on Pre-failure deformation characteristics of geomaterials,* Sapporo, Japan, Vol.2, pp.947-1063.

APPENDIX A

A-1 Modified Cam-Clay model with η^*

In conventional critical state soil mechanics, the stress ratio η is generally defined as:

$$\eta = \sqrt{\frac{3}{2}\boldsymbol{\eta}\cdot\boldsymbol{\eta}}\,, \tag{A-1}$$

However, Sekiguchi and Ohta (1977) introduced the following stress invariant, instead of conventional η, in order to express the rotation of the plastic potential:

$$\eta^* = \sqrt{\frac{3}{2}\hat{\boldsymbol{\eta}}\cdot\hat{\boldsymbol{\eta}}}\,. \tag{A-2}$$

In Equations (A-1) and (A-2)

$$\hat{\boldsymbol{\eta}} = \boldsymbol{\eta} - \boldsymbol{\beta}\,,\quad \boldsymbol{\eta} = \frac{\boldsymbol{S}}{p'}\,,\quad \boldsymbol{S} = \boldsymbol{T}' + p'\boldsymbol{I} \quad \text{and} \quad p' = -\frac{1}{3}\mathrm{tr}\boldsymbol{T}'\,, \tag{A-3}$$

where $\boldsymbol{I}$ is the identity tensor and $\boldsymbol{T}'$ denotes the Cauchy effective stress tensor, and $\boldsymbol{\beta}$ is the axis of rotation tensor. The shape of the plastic potential of the modified Cam-Clay is then expressed, when η^* is introduced, as follows:

$$f(p', \eta^*) = \mathrm{MD}\ln\frac{p'}{\tilde{p}'_0} + \mathrm{MD}\ln\frac{\mathrm{M}^2 + \eta^{*2}}{\mathrm{M}^2} = \varepsilon_v^p \tag{A-4}$$

in which D is a material constant. The $\tilde{p}'_0$ in Equation (A-4) is found to be the mean effective stress on the modified Cam-Clay yield surface that coincides with the initial mean effective stress p'_0 of the soil in the reference state. Note that D is expressed in terms of $\tilde{\lambda}$, $\tilde{\kappa}$ and M in the following equation:

$$\mathrm{D} = \frac{\tilde{\lambda} - \tilde{\kappa}}{\mathrm{M}(1 + \mathrm{e}_0)}\,. \tag{A-5}$$

Note also that

$$\mathrm{N}-\Gamma=(\tilde{\lambda}-\tilde{\kappa})\ln 2 \tag{A-6}$$

which is because the interpolation between N and Γ is somewhat different from the original Cam-Clay model. Essentials of the modified Cam-Clay model can be found in Muir Wood (1995).

The objective of the use of η^*, instead of η, is to express anisotropic plastic behavior of soils. Evolution of anisotropy, in soils, naturally proceeds as plastic deformation proceeds (*i.e.*, stress induced anisotropy). Therefore the $\boldsymbol{\beta}$ in Equation (A-3) is generally the variable of plastic stretching, as discussed later in this study and also by Hashiguchi and Chen (1998).

A-2 Model formulation

In this main text, formulations are made using a finite deformation scheme satisfying objectivity.

Super-subloading concepts are introduced to Equation (A-4). The current stresses are generally considered on the subloading surface:

$$\begin{aligned} &f(p',\eta^*)+\mathrm{MD}\ln R^*-\mathrm{MD}\ln R+\int_0^t J\mathrm{tr}\boldsymbol{D}^p d\tau \\ &=\mathrm{MD}\ln\frac{p'}{\tilde{p}'_0}+\mathrm{MD}\ln\frac{\mathrm{M}^2+\eta^{*2}}{\mathrm{M}^2} \\ &+\mathrm{MD}\ln R^*-\mathrm{MD}\ln R+\int_0^t J\mathrm{tr}\boldsymbol{D}^p d\tau=0 \end{aligned} \tag{A-7}$$

where $\boldsymbol{D}^p$ denotes the plastic components of the stretching tensor $\boldsymbol{D}$. Both $\boldsymbol{D}$ and $\boldsymbol{D}^p$ are defined as positive in extension. The J in the above equation is the Jacobian determinant of the deformation gradient tensor $\boldsymbol{F}$, which is expressed in terms of specific volume as follows:

$$J=\det\boldsymbol{F}=\frac{1+e}{1+e_0} \tag{A-8}$$

where $1+e$ and $1+e_0$ are the specific volumes at the current (time t) and the reference (time $t=0$) state, respectively.

R denotes the state of overconsolidation and R^* denotes the structured state. Both R and R^* take their values between zero and one. Mathematically, R is the "surface size ratio" of the ***subloading surface*** to the ***superloading surface***:

$$R=\frac{p'}{\overline{p}'}=\frac{q}{\overline{q}},\quad 0<R\le 1\quad\text{and}\quad \overline{\eta}\left(=\frac{\overline{q}}{\overline{p}'}\right)=\eta. \tag{A-9}$$

Note here that $1/R$ gives the overconsolidation ratio. Similarly, R^* defines the surface size ratio of the plastic potential of normally consolidated and least structured soil ($R^*=1$) to the superloading surface:

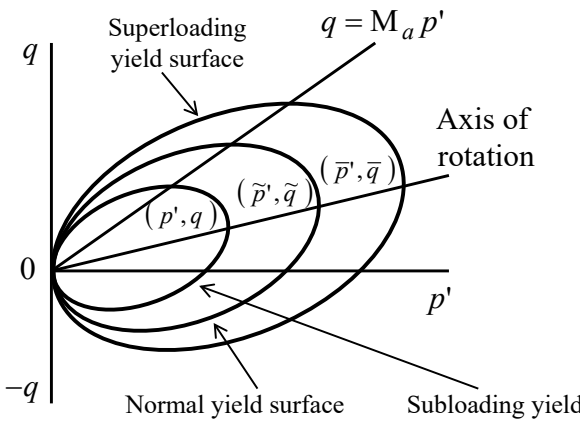

Fig. A-1 Three loading surfaces.

$$R^*=\frac{\tilde{p}'}{\overline{p}'}=\frac{\tilde{q}}{\overline{q}},\quad 0<R^*\le 1\quad\text{and}\quad \tilde{\eta}\left(=\frac{\tilde{q}}{\tilde{p}'}\right)=\overline{\eta}(=\eta). \tag{A-10}$$

The superloading surface and the normal surface are obtained as follows:

$$\begin{aligned} &f(\overline{p}',\overline{\eta}^*)+\mathrm{MD}\ln R^*+\int_0^t J\mathrm{tr}\boldsymbol{D}^p d\tau \\ &=\mathrm{MD}\ln\frac{\overline{p}'}{\tilde{p}'_0}+\mathrm{MD}\ln\frac{\mathrm{M}^2+\overline{\eta}^{*2}}{\mathrm{M}^2}+\mathrm{MD}\ln R^*+\int_0^t J\mathrm{tr}\boldsymbol{D}^p d\tau=0 \end{aligned}$$

(the superloading surface) (A-11)

$$\begin{aligned} &f(\tilde{p}',\tilde{\eta}^*)+\int_0^t J\mathrm{tr}\boldsymbol{D}^p d\tau \\ &=\mathrm{MD}\ln\frac{\tilde{p}'}{\tilde{p}'_0}+\mathrm{MD}\ln\frac{\mathrm{M}^2+\tilde{\eta}^{*2}}{\mathrm{M}^2}+\int_0^t J\mathrm{tr}\boldsymbol{D}^p d\tau=0 \end{aligned}$$

(the normal plastic potential surface) (A-12)

The super/subloading surfaces together with the normal surface are illustrated in $p'-q$ stress space when an axisymmetric stress state is considered (Fig.A-1).

A-3 Normality rule and consistency condition

Plastic behavior of soil is assumed to follow the associated flow rule,

$$\boldsymbol{D}^p=\lambda\frac{\partial f}{\partial\boldsymbol{T}'}\quad(\lambda>0) \tag{A-13}$$

in which λ denotes the plastic multiplier. On the basis of the theory of plasticity, Prager's consistency condition

$$\frac{\partial f}{\partial\boldsymbol{T}'}\cdot\dot{\boldsymbol{T}}'+\frac{\partial f}{\partial\boldsymbol{\beta}}\cdot\dot{\boldsymbol{\beta}}+J\mathrm{tr}\boldsymbol{D}^p+\mathrm{MD}\frac{\dot{R}^*}{R^*}-\mathrm{MD}\frac{\dot{R}}{R}=0 \tag{A-14}$$

should determine the size of the subsequent plastic potential surface. Note here that corotational rate tensors for $\boldsymbol{T}'$ and $\boldsymbol{\beta}$,

$$\overset{\circ}{\boldsymbol{\beta}} = \dot{\boldsymbol{\beta}} + \boldsymbol{\beta\Omega} - \boldsymbol{\Omega\beta} \tag{A-15}$$

and

$$\overset{\circ}{\boldsymbol{T}}' = \dot{\boldsymbol{T}}' + \boldsymbol{T}'\boldsymbol{\Omega} - \boldsymbol{\Omega}\boldsymbol{T}' \tag{A-16}$$

lead from Equation (A-14) to

$$\frac{\partial f}{\partial \boldsymbol{T}'} \cdot \overset{\circ}{\boldsymbol{T}}' + \frac{\partial f}{\partial \boldsymbol{\beta}} \cdot \overset{\circ}{\boldsymbol{\beta}} + J\mathrm{tr}\boldsymbol{D}^p + \mathrm{MD}\frac{\dot{R}^*}{R^*} - \mathrm{MD}\frac{\dot{R}}{R} = 0 \tag{A-17}$$

(*see* details in APPENDIX B). $\overset{\circ}{\boldsymbol{T}}'$ and $\overset{\circ}{\boldsymbol{\beta}}$ are both objective rate tensors (Green and Naghdi (1965)), in which $\boldsymbol{\Omega} = \dot{\boldsymbol{R}}\boldsymbol{R}^{\mathrm{T}}$ and $\boldsymbol{R}$ represents the rotation tensor. The superscript "T" denotes the transpose operation.

A-4 Evolution laws for R, R and* $\boldsymbol{\beta}$

Evolution laws for R and R^* define the material time derivatives of these variable as positive scalar functions relating to plastic stretching. As a measure of ongoing plastic deformation, the norm of plastic stretching $\|\boldsymbol{D}^p\|$ is adopted.

The material time derivative of R is assumed to follow:

$$\dot{R} = JU\|\boldsymbol{D}^p\| \tag{A-18}$$

where positive scalar function U is a function of R that satisfies

$$U(0) = \infty \quad \text{and} \quad U(1) = 0 \tag{A-19}$$

In the present study,

$$U = -\frac{m}{\mathrm{D}}\ln R \tag{A-20}$$

is assumed for simplicity (Hashiguchi, 1989), in which m is a positive material constant.

On the other hand, in the numerical examples of the paper, the measure of plastic deformation of clay is given in a different form from that of sand. That is, for clay

$$\dot{R}^* = JU^*\|\boldsymbol{D}^p\| \tag{A-21}$$

is assumed for the evolution law of R^*, while for sand

$$\dot{R}^* = JU^*\sqrt{\frac{2}{3}}\|\boldsymbol{D}_s^p\| \tag{A-22}$$

using $\boldsymbol{D}_s^p = \boldsymbol{D}^p - \mathrm{tr}\boldsymbol{D}^p\boldsymbol{I}/3$. In Equations (A-21) and (A-22), U^* is a positive scalar function of R^*. Asaoka, Nakano and Noda (2000a) derived the following constraints on U^*,

$$U^*(0) = 0 \quad \text{and} \quad U^*(1) = 0 \tag{A-23}$$

from which the beta function

$$U^* = \frac{a}{\mathrm{D}}R^{*b}(1-R^*)^c \tag{A-24}$$

is assumed for generality. The parameters *a, b and c* are positive material constants. The first two constants b and c are set at a value of one for simplicity throughout the present study.

For the evolution law of $\boldsymbol{\beta}$, objective material time derivative $\overset{\circ}{\boldsymbol{\beta}}$ is formulated through the following four steps (Hashiguchi and Chen, 1998):

1) Evolution of anisotropy is assumed to proceed with $\|\boldsymbol{D}_s^p\|$,

2) The rotation of the current plastic potential is limited to

$$\|\boldsymbol{\beta}\| = m_b \tag{A-25}$$

which is called, by Hashiguchi and Chen (1998), the *"limit surface for rotational hardening*" or the "*rotational limit surface*".

3) Rotational variable rate $\overset{\circ}{\boldsymbol{\beta}}$ is assumed to have the same direction as that of

$$\boldsymbol{\eta}_b = m_b\frac{\hat{\boldsymbol{\eta}}}{\|\hat{\boldsymbol{\eta}}\|} - \boldsymbol{\beta} \tag{A-26}$$

4) For the monotonic proportional loading with $\boldsymbol{\eta}$ = const., *i.e.* the so-called anisotropic consolidation, $\boldsymbol{\beta}$ is then naturally considered to reach $\boldsymbol{\eta}$ gradually, which leads to $\|\hat{\boldsymbol{\eta}}\| = 0$.

$\overset{\circ}{\boldsymbol{\beta}}$ is then given in the following form.

$$\overset{\circ}{\boldsymbol{\beta}} = J\frac{br}{\mathrm{D}}\sqrt{\frac{2}{3}}\|\boldsymbol{D}_s^p\|\|\hat{\boldsymbol{\eta}}\|\boldsymbol{\eta}_b \tag{A-27}$$

in which a material constant *br* determines the rate of the evolution of anisotropy.

A-5 Plastic multiplier λ *in terms of stresses*

Substituting the evolution laws given in Equations (A-18), (A-21) or (A-22), and (A-27) into Equation (A-17) and applying the normality rule, Equation (A-13), one gets λ as follows:

$$\lambda = \frac{\dfrac{\partial f}{\partial \boldsymbol{T}'} \cdot \overset{\circ}{\boldsymbol{T}}'}{J\dfrac{\mathrm{MD}}{p'(\mathrm{M}^2+\eta^{*2})}(\mathrm{M}_s{}^2 - \eta^2)} \tag{A-28}$$

in which, for clay

$$\mathrm{M}_s{}^2 = \mathrm{M}_a{}^2 + br\frac{4\mathrm{M}\eta^{*2}}{\mathrm{M}^2+\eta^{*2}}\left(m_b\eta^* - \sqrt{\frac{3}{2}}\hat{\boldsymbol{\eta}}\cdot\boldsymbol{\beta}\right) - \mathrm{MD}\left(\frac{U^*}{R^*} - \frac{U}{R}\right)\sqrt{6\eta^{*2} + \frac{1}{3}(\mathrm{M}_a{}^2 - \eta^2)^2} \tag{A-29}$$

and, for sand

$$\mathrm{M}_s{}^2 = \mathrm{M}_a{}^2 + br\frac{4\mathrm{M}\eta^{*2}}{\mathrm{M}^2+\eta^{*2}}\left(m_b\eta^* - \sqrt{\frac{3}{2}}\hat{\boldsymbol{\eta}}\cdot\boldsymbol{\beta}\right) - \mathrm{MD}\left\{\frac{U^*}{R^*}2\eta^* - \frac{U}{R}\sqrt{6\eta^{*2} + \frac{1}{3}(\mathrm{M}_a{}^2 - \eta^2)^2}\right\} \tag{A-30}$$

$$\mathrm{M}_a{}^2 = \mathrm{M}^2 + \zeta^2 \tag{A-31}$$

and

$$\zeta = \sqrt{\frac{3}{2}\boldsymbol{\beta}\cdot\boldsymbol{\beta}} = \sqrt{\frac{3}{2}}\|\boldsymbol{\beta}\|. \qquad \text{(A-32)}$$

The new parameter M_s for structured and overconsolidated soil with induced anisotropy varies with the evolution of both the soil structure and overconsolidation and also with the evolution of anisotropy, in which the "critical state parameter" M is constant throughout.

A-6 The threshold stress ratio between softening and hardening of soils

Based on the theory of plasticity, when soil is under loading, it holds that

$$\lambda > 0 \qquad \text{(A-33)}$$

Given that λ is positive, Equation (A-28) suggests that there exist following three cases for loading:

$$\begin{aligned} &\frac{\partial f}{\partial \boldsymbol{T}'}\cdot\overset{\circ}{\boldsymbol{T}}' > 0 \quad \text{when} \quad \eta^2 < \mathrm{M}_s{}^2 \\ &\frac{\partial f}{\partial \boldsymbol{T}'}\cdot\overset{\circ}{\boldsymbol{T}}' = 0 \quad \text{when} \quad \eta^2 = \mathrm{M}_s{}^2 \\ &\frac{\partial f}{\partial \boldsymbol{T}'}\cdot\overset{\circ}{\boldsymbol{T}}' < 0 \quad \text{when} \quad \eta^2 > \mathrm{M}_s{}^2 \end{aligned} . \qquad \text{(A-34)}$$

Since η is positive by definition, $\eta = \mathrm{M}_s$ is thus found to give the threshold stress ratio between hardening and softening.

A-7 Constitutive equation and loading criterion

Substituting an elastic response,

$$\overset{\circ}{\boldsymbol{T}}' = \boldsymbol{E}\boldsymbol{D}^e \qquad \text{(A-35)}$$

into Equation (A-28), and solving it with respect to λ, one gets the plastic multiplier in terms of stretching:

$$\Lambda = \lambda = \frac{\dfrac{\partial f}{\partial \boldsymbol{T}'}\cdot\boldsymbol{E}\boldsymbol{D}}{\dfrac{\partial f}{\partial \boldsymbol{T}'}\cdot\boldsymbol{E}\dfrac{\partial f}{\partial \boldsymbol{T}'} + J\,\dfrac{\mathrm{MD}}{p'(\mathrm{M}^2+\eta^{*2})}(\mathrm{M}_s{}^2-\eta^2)} . \qquad \text{(A-36)}$$

In Equation (A-35), $\boldsymbol{D}^e$ denotes the elastic components of stretching and $\boldsymbol{E}$ the elastic modulus tensor. Employing the plastic multiplier Λ in terms of stretching, and taking Equation (A-17) into consideration, one gets the linear rate type constitutive equation from Equation (A-35):

$$\overset{\circ}{\boldsymbol{T}}' = \boldsymbol{E}\boldsymbol{D} - \Lambda\boldsymbol{E}\frac{\partial f}{\partial \boldsymbol{T}'} . \qquad \text{(A-37)}$$

The detailed form of Equation (A-37) is given in APPENDIX C.

Note here that, when soil parameters satisfy the condition of the denominator of Λ being positive, the loading criterion

$$\Lambda > 0 \qquad \text{(A-38)}$$

can be rewritten simply in terms of the numerator of Λ as follows:

$$\frac{\partial f}{\partial \boldsymbol{T}'}\cdot\boldsymbol{E}\boldsymbol{D} > 0 . \qquad \text{(A-39)}$$

These parameters are taken to be the soil parameters throughout this study.

A-8 Plastic volume compression and plastic volume expansion

Since the plastic potential surface rotates with ongoing plastic deformation, the watershed between plastic volume compression and plastic volume expansion naturally also moves with ongoing plastic deformation.

Note here that

$$-\mathrm{tr}\boldsymbol{D}^p = -\lambda\,\mathrm{tr}\frac{\partial f}{\partial \boldsymbol{T}'} = \lambda\frac{\mathrm{MD}}{p'(\mathrm{M}^2+\eta^{*2})}(\mathrm{M}_a{}^2-\eta^2) . \qquad \text{(A-40)}$$

Then, the watershed between plastic volume compression and plastic volume expansion in terms of the stress ratio is given by $\eta^2 = \mathrm{M}_a{}^2$, which classifies the volume change behavior as follows:

$$\begin{aligned} &-\mathrm{tr}\boldsymbol{D}^p > 0 \quad \text{when} \quad \eta^2 < \mathrm{M}_a{}^2 \\ &-\mathrm{tr}\boldsymbol{D}^p = 0 \quad \text{when} \quad \eta^2 = \mathrm{M}_a{}^2 \\ &-\mathrm{tr}\boldsymbol{D}^p < 0 \quad \text{when} \quad \eta^2 > \mathrm{M}_a{}^2 \end{aligned} . \qquad \text{(A-41)}$$

The existence of *"the limit surface for rotational hardening"* gives the following constraint to M_a:

$$\mathrm{M}_a{}^2 \le \mathrm{M}^2 + \frac{3}{2}m_b{}^2 . \qquad \text{(A-42)}$$

A-9 Model characteristics

In conventional critical state soil mechanics, the critical state stress ratio, M, is the threshold both for hardening and softening and for plastic volume compression and plastic volume expansion. Therefore, hardening is always associated with plastic volume compression and softening is always associated with plastic volume expansion. Furthermore, the threshold value M is constant throughout the loading procedure. However, when the evolution laws of the soil structure and overconsolidation are considered, the threshold between hardening and softening given by M_s is a variable of ongoing plastic deformation. The same is true for the threshold between plastic volume compression and plastic volume expansion. When the rotational hardening rule is considered, the evolution of anisotropy gives the threshold M_a also as a variable of ongoing plastic deformation. Furthermore, Equation (A-29) or (A-30) suggests that it is not always trivial whether M_s is larger than M_a, or not. In other words, hardening is possible even with plastic volume expansion and softening is also possible during plastic volume compression.

The general tendency of the movement of M_s is summarized as follows. In Equation (A-24), consider the case of b=1 for simplicity, as assumed throughout this study. The substitution of Equation (A-20) and (A-24) with b=1 into $U^*/R^* - U/R$ yields

$$\frac{U^*}{R^*}-\frac{U}{R}=\frac{1}{\mathrm{D}}\{aR^*\ (1-R^*)^c-\frac{m\ln R}{R}\} \tag{A-43}$$

which increases when $R^*\rightarrow 1$ and decreases when $R\rightarrow 1$. Equation (A-29) or (A-30) indicates that the decay of the structure (*i.e.*, $R^*\rightarrow 1$) raises the value of M_s, while the loss of overconsolidation (*i.e.,* $R\rightarrow 1$) lowers it.

The effect of the evolution of anisotropy upon M_s and M_a is clearly observed when a soil in the fully remolded and normally consolidated state (*i.e.*, $R^*=1$, and $R=1$) is considered. In this case, since Equation (A-29) or (A-30) simply becomes

$$\mathrm{M}_s{}^2=\mathrm{M}_a{}^2+br\frac{4\mathrm{M}\eta^{*2}}{\mathrm{M}^2+\eta^{*2}}(m_b\eta^*-\sqrt{\frac{3}{2}}\hat{\boldsymbol{\eta}}\cdot\boldsymbol{\beta}) \tag{A-44}$$

then, based on Equation (D-1) in APPENDIX D, one has

$$\mathrm{M}_a{}^2\le\mathrm{M}_s{}^2 \tag{A-45}$$

which indicates that hardening is still possible during plastic volume expansion when the stress ratio satisfies

$$\mathrm{M}_a{}^2<\eta^2<\mathrm{M}_s{}^2\,. \tag{A-46}$$

Since hardening during plastic volume expansion at high stress ratios is a typical behavior of overconsolidated soils, it is called the "quasi-overconsolidation effect" in this study. In other words, when high levels of stress-induced anisotropy develop, normally consolidated soil still exhibits overconsolidation-like behavior at high stress ratios.

Here, the important thing to appreciate is that all the effects on the movements of M_s and M_a are the combined effects of the following three factors: decay of the structure, loss of overconsolidation and evolution of anisotropy, that occur as plastic deformation proceeds.

APPENDIX B

USE OF COROTATIONAL RATE TENSOR

For the scalar function $f(p',\eta^*)$ as defined in Equation (A-4), since

$$\frac{\partial f}{\partial p'}\dot{p}'=\frac{\partial f}{\partial p'}\mathring{p}', \tag{B-1}$$

$$\frac{\partial f}{\partial\boldsymbol{\eta}}=-\frac{\partial f}{\partial\boldsymbol{\beta}}\left(=\frac{\partial f}{\partial(\boldsymbol{\eta}-\boldsymbol{\beta})}\right) \tag{B-2}$$

and

$$\frac{\partial f}{\partial(\boldsymbol{\eta}-\boldsymbol{\beta})}\cdot(\dot{\boldsymbol{\eta}}-\dot{\boldsymbol{\beta}})=\frac{\partial f}{\partial(\boldsymbol{\eta}-\boldsymbol{\beta})}\cdot(\mathring{\boldsymbol{\eta}}-\mathring{\boldsymbol{\beta}}) \tag{B-3}$$

then, employing $\mathring{\boldsymbol{T}}'$ (Equation (A-15)) and $\mathring{\boldsymbol{\beta}}$ (Equation (A-16)), it follows simply that

$$\frac{\partial f}{\partial\boldsymbol{T}'}\cdot\dot{\boldsymbol{T}}'+\frac{\partial f}{\partial\boldsymbol{\beta}}\cdot\dot{\boldsymbol{\beta}}=\frac{\partial f}{\partial\boldsymbol{T}'}\cdot\mathring{\boldsymbol{T}}'+\frac{\partial f}{\partial\boldsymbol{\beta}}\cdot\mathring{\boldsymbol{\beta}} \tag{B-4}$$

Equation (B-4) can be used to make the constitutive equation linear with respect to $\boldsymbol{D}$.

APPENDIX C

CONCRETE FORM OF CONSTITUTIVE MODEL

The rate type constitutive equation (Equation (A-37)) for the modified Cam-Clay model with rotational hardening and Super-subloading surfaces can be written as follows:

$$\mathring{\boldsymbol{T}}'=(\widetilde{K}-\frac{2}{3}\widetilde{G})\mathrm{tr}\boldsymbol{D}\boldsymbol{I}+2\widetilde{G}\boldsymbol{D}-\frac{(6\widetilde{G}\hat{\boldsymbol{\eta}}\cdot\boldsymbol{D}-\widetilde{K}\alpha\mathrm{tr}\boldsymbol{D})(6\widetilde{G}\hat{\boldsymbol{\eta}}-\widetilde{K}\alpha\boldsymbol{I})}{12\eta^{*2}\ \widetilde{G}+\widetilde{K}\alpha^2+h} \tag{C-1}$$

where

$$\widetilde{K}=\frac{1+\mathrm{e}}{\widetilde{\kappa}}p'\left(=\frac{J(1+\mathrm{e}_0)}{\widetilde{\kappa}}p'\right),\ \widetilde{G}=\frac{3(1-2\nu)}{2(1+\nu)}\widetilde{K}$$

$$\alpha=\mathrm{M}_a{}^2-\eta^2\ \text{ and }\quad h=Jp'\frac{\mathrm{M}^2+\eta^{*2}}{\mathrm{MD}}\left(\mathrm{M}_s{}^2-\eta^2\right). \tag{C-2}$$

APPENDIX D

PROOF OF THE INEQUALITY (A-45)

$$m_b\eta^*-\sqrt{\frac{3}{2}}\hat{\boldsymbol{\eta}}\cdot\boldsymbol{\beta}\ge\|\boldsymbol{\beta}\|\eta^*-\sqrt{\frac{3}{2}}\hat{\boldsymbol{\eta}}\cdot\boldsymbol{\beta}=\|\boldsymbol{\beta}\|\eta^*\left(1-\frac{\hat{\boldsymbol{\eta}}}{\|\hat{\boldsymbol{\eta}}\|}\cdot\frac{\boldsymbol{\beta}}{\|\boldsymbol{\beta}\|}\right)\ge 0\,. \tag{D-1}$$